

A study of the mechanisms regulating cytokinesis and tissue morphogenesis during *C. elegans* embryogenesis

Karina Mastronardi

A Thesis
in the Department
of
Biology

Presented in Partial Fulfillment of the Requirements
For the Degree of
Doctor of Philosophy (Biology) at
Concordia University
Montreal, Quebec, Canada

October 2021

©Karina Mastronardi, 2021

CONCORDIA UNIVERSITY
School of Graduate Studies

This is to certify that the thesis prepared

By: Karina Mastronardi

Entitled: A study of the mechanisms regulating cytokinesis and tissue morphogenesis during *C. elegans* embryogenesis

and submitted in partial fulfillment of the requirements for the degree of

Doctor of Philosophy (Biology)

complies with the regulations of the University and meets the accepted standards with respect to originality and quality.

Signed by the final Examining Committee:

_____	Chair
Dr. Natalie Phillips	
_____	External Examiner
Dr. Sylvia Santosa	
_____	External Examiner
Dr. Christian Rocheleau	
_____	Examiner
Dr. Jean-Claude Labbe	
_____	Examiner
Dr. Malcolm Whiteway	
_____	Supervisor
Dr. Alisa Piekny	

Approved by _____
Dr. Robert Weladji, Graduate Program Director

Wednesday, October 20th, 2021

Dr. Pascale Sicotte, Dean of Faculty of Arts and Science

Abstract

A study of the mechanisms regulating cytokinesis and tissue morphogenesis during *C. elegans* embryogenesis

**Karina Mastronardi, PhD.
Concordia University, 2021**

Morphogenesis and cytokinesis are both regulated by cytoskeletal dynamics. In Chapter 2, we explore *C. elegans* anterior morphogenesis, where the epidermis covers the head of the embryo and helps to form an anterior lumen with the pharynx. Mechanisms must be coordinated at both the cellular and tissue levels to give rise to complex structures, which have been challenging to study *in vivo*. We determined how cells from three different tissues are coordinated for anterior morphogenesis. By examining the localization of the polarity protein PAR-6, we observed how polarized projections from pharyngeal, neuroblasts (neuronal precursor cells) and epidermal cells form specific patterns. We proposed that the cells forming these patterns provide and/or respond to cues that regulate epidermal cell migration. In support of this, we found that disruption of the pharyngeal cells or neuroblasts affected the rate of epidermal cell migration and epithelialization of the pharynx, while altering epidermal cell fate caused lumen positioning defects. Our studies are the first to characterize anterior morphogenesis and lay the framework for identifying how cell patterns are controlled at the molecular level.

In Chapter 3, we show how cytokinesis is regulated in different cell types. Cytokinesis occurs at the end of mitosis due to the ingression of an actomyosin ring that cleaves the cell into two daughters. However, the pathways controlling ring assembly are not fully understood and likely vary with cell type. Our lab found that the Ran pathway spatially regulates ring position in response to chromatin in mammalian cells (Beaudet et al, 2017; Beaudet et al., 2020). We tested the hypothesis that the requirement for the Ran pathway changes with cell fate in the early *C.*

elegans embryo. The zygote (P0) divides asymmetrically to give rise to AB and P1 cells with different fates, and we found that each cell has distinct ring assembly kinetics. The differences in AB and P1 cell kinetics are due to differences in the levels of inherited actomyosin, and the Ran pathway. Importantly, we found that the Ran pathway could regulate different downstream targets in AB vs. P1 cells that control ring assembly.

Acknowledgements

First and foremost, I would like to thank my supervisor, Dr. Alisa Piekny. Alisa, I have known you for most of my adult life (yes, it's true). In that time, you went from being just one of my professors, to one of my favourite professors, to my PI and finally, my mentor and friend. Thank you for giving me a chance and taking me on as a green grad-student all those years ago and, more importantly, thanks for helping me to grow and mature as a scientific researcher.

I would also like to thank the Centre for Microscopy and Cellular Imaging at Concordia University. Dr. Chloe van Oostende, thank you for all the training when I was so very inexperienced; Dr. Chris Law, thank you for the countless Swept glitch fixes and analysis computer troubleshooting expertise.

Grim (aka. Dr. Stephanie Grimbert), you are the best partner I could have ever asked for; I will be forever proud of what we accomplished together. Victoria, I am so grateful for all your help, especially during revision time, you were a pleasure to have on the team. Imge, thank you for picking up the cytokinesis project and seeing it through to the finish line.

Of course, I need to thank my fellow lab mates, Danny and Dilan, and honorary lab members, Samantha and James, for the countless pep talks and never-ending support. I couldn't have asked for a better group of people to be stuck in the grad-school trenches with.

Lastly, I would like to thank my parents for always supporting me. Parentals, thank you for letting me find my own way but always being there to guide and motivate me. You guys are the best and I love you both very much.

Dedications

To my long-suffering and supremely patient husband, I dedicate this thesis to you. Dave, thank you for supporting our family all the while putting up with a pregnant, PhD candidate writing her doctoral thesis. You are, most definitely, the real MVP. Noah and I are so lucky to have you. I love you.

Contribution of Authors

Figure 13: Dr. Stephanie Grimbert and I both contributed to the time-lapse images. Dr. Ryan Christensen acquired all images in D.

Figure 14: Dr. Stephanie Grimbert and I both contributed to the time-lapse images. Victoria Richard contributed to D and E.

Figure 15: Dr. Stephanie Grimbert, Victoria Richard and I contributed to the time-lapse images.

Figure 16: Dr. Stephanie Grimbert and I both contributed to the time-lapse images.

Figure 17: Dr. Stephanie Grimbert and I both contributed to the time-lapse images.

Figure 18: Dr. Stephanie Grimbert and I both contributed to the time-lapse images. Victoria Richard contributed to D.

Figure 19: Dr. Stephanie Grimbert and I both contributed to the time-lapse images.

Figure 20: Chris Law plotted the heat map. Imge Ozugergin performed the statistical analysis.

Figure 21: Imge Ozugergin and I both contributed to the time-lapse images. Imge Ozugergin performed the statistical analysis.

Figure 22: Imge Ozugergin and I both contributed to the time-lapse images. Imge Ozugergin performed the statistical analysis.

Figure 23: Imge Ozugergin and I both contributed to the time-lapse images.

Figure 26: Imge Ozugergin and I both contributed to the time-lapse images.

Table of Contents

List of figures	xii
List of abbreviations	xiv
Chapter 1: General Introduction	1
1.1. Preamble.....	1
1.2. <i>C. elegans</i> embryonic development – a brief overview.....	2
1.3. The first cell division.....	5
1.3.1 Divisions in the early embryo.....	14
1.4. Tissue morphogenesis.....	15
1.4.1 Gastrulation.....	15
1.4.2. Epidermal morphogenesis.....	16
1.4.3. Pharyngeal and intestinal polarization – forming a lumen.....	21
1.4.4. Neuroblast morphogenesis.....	26
1.5. Cytoskeletal regulators.....	29
1.5.1. Rho-GTPases.....	29
1.5.2. Actin.....	31
1.5.3. Myosin.....	31
1.5.4. Anillin.....	34
1.6. Thesis summary.....	36
Chapter 2: Multi-tissue patterning drives anterior morphogenesis of the <i>C. elegans</i> embryo	38

2.1. Abstract.....	38
2.2. Introduction.....	39
2.3. Materials and Methods.....	44
2.3.1. Strains.....	44
2.3.2. RNAi.....	45
2.3.3. Microscopy.....	46
2.3.4. Image analysis.....	47
2.4. Results.....	50
2.4.1. Dynamic cell movements and patterning occur during anterior morphogenesis....	50
2.4.2. The arcade cells of the pharynx form a stable rosette.....	54
2.4.3. Distinct patterns of PAR-6 foci form in the anterior region of the embryo.....	57
2.4.4. Junction proteins are enriched in foci at the anterior of the embryo.....	61
2.4.5. Ventral and dorsal epidermal cells migrate to an anterior-ventral position.....	64
2.4.6. Anterior epidermal cell migration depends on the arcade cells and subsets of anterior neuroblasts.....	68
2.4.7. Epidermal cells determine the position of the lumen.....	72
2.5. Discussion.....	74
2.6. Conclusion and model.....	77

Chapter 3: Cytokinesis is regulated differently in cells with different fates in the early

<i>C.elegans</i> embryo.....	79
3.1. Preface.....	79
3.2. Abstract.....	80

3.3. Introduction.....	82
3.4. Materials and Methods.....	88
3.4.1. Strains.....	88
3.4.2. RNAi.....	88
3.4.3. Microscopy.....	89
3.4.4. Image analysis.....	89
3.4.5. Quantitative data analysis.....	90
3.4.6. Statistical analysis.....	91
3.5. Results.....	92
3.5.1. Cells with different fates have unique ring closure kinetics.....	92
3.5.2. Differences in ring closure kinetics are cell fate-dependent.....	95
3.5.3. Regulators of actomyosin contractility control ring kinetics in P0, AB and P1 cells.....	98
3.5.4. The Ran pathway uniquely regulates ring closure kinetics in AB vs. P1 cells.....	102
3.5.5. The regulation of ring closure kinetics by the Ran pathway is dependent on <i>ect-2</i>	108
3.5.6. Anillin is differently regulated by the Ran pathway in AB and P1 cells.....	108
3.6. Discussion.....	113
Chapter 4: Overview and conclusions.....	118
4.1. Chapter 2 Conclusions.....	118
4.2. Chapter 2 Perspectives.....	120
4.3. Chapter 3 Conclusions.....	121

4.4. Chapter 3 Perspectives.....	125
References.....	126
Supplemental Figures.....	146

List of figures

Figure 1. Asymmetric divisions of the early <i>C. elegans</i> embryo.....	3
Figure 2. Schematic overview of developmental timing of morphogenetic events during <i>C. elegans</i> embryogenesis.....	4
Figure 3. Anterior-posterior polarity in the one-cell <i>C. elegans</i> embryo.....	6
Figure 4. Cytokinesis.....	10
Figure 5. Model for the role of aster-based signaling during cytokinesis.....	12
Figure 6. <i>C. elegans</i> embryonic morphogenesis.....	17
Figure 7. Pharyngeal morphogenesis.....	23
Figure 8. Schematic of the <i>C. elegans</i> adherens junction.....	25
Figure 9. Schematics show neuroblast bridge formation during <i>C. elegans</i> ventral enclosure....	28
Figure 10. F-actin formation in lamellipodia/filopodia.....	32
Figure 11. Structure and function of non-muscle myosin.....	33
Figure 12. The structure and location of anillin during cytokinesis.....	35
Figure 13. Cells ingress during anterior morphogenesis.....	52
Figure 14. The pharyngeal arcade cells form a rosette.....	55
Figure 15. Distinct patterns formed by PAR-6 foci correlate with the migrating anterior epidermal cells.....	59
Figure 16. Adhesion junctions are enriched in subsets of cells during anterior morphogenesis.....	62
Figure 17. Projections form at the leading edge of the migrating anterior ventral epidermal cells.....	66
Figure 18. Disrupting neuroblast division causes delays in anterior epidermal cell migration....	70

Figure 19. Altering epidermal cell fate causes a change in lumen position.....	73
Figure 20. P0, AB and P1 cells have unique ring closure kinetics.....	93
Figure 21. Altering cell fate affects ring closure kinetics.....	96
Figure 22. Ring closure kinetics in P0, AB and P1 cells are dependent on regulators of contractility.....	99
Figure 23. The Ran pathway regulates cytokinesis in early <i>C. elegans</i> embryos.....	103
Figure 24. Ran-3/RCC1 is not required for polarity or spindle assembly in the early embryo..	107
Figure 25. Depleting regulators of contractility suppresses the Ran-GEF/RCCI phenotype....	109
Figure 26. ANI-1 is differently regulated by the Ran pathway in AB vs. P1 cells.....	110

List of Abbreviations

14-3-3	14-3-3 protein named after elution fraction and migration position following chromatography
ABD	Actin binding domain
AHD	Anillin Homology domain
AJM-1	Adherens junction marker 1
ANI-1	Anillin
AP	Anterior-posterior axis
Arp2/3	Actin-related protein-2/3 (<i>C. elegans</i> ARX-2/3)
AIR-1	Aurora A kinase
CeAJ	<i>C. elegans</i> adherens junction
CCC	catenin-cadherin complex
Cdc42	Cell division control protein 42 (<i>C. elegans</i> CDC-42)
Cdk1	Cyclin-dependent kinase 1 (<i>C. elegans</i> CDK-1)
CGC	Caenorhabditis Genetics Center
CPC	Chromosomal passenger complex
Cyk4	Cytokinesis defect 4 (<i>C. elegans</i> CYK-4; human MgcRacGAP; <i>Drosophila</i> RacGAP50C)
CRISPR/Cas9	Clustered regularly interspaced short palindromic repeats/CRISPR associated protein 9
DAC	DLG-1/AJM-1 complex
DIC	Differential interference contrast
DLG-1	<i>Drosophila</i> discs large homologue 1

DNA	Deoxyribonucleic acid
E-cadherin	Epidermal cadherin
Ect2	Epithelial cell transformer sequence 2 (<i>C. elegans</i> ECT-2)
ELC	Myosin essential light chain
ERM	Ezrin/Radixin/Moesin
F-actin	Filamentous actin
FH1/2	Formin homology (domain) 1/2
GAP	Guanine nucleotide activating protein
GEF	Guanine nucleotide exchange factor Gex – gut on the exterior
GFP	Green fluorescent protein
GDP	Guanosine diphosphate
GTP	Guanosine triphosphate
GTPase	Guanosine triphosphatase
H2B	Histone H2B
HILO	Highly inclined and laminated optical sheet microscopy
HMP-1/2	Humpback dorsal lumps 1/2
HMR-1	Hammerhead embryonic lethal 1
Imp- a/b	Importin-a/b- nuclear transport receptors
L1/2/3/4	<i>C. elegans</i> larval stage (1-4)
L4440	Ligation number 4440/feeding vector
LGN	Mammalian homolog of Pins
LUTs	Look up tables
MAB-20	Male abnormal (human semaphorin-2A)

mCherry	Monomeric cherry fluorescent protein
mDia1/2	Mammalian diaphanous ½
MEL-11	Myosin phosphatase
MHC	Myosin heavy chain (<i>C. elegans</i> NMY-1/2)
MKLP1	Kinesin-like protein KIF23 (<i>C. elegans</i> ZEN-4)
MLC	Myosin light chain
MLCK	Myosin light chain kinase
MP-GAP	M phase GTPase activating protein
MT	Microtubules
NMY-2	Non-muscle myosin II
N-term	N-terminus or NH2-terminus
n.s.	Not significant
NIH	National Institute of Health
OP-50	Escherichia coli strain OP50/ <i>C. elegans</i> feeding bacteria
PAK-1	p21-activated kinase
PAR	Partitioning protein
Pat	Paralyzed arrest at twofold
PH	Pleckstrin Homology
PIE-1	Pharynx and intestine in excess 1
PIX-1	PAK interacting exchange factor homolog 1
Pins	Partner of Inscuteable
Plk1	Polo-like kinase 1 (<i>C. elegans</i> PLK-1)
PLX-2	Plexin 2

Rac1	Receptor-adenylate cyclase protein (<i>C. elegans</i> CED-10)
Ran	Ras-related nuclear protein GTPase (<i>C. elegans</i> RAN-1)
RanGAP	Ran GTPase activating protein
RBD	Rho-binding domain
RCC1	Regulator of chromosome condensation 1 (<i>C. elegans</i> RAN-3)
RDE-1	RNAi defective 1
RhoA	Ras homolog family, member A (<i>C. elegans</i> RHO-1)
RLC	Myosin regulatory light chain
RNAi	Ribonucleic Acid interference
ROCK	Rho-associated protein kinase (<i>C. elegans</i> LET-502)
ROI	Region of interest
S2 cells	Schneider 2 cells
SAX-3	Sensory axon guidance 3
SD	Standard deviation
SEM	Standard error of the mean
SMA-1	Small 1
TIRF	Total internal reflection fluorescence (microscope)
TPXL-1	Targeting protein for xenopus
UNC-4/40/119	uncoordinated 4/40/119
VAB-1/2/10	Variable abnormal morphology 1/2/10
VE	Ventral enclosure
WASp	Wiskott-Aldrich syndrome protein (<i>C. elegans</i> WSP-1)
WAVE/SCAR	WASp-family verprolin homology protein/suppressor of cAMP receptor

(*C.elegans* WVE-1, GEX-2/3)

Wnt

Drosophila wingless

Chapter 1: General Introduction

1.1. Preamble

Developmental biology aims to understand the myriad of processes that lead from the fertilized egg to the successful formation of a multicellular organism (Love, 2008; Minelli, 2011). This area of research includes identifying the mechanisms that regulate the coordination of cell division, changes in cell shape and migration to give rise to tissues and organs. When these mechanisms fail to function properly this can be detrimental for an organism.

Our current knowledge of developmental biology comes from the use of model organisms including invertebrates such as *Caenorhabditis elegans* (hereafter *C. elegans*) and *Drosophila melanogaster*, and vertebrates such as *Xenopus laevis*, echinoderms and mice (Davis, 2004; Leonelli and Ankeny, 2011). *C. elegans* is an excellent model organism to study the mechanisms controlling cell division, cell shape changes and migration during embryogenesis for morphogenesis of several tissues that comprise the adult animal. *C. elegans* is a non-parasitic, soil-dwelling nematode that grows up to 1 mm in length, and is amenable to microscopy due to its transparency, genetic studies, transgenics and RNAi, to name a few. It has a short life span and large brood size and has the ability to self-fertilize as hermaphrodites. Most relevant for development, each tissue has a well-defined, stereotypical number of cells with a mapped lineage, which can be used to determine when a tissue has not developed properly. These attributes make *C. elegans* an excellent model organism to study the mechanisms that control cell-specific changes crucial for tissue morphogenesis and development.

1.2. *C. elegans* embryonic development – a brief overview

After fertilization, the first division in the *C. elegans* zygote occurs asymmetrically to give rise to two daughter cells that already have distinct fates. This division occurs in the anterior-posterior axis, where the P1 posterior daughter is fated to give rise to more P-daughters that will give rise to the germline, and the AB anterior daughter is fated to become the other tissues. The P1 divides asymmetrically to give rise to the EMS (fated to become the endoderm and mesoderm) and P2 daughter, while the AB daughters divide symmetrically. During these early divisions, the body axes and cell fates are determined (Figure 1; Sulston et al., 1983). At the 26-cell stage, gastrulation begins when small groups of cells ingress into the interior of the embryo. Gastrulation plays an integral role for the development of the worm by internalizing endodermal, mesodermal and germ-line precursors (Figure 2; Nance and Priess, 2002; Nance et al., 2005). As gastrulation occurs, the embryo also undergoes ventral cleft closure, where the neuroblasts (neuronal precursor cells) move into fill the space left by the various cell movements (Figure 2). Another major event that occurs is the intercalation and migration of epidermal cells to initiate epidermal morphogenesis. The epidermal cells are born on the dorsal surface of the embryo and assemble into six rows. Through an event called dorsal intercalation, the cells in the inner two rows interdigitate to form a single row of cells (Figure 2; Chisholm and Hardin, 2005). Ventral enclosure occurs after dorsal intercalation when the ventral epidermal cells collectively migrate towards the ventral midline to cover the belly of the embryo in a layer of epidermis (Figure 2; Chisholm and Hardin, 2005). Ventral enclosure occurs in two distinct stages, where a pair of leading cells migrate toward the midline, followed by the purse-string like constriction of a pocket formed by the posterior ventral epidermal cells. After ventral enclosure, the lateral epidermal cells undergo shape changes to initiate elongation, where the embryo adopts its vermiform-like shape.

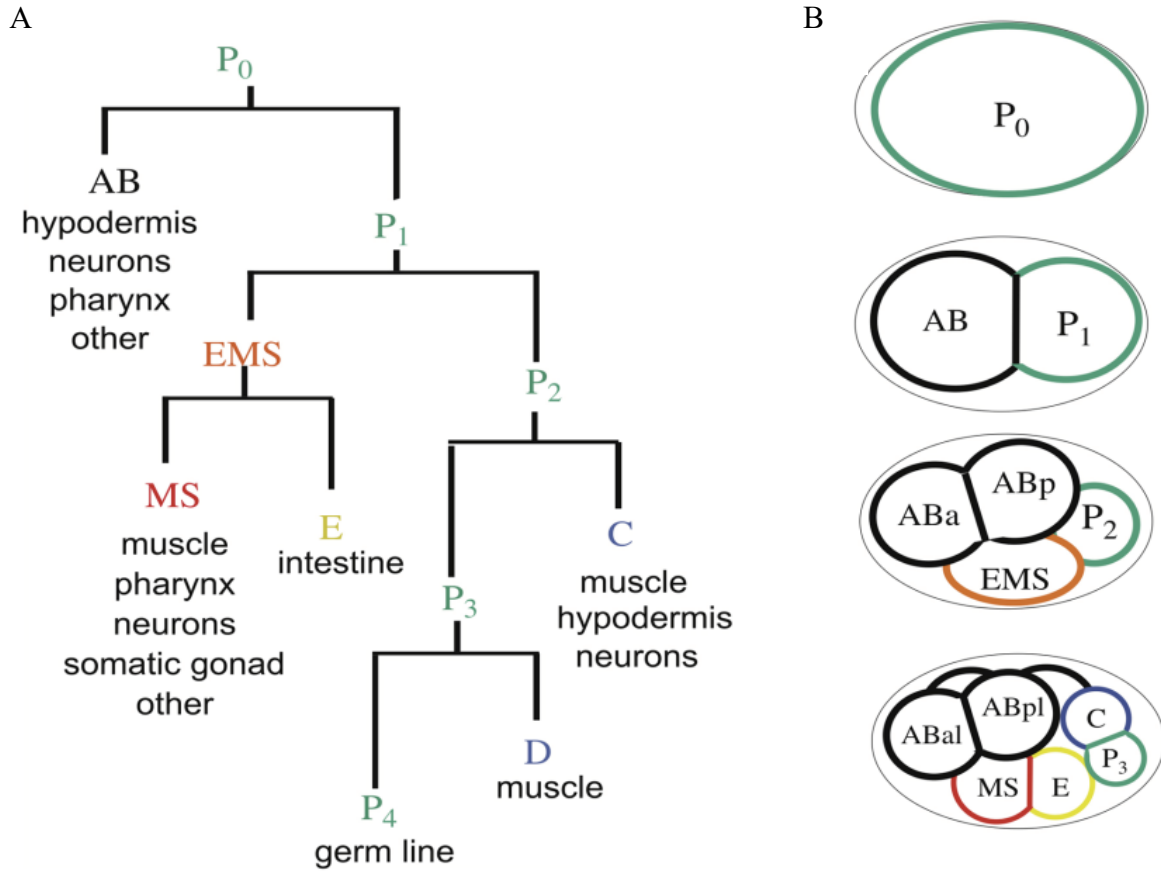


Figure 1. Asymmetric divisions of the early *C. elegans* embryo. **A)** Diagram showing the invariant cell lineage of the early embryo. The major cell types produced from the founder cells are shown. **B)** Diagram shows the symmetric (black) and asymmetric (color) division of the early embryo that generates the six founder cells. The germ-line precursor P cells are in green. Anterior is to the left while posterior is to the right. Figure taken from Rose and Gönczy, 2014.

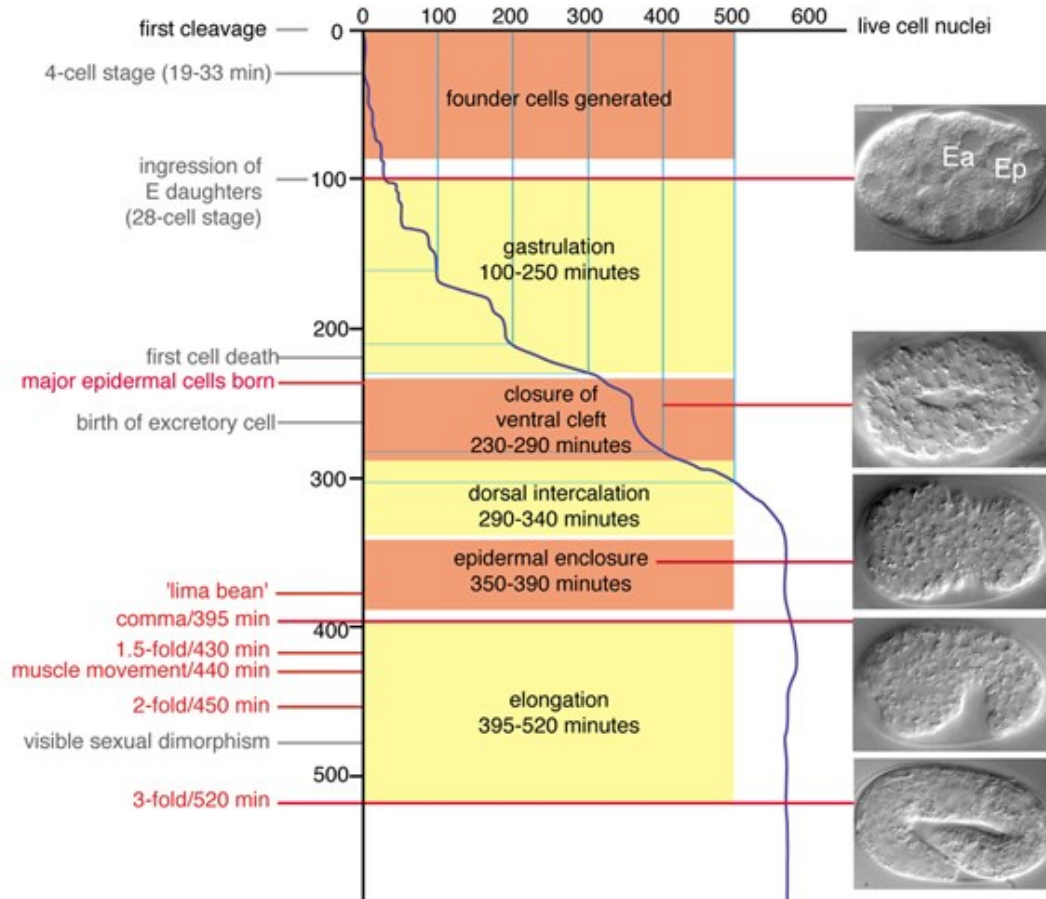


Figure 2. Schematic overview of developmental timing of morphogenetic events during *C. elegans* embryogenesis. Developmental landmarks are shown with representative Differential Interference Contrast (DIC) microscopy images of embryos at corresponding stages. Epidermal morphogenesis occurs between ~290-520 minutes after the first cleavage and includes dorsal intercalation, epidermal (ventral) enclosure and elongation. Figure adapted from Chisholm and Hardin, 2005.

Coincident with epidermal morphogenesis, the pharyngeal and intestinal cells polarize to form a well-defined lumen that is coordinated with the epidermal cells at the anterior and posterior of the embryo (Leung et al, 1999; Portereiko and Mango, 2001; Rasmussen et al, 2012). Also, at this time, the neuroblasts undergo morphogenesis, similar to convergent extension, to lengthen the tissue in line with the overlying epidermis (Wernike et al., 2016). Neuroblasts at the anterior also ingress to be positioned closer to the developing pharynx where they will form a nerve ring (the brain), where the glial cells act as guides to position the different neuronal cell bodies at their correct location (Rapti et al., 2017; Barnes et al., 2020). Another tissue that also develops is the muscle, which initiates during mid-embryogenesis where the muscle cells form into 4 quadrants that mature underneath the developing epidermis (Williams and Waterston, 1994; Chisholm and Hardin, 2005; Vuong-Brender et al., 2016). At about the two-fold stage, muscle contractions begin, causing the embryo to start twitching. This twitching drives the last stages of elongation via a mechanotransduction between the dorsal-ventral muscles and the epidermis (Zhang et al., 2011; Lardennois et al., 2019).

1.3. The first cell division

The anterior-posterior (AP) axis is already established in the zygote as the position of the centrosome provided by the sperm defines the future posterior (Cuenca et al., 2003; Munro et al., 2004; Rose and Gonczy, 2014; Gan and Motegi, 2021). Fertilization leads to a series of events necessary for symmetry breaking of the oocyte, the first of which is the local cessation of surface contractions (Figure 3; Rose and Gonczy, 2014; Gan and Motegi, 2021). Surface contractions require the Rho-GTPase RHO-1 (*discussed in detail later*) which promotes activity and contraction

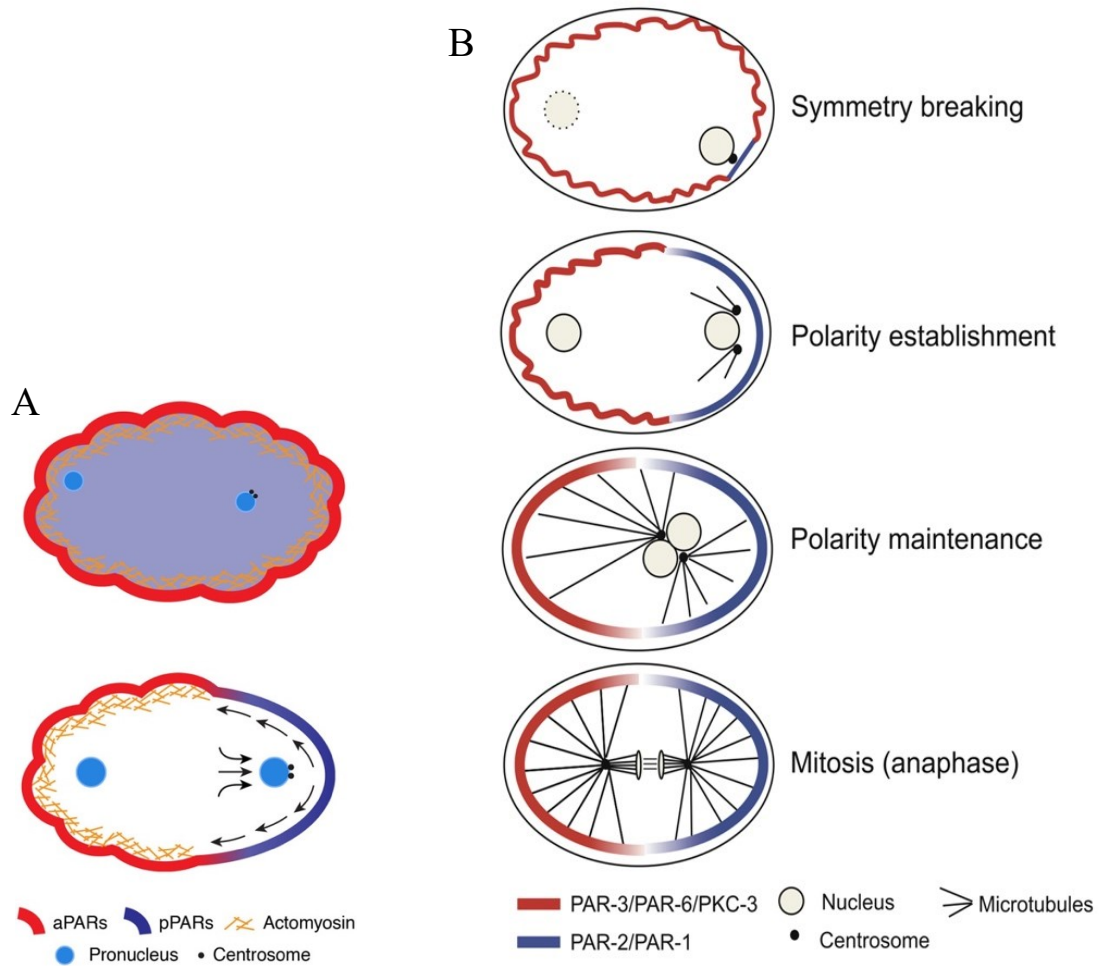


Figure 3. Anterior-posterior polarity in the one-cell *C. elegans* embryo. A) Before symmetry breaking, the anterior PARs are distributed evenly along the cortex while the posterior PARs are localized throughout the cytoplasm. The sperm-derived centrosome initiates symmetry breaking which results in the contractile actomyosin network to become segregated toward the anterior pole via cortical flows whereas the posterior PARs move from the cytoplasm to the posterior pole. **B)** Schematic showing the distribution of the anterior (red) and posterior (blue) PAR proteins. During polarity establishment, PAR-2 expands towards the anterior while PAR-6 retracts from the anterior. Anterior polarity is maintained by the mutual inhibition of the anterior and posterior cortical domains. Figure adapted from Gan and Moteği, 2021 (A) and Rose and Gönczy, 2014 (B)

of the cortical actomyosin network (Figure 3; Motegi and Sugimoto, 2006; Schonegg and Hyman, 2006). RHO-1 inactivation near the sperm centrosome, therefore, plays a major role in initiating AP polarity establishment. The partitioning of the cortex relies upon the asymmetric distribution of PAR proteins at the cell cortex which further establishes AP polarity (Kemphues and Strome, 1997). The *par* genes (for partitioning defective; *discussed in detail later*), result in the generation of daughter cells with the appropriate cell fate and size (Kemphues and Strome, 1997). The anterior PAR complex (PAR-3, PAR-6 and PKC-3) and the posterior PARs (PAR-1 and PAR-2) form two mutually exclusive domains which help to promote AP establishment (Figure 3). There is feedback between actomyosin contractility and the PAR proteins that help to form and maintain these domains.

One of the important functions of AP polarity is to position the spindle in the P0 embryo, which initially assembles in the cell center, in order for the first division to occur asymmetrically and, subsequently, to successfully partition cell-fate determinants (Kotak and Gonczy, 2013). During cell division, several types of microtubules emanate from the spindle poles. One type, the astral microtubules, project outwards from the spindle poles towards the cortex and pulling forces exerted on the plus-end of these asters at the cell cortex are essential for accurate spindle position (Rose and Gonczy, 2005; Kotak and Gonczy, 2013). Although formed in the center of the cell, the spindle is displaced towards the posterior of the cell through unequal pulling forces regulated by cortical PAR proteins (Grill et al., 2001; Labbe et al., 2004)

These pulling forces require the contribution of a ternary complex composed of $G\alpha$, GPR-1/2 and LIN-5, as their depletion results in the near absence of pulling forces on astral microtubules and as a consequence, the spindle remains centrally located and the first division is symmetric (Gotta and Ahringer, 2001; Colombo et al., 2003; Kotak and Gonczy, 2013). The entire complex

is anchored at the cell cortex where it is able to interact with the microtubule minus-end directed motor protein dynein. Dynactin, the dynein activator, helps to target dynein to the specific cellular locations it needs to be, links dynein to cargo and seems to be essential for all of dynein's cellular functions (Schroer, 2004; Kardon and Vale, 2009). Dynein is able to associate with the LIN-5 component of the $G\alpha$, GPR-1/2 and LIN-5 complex and generate force in various ways. Dynein can essentially anchor the depolymerizing microtubules to the cell cortex via $G\alpha$, GPR-1/2 and LIN-5 and the act of depolymerization generates the actual pulling force that repositions the spindle (Kozlowski et al., 2007). Dynein may also exert pulling forces directly through its motor activity, although this would need to be done in a cooperative manner in order to generate the forces required for spindle repositioning (Kotak and Gonczy, 2013; Rai et al., 2013). Interestingly, spindle-severing experiments following temperature shift of conditional mutant alleles of the dynein heavy chain gene *dhc-1*, mild RNAi-mediated inactivation of the dynein-associated lissencephaly protein-1 (LIS-1) or depletion of the dynein-associated component roadblock (DYRB-1) all show significant reduction of pulling forces (Labbe et al., 2004; Couwenbergs et al., 2007; Nguyen-Ngoc et al., 2007; Kotak and Gonczy, 2013). Additionally, laser irradiation experiments of the anterior or posterior aster revealed a stronger net pulling force present on the posterior aster compared with the anterior aster. This uneven tension results in double the amount of posterior movement of the posterior centrosome when compared to the anterior movements of the anterior centrosome, which contributes to the asymmetric positioning of the spindle for cytokinesis (Labbe et al., 2004).

As the division plane is established by spindle position, the cortex undergoes dramatic changes to assemble an actomyosin ring in the overlying plane for cytokinesis. Cytokinesis, the last stage of mitosis, is tightly regulated in both space and time to ensure that cell components are

properly inherited by the two daughter cells (Figure 4; Green et al., 2012; Glotzer, 2017; Pintard and Bowerman, 2019). Successful cytokinesis requires the formation of a contractile ring which pulls in the overlying cortex to cleave the cell into two daughters (Green et al., 2012; Glotzer 2017; Pintard and Bowerman, 2019). The machinery that regulates cytokinesis is highly conserved among metazoans, and our knowledge of this process comes from studies that include the early *C. elegans* zygote.

Spindle-dependent mechanisms lead to the formation of an equatorial zone of active RhoA (RhoA-GTP; RHO-1). In echinoderm embryos, if the mitotic spindle is shifted to a new position during anaphase, RhoA and the furrow will also shift their positions to once again be over the midplane of the newly repositioned spindle (Rappaport, 1971). Ect2 (Rho-GEF; ECT-2) is a guanine nucleotide exchange factor that generates active RhoA for cytokinesis, as depletion of either RHO-1 or ECT-2 causes failed cytokinesis in the zygote (Prokopenko et al., 1999; Tatsumoto et al., 1999; Jantsch-Plunger et al., 2000). Active RhoA binds to the effector Rho kinase (ROCK; LET-502), which induces myosin light chain phosphorylation, filament assembly, and motor activation (Kosako et al. 2000; Piekny and Mains, 2002). Active RhoA also binds to and activates formins (mDia1; CYK-1), which nucleate the assembly of unbranched actin filaments. Additionally, RhoA recruits other effectors including anillin (ANI-1), a scaffold protein that can interact with RhoA, F-actin, microtubules and myosin (NMY-2) (Straight et al. 2005; Piekny and Glotzer, 2008; Piekny and Maddox, 2010; Sun et al. 2015; Pintard and Bowerman, 2019).

Studies in several systems revealed that the central spindle protein Cyk4 (CYK-4) is required for ECT-2 function. The central spindle arises between sister chromatids during anaphase. Several microtubule-associated and kinesin motor proteins mediate bundling of the antiparallel microtubules that make up the central spindle (Glotzer, 2009). The two main central spindle

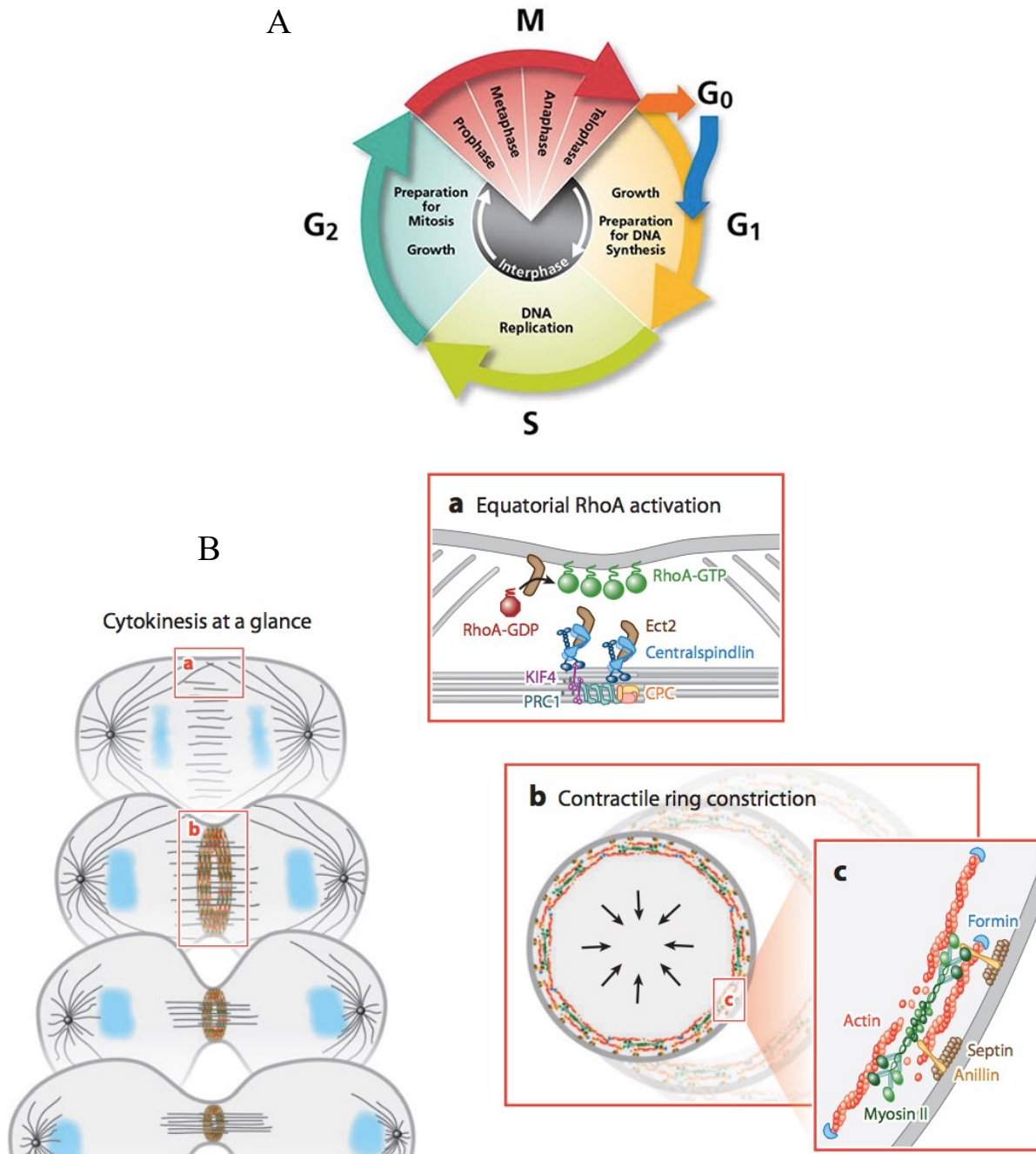


Figure 4. Cytokinesis. **A)** The schematic shows that cytokinesis occurs at the end of mitosis to complete the cell cycle. **B)** (a) An active zone of RhoA is generated at the equatorial zone of the cell. This occurs through a combination of positive signaling from the central spindle (via Ect2), and negative signaling from the astral microtubules (MTs). (b) Active RhoA coordinates the assembly of the actomyosin ring. (c) The contractile ring is made up of filamentous actin (F-actin; nucleated by formin) and myosin and is anchored to the membrane by anillin, which also recruits the membrane-associated filament, septin. Figure adapted from Green et al., 2012.

regulators are the centralspindlin complex and the chromosomal passenger complex (CPC). Centralspindlin is a heterotetrameric complex composed of a dimer of MKLP1 (ZEN-4) bound to a dimer of CYK-4 (Mishima et al., 2002; Glotzer, 2009). This complex is also required for the activation of Ect2 in multiple animal cell types. Membrane-localized centralspindlin is inhibited by 14-3-3 in the polar regions of the cell, while Aurora B kinase activity, via the CPC at the midzone, overrides this inhibition by phosphorylation of MKLP1. At the midzone, the Polo-like kinase Plk1 (PLK-1) phosphorylates Cyk4, which could release it to the overlying membrane where it forms a complex with Ect2 that generates active RhoA. The precise mechanism by which Cyk4 does this is not known, but lipid-binding is essential for their function (Petronczki et al., 2007; Wolfe et al., 2009; Basant et al., 2015; Glotzer, 2017).

Astral microtubules also regulate ring assembly by regulating the zone of active RhoA and localization of ring proteins. Astral microtubules emanate toward the polar regions of the cell where they inhibit the localization of contractile proteins (Tse et al., 2011; van Oostende Triplet et al., 2014; Chapa-Y-Lazo et al., 2020). Experiments in *C. elegans* revealed that both the central spindle and astral microtubules help to position the contractile ring (Dechant and Glotzer, 2003; Lewellyn et al., 2010). Astral microtubules prevent the accumulation of contractile proteins at the cell poles by promoting their removal or excluding them from the cortex. Mutant embryos that had fewer astral microtubules were shown to generate ectopic furrows while embryos that had more astral microtubules in the equatorial zone resulted in delayed furrowing (Figure 5; Dechant and Glotzer, 2003; Werner et al., 2007; Lewellyn et al., 2010; Tse et al., 2011). It seems that this mechanism is conserved since treating mammalian cells with low doses of nocodazole, a microtubule-depolymerizing drug, causes the partial depletion of astral microtubules resulting in a broader zone of RhoA activity (Chang et al., 2008). As the centrosomes separate during

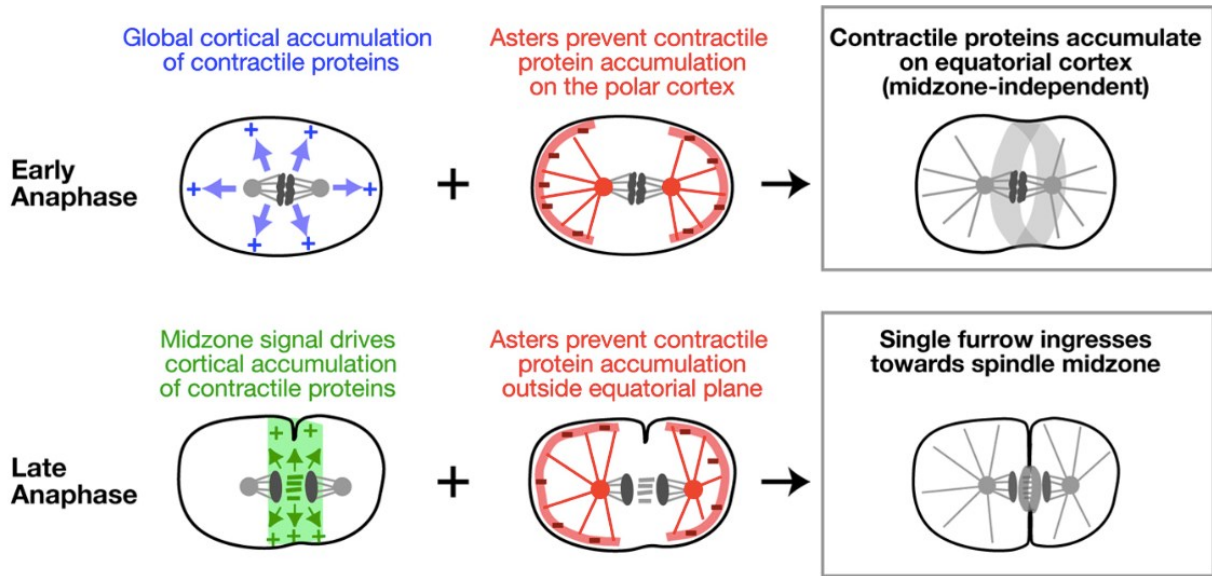


Figure 5. Model for the role of aster-based signaling during cytokinesis. In early anaphase, there is a global increase in cortical contractility (blue arrows) while aster mediated inhibition excludes contractile proteins from the anterior and posterior cortex (red lines). This leads to enrichment of contractile proteins at the equatorial cortex. As the midzone assembles in late anaphase, it provides a spatially restricted signal mediated by centralspindlin and the CPC (green arrows/zone) which further promotes accumulation of contractile proteins. Figure adapted from Lewellyn et al., 2010.

anaphase, the furrow always forms at the region with the lowest density of astral microtubules (Dechant and Glotzer, 2003). Intriguingly, evidence supports a distinct role for the central spindle and astral microtubule pathways; laser ablation and genetic studies that spatially separate the two pathways resulted in the formation of multiple furrows in response to their respective furrow-inducing signal (Bringmann and Hyman, 2005; Werner et al., 2007).

Several microtubule-independent mechanisms also influence the division plane (Deng et al., 2007; von Dassow et al., 2009; Cabernard et al., 2010; Sedzinski et al., 2011; Kiyomitsu and Cheeseman, 2013; Zanin et al., 2013; Rodrigues et al., 2015). In the zygote, MPGAP (RGA-3/4) globally inhibits RHO-1, since depleting RGA-3/4 leads to hypercontractility and increased levels of active RHO-1 throughout the cell cortex (Zanin et al., 2013). This inhibition is presumably overcome by ECT-2 in the equatorial plane. In addition, ECT-2 is also regulated by NOP-1 in the early zygote (Tse et al., 2012). NOP-1 promotes the cortical accumulation of myosin, anillin and actin at the furrows during pseudocleavage, which occurs after sperm entry and before the first cell division (Rose et al., 1995; Morton et al., 2012; Tse et al., 2012). NOP-1 subsequently functions redundantly with CYK-4 to regulate ECT-2 activity for the ring assembly in the first division (Rose et al., 1995; Morton et al., 2012; Tse et al., 2012). Another study showed that the clearing of F-actin and anillin from the polar cortex requires the astral microtubule-based TPXL-1 mediated activation of Aurora A kinase/AIR-1 (Mangal et al., 2018). Their model suggests that during anaphase, TPXL-1 binds to centrosomal microtubules where it recruits and activates AIR-1. This creates a phosphorylation gradient of AIR-1 which causes the clearing of RhoA activity and contractile proteins from the polar cortex (Mangal et al., 2018). However, whether AIR-1 activity directly affects RhoA and/or anillin localization remains unclear; further evidence is

required since few molecular regulators of the astral pathway are known (Basant and Glotzer, 2018).

1.3.1 Divisions in the early embryo

Once the ring has ingressed and formed a midbody, the division of the AB and P1 daughters occurs to form four daughter cells each with a distinct cell lineage by conserved cell-fate signaling pathways (Rose and Gonczy, 2014; Davies et al., 2018). The AB cell divides symmetrically and its descendants, ABa and ABp, will form the hypodermis, nervous system and the pharynx. Meanwhile, the P1 cell divides asymmetrically to produce an EMS daughter, which gives rise to the MS and E blastomeres, and a P2 daughter that is fated to become the germline after more asymmetric divisions (Figure 1; Sulston et al., 1983). Cytokinetic variation, which is the result of cell-type specific regulatory mechanisms, can be classified into two distinct groups: cell-intrinsic and cell-extrinsic regulation. Cell-intrinsic regulation usually involves cell polarity proteins that promote cytokinesis during asymmetric cell division (Cabernard et al., 2010; Jordan et al., 2016; Davies et al., 2018). Cell-extrinsic regulation typically involves cell-fate signalling via Wnt and Src (Fumoto et al., 2012; Soeda et al., 2013; Davies et al., 2018) while cell-cell adhesion junctions have been found to regulate contractile ring constriction in epithelial cells (Guillot and Lecuit, 2013; Daniel et al., 2018). In order to demonstrate the mechanisms of cytokinetic variation, a recent study by Davies et al., 2018 inactivated two cytokinesis proteins that are essential for contractile ring constriction in the one-cell embryo, non-muscle myosin II (NMY-2) and formin (CYK-1). They discovered that in the ABa and ABp blastomeres (AB daughters), cytokinesis is affected by reduced CYK-1 activity. However, in the EMS and P2 blastomeres (P1 daughters), decreased CYK-1 mediated F-actin activity did not affect cytokinesis in these cells (Davies et al.,

2018). Interestingly, these cell-types specific differences did not require NMY-2 activity during cytokinesis (Davies et al., 2018). Furthermore, in order to differentiate between cell-intrinsic and cell-extrinsic regulation of these cells, cell isolation and blastomere pairing experiments were performed. These experiments revealed that P2 cytokinesis is cell-intrinsically regulated as isolating it still resulted in robust cell division (Davies et al., 2018). Contrastingly, EMS cell division relies on cell-extrinsic regulation, namely, direct cell contact with P2 and cell-fate signalling via SRC-1 (Davies et al., 2018).

Our lab has recently discovered a microtubule-independent chromatin-sensing pathway which is governed by active Ran and its coeffectors in cultured mammalian cells (Beaudet et al., 2017; Beaudet et al., 2020). Since the role of the Ran pathway has not yet been shown in cytokinesis in *C. elegans*, studying these mechanisms that regulate cell division *in vivo* is crucial to gain a better understanding of their biological significance. Cytokinesis is a very tightly regulated process in both space and time and studying the requirements of Ran as well as the role and regulation of various contractile proteins in cells of different fates is crucial for development.

1.4. Tissue morphogenesis

After the early divisions establish the body axes and cell fates, specific subsets of cells undergo changes in polarity that govern changes in their shape and migration required to control their position for signaling and to develop tissues.

1.4.1 Gastrulation

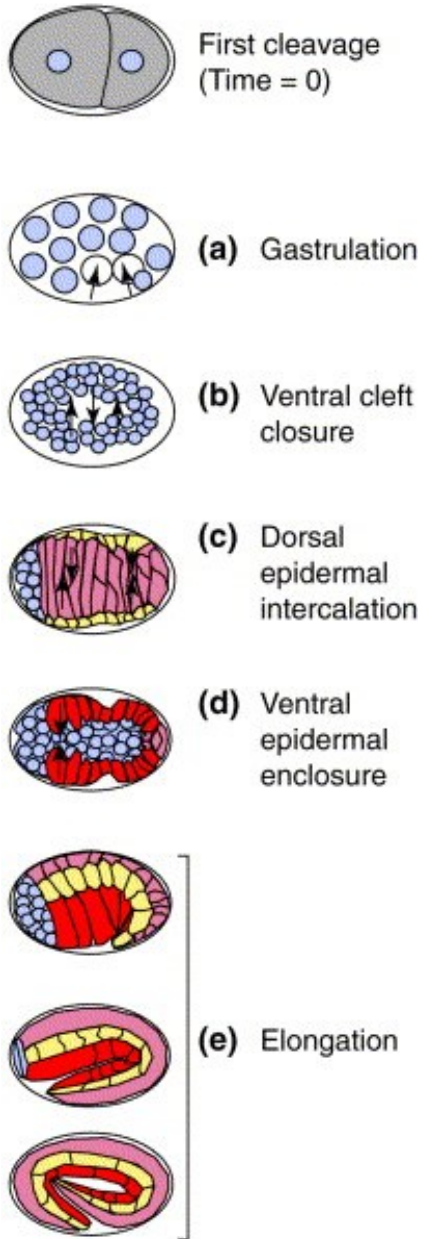
At the 26-28 cell stage, gastrulation begins when small groups of cells ingress at various times into the interior of the embryo (Sulston et al.1983; Nance and Priess 2002; Harrell and

Goldstein, 2011). Gastrulation plays an integral role for the development of the worm by internalizing endodermal, mesodermal and germ-line precursors (Figure 6A; Nance and Priess, 2002; Nance et al., 2005; Harrell and Goldstein, 2011). Gastrulation of the E daughters requires the PAR proteins to define apical-basal surfaces that will then properly pattern cell adhesions (Nance et al., 2005). Depleting apical PAR proteins prior to gastrulation resulted in slowed endodermal cell internalization, suggesting that these proteins contribute partially redundantly to gastrulation (Nance et al., 2003; Goldstein and Nance, 2020). Once apical surfaces have been defined, myosin accumulation at these surfaces helps the cells to subsequently constrict and ingress (Nance and Priess, 2002). In embryos depleted of anterior PARs, myosin failed to enrich apically in endodermal cells (Nance et al., 2003; Goldstein and Nance, 2020). Gastrulation is complete once the dorsally-born epidermal cells begin to intercalate and migrate ventrally, which are the processes known as dorsal intercalation and ventral enclosure, respectively (Chisholm and Hardin, 2005; Nance et al., 2005).

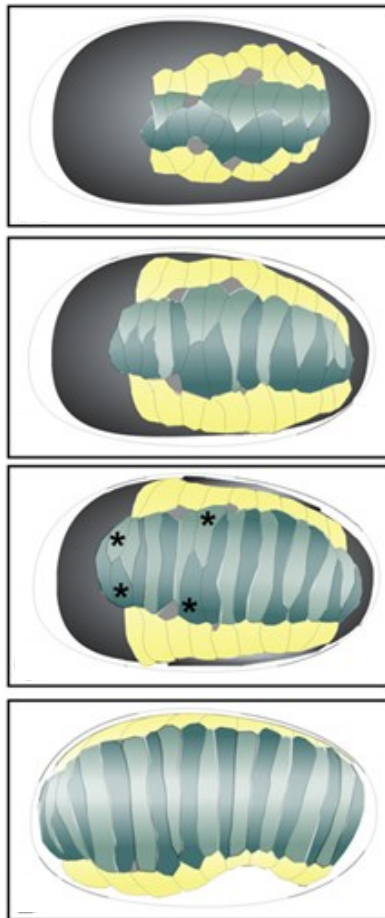
1.4.2. Epidermal morphogenesis

After the epidermal cells are born, the cells undergo shape changes and migration to define the dorsal, lateral and ventral regions of the tissue (Figure 6B, C; Chisholm and Hardin, 2005). The mechanism that drives dorsal intercalation to define the dorsal epidermis involves the regulation of actin-mediated protrusions controlled by Rac and Cdc42 and their downstream effectors the WAVE/SCAR and WASP complexes (*discussed in detail later*) (Walck-Shannon et al., 2015). Similarly, actin-mediated protrusions also regulate migration of the leading pair of ventral epidermal cells where filipodial/lamellipodial projections that are rich in short, branched F-actin are required for their movement to the ventral midline (Chisholm and Hardin, 2005).

A
C. elegans embryonic
 morphogenesis



B
 Dorsal intercalation



C
 Ventral enclosure

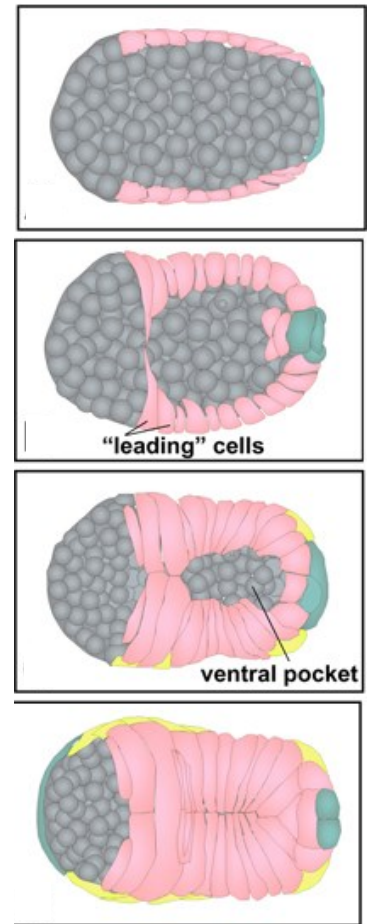


Figure 6. *C. elegans* embryonic morphogenesis. **A)** Outline of the major morphogenetic events. Dorsal epidermal cells are shown in pink, ventral epidermal cells are shown in red, lateral seam cells are shown in yellow and the neuronal precursor cells (neuroblasts) are shown in blue. **B)** Cartoon schematic of the different stages of dorsal intercalation. The dorsal cells are light and dark green and the seam cells (lateral epidermal cells) are yellow. At the onset of dorsal intercalation, the dorsal cells become wedge-shaped and interdigitate between their partners on the opposite side of the dorsal midline (top two rows). As they intercalate, the dorsal epidermal cells also elongate until they establish contacts and form adhesion junctions with the lateral seam cells (third row). A complete dorsal sheet is established once all of the dorsal cells have fully elongated (bottom row). **C)** Cartoon schematics of an embryo going through ventral enclosure. The ventral epidermal cells are pink, the seam cells are yellow and the dorsal cells are teal. The grey cells are underlying neuronal precursor cells (neuroblasts). Two pairs of leading-edge cells migrate toward the ventral midline using actin-rich protrusions and then the ventral pocket closes over the embryo. Figure adapted from Chin-Sang and Chisholm, 2000; Chisholm and Hardin, 2005.

Inactivating these cells by ablation or inhibiting F-actin polymerization disrupts ventral enclosure by either slowing down or completely halting migration (Williams-Masson et al., 1997). During the second stage of ventral enclosure, the posterior ventral epidermal (pocket) cells become wedge-shaped and form a ring that then constricts closed over the ventral surface of the embryo (Chisholm and Hardin, 2005; Zhang et al., 2010). Long F-actin cables accumulate along the junction-free edge of the pocket epidermal cells in a supracellular manner, thereby forming an actin ring around the ventral pocket (Williams-Masson et al., 1997). Additionally, myosin localizes with a similar pattern to actin and our lab showed that it is required for ventral pocket closure (Fotopoulos et al. 2013; Wernike et al. 2016). Successful ventral enclosure requires cues from the underlying neuroblasts which are the neuronal precursor cells. Different subsets of neuroblasts have been implicated in providing chemical cues that mediate ventral epidermal cell migration, suggesting that neuroblast positioning and signaling to the overlying epidermal cells is important for efficacious ventral enclosure (Chin-Sang et al., 1999; Roy et al., 2000; Chin-Sang et al., 2002; Patel et al., 2008; Bernadskaya et al., 2012; Ikegami et al., 2012).

After the ventral pocket closes, the lateral epidermal cells undergo cell shape changes to elongate the embryo into a vermiform shape. Elongation primarily occurs by myosin-mediated contraction of highly organized actin filaments within the seam cells (lateral epidermal cells). The forces generated by myosin cause these cells to squeeze from cuboidal to cylindrical in shape along the anterior-posterior axis, thereby elongating the worm (Priess and Hirsch, 1986; Wissmann et al., 1997; Piekny et al., 2000; Piekny et al., 2003). Elongation can be divided into two phases, early and late. Early elongation initiates when both actin microfilaments and microtubules become very highly organized within the dorsal and ventral epidermal cells (Williams-Masson et al., 1997; Costa et al., 1998; Chisholm and Hardin, 2005). Actomyosin-mediated contractions are mainly

regulated by phosphorylation of MLC-4, the myosin regulatory light chain that is expressed in high levels in the seam cells (*discussed in detail later*) by LET-502 (Rho-binding kinase), and PAK-1 (Rac effector kinase). These kinases function in an antagonistic manner with MEL-11 (myosin phosphatase). MLC-4 phosphorylation leads to actomyosin contractility while its dephosphorylation leads to relaxation (Wissmann et al., 1997; Shelton et al., 1999; Piekny et al., 2000; Piekny et al., 2003; Chisholm and Hardin, 2005; Gally et al., 2009; Martin and Goldstein, 2014). The LET-502/MEL-11 pathway, which is governed upstream by RHO-1, is also an essential regulator of cytokinesis (Wissmann et al., 1997; Piekny et al., 2000; Piekny et al., 2003). A second pathway involves the Rac effector PAK-1 and its activator PIX-1, where PAK-1 can also phosphorylate MEL-11 and therefore control actomyosin contractility in the seam cells (Martin et al., 2016). RhoA and Rac1 pathways involving the RhoA effector LET-502 and the Rac regulator and effector PIX-1 and PAK-1, respectively, seem to control early elongation in parallel (Piekny et al., 2003; Gally et al., 2009; Martin et al., 2014; Martin and Goldstein, 2016). As the embryo approaches the two-fold stage, late elongation mechanisms begin to take over as muscle cells located under the dorsal and ventral epidermal cells start to contract (Vuong-Brender et al., 2016). For instance, mutations causing complete abolishment of muscle function result in failure to elongate beyond the two-fold stage. These mutations are classified as Pat mutations, which result in a paralyzed at two-fold phenotype (Williams and Waterston, 1994; Chisholm and Hardin, 2005). Interestingly, in these mutants, elongation proceeds normally up until the two-fold stage, likely because early elongation is governed by the mechanisms discussed above, namely in the epidermal seam cells. However, beyond the two-fold stage, elongation requires both the epidermis and muscle activity, namely in the dorsal and ventral epidermal cells, as the tension created by muscle twitching activates a mechanotransduction cascade in the epidermis that promotes body axis

elongation (Zhang et al., 2011; Lardennois et al., 2019). Muscles attach to the exoskeleton through transepithelial structures called fibrous organelles (FOs) which also span through the dorsal and ventral epidermal cells (Francis and Waterston, 1991; Vuong-Brender et al., 2016). This is accomplished by the two hemidesmosome-like junctions present in epidermal cells, one apical and the other basal, connected by intermediate filaments which transmit mechanical tension exerted by muscles when they contract (Zhang and Labouesse, 2010; Zhang et al., 2011; Vuong-Brender et al., 2016; Lardennois et al., 2019). Muscle contractions create tension in the longitudinal axis that is then transmitted to the overlying epidermis where the dorsal and ventral cells become locally compressed and longitudinally stretched (Zhang et al., 2011; Vuong-Brender et al., 2016). Ultimately, the tension created by the muscle contraction is relayed to the hemidesmosomes and this initiates the mechanotransduction pathway in the epidermis via PAK-1, PIX-1, GIT-1 (an adaptor protein) and CED-10, which result in the phosphorylation of intermediate filaments and their further recruitment to the hemidesmosomes (Zhang et al., 2011; Vuong-Brender et al., 2016).

While many aspects of epidermal morphogenesis have been extensively studied, after the epidermal cells meet at the ventral midline and cover the belly of the embryo, not much is known regarding how the anterior of the embryo becomes epithelialized before elongation and twitching begins. While this epithelialization most certainly involves the epidermal cells, how other tissues contribute, such as the underlying neuroblasts, has yet to be elucidated. In addition to epithelialization, lumen formation is required in order to form the future mouth of the worm and could mean that the most anterior portion of the gut, the pharynx, could also be involved.

1.4.3. Pharyngeal and intestinal polarization – forming a lumen

The *C. elegans* digestive tract consists primarily of a series of interconnected tubes,

primarily the pharynx and the intestine. The pharynx develops from pharyngeal precursor cells that cluster together to form a primordium in the interior of the embryo, which initiates during ventral enclosure. During pharyngeal morphogenesis, a subset of cells reorient their apicobasal polarity and become wedge-shaped to form a highly visible and stable rosette, which subsequently transforms into a short, cylindrical epithelial cyst (Albertson and Thomson, 1976; Horner et al., 1998; Leung et al., 1999; Mango, 2009; Portereiko and Mango, 2001; Portereiko et al., 2004; Rasmussen et al., 2012). Pharyngeal cell fate is determined by expression of the transcription factor FoxA (PHA-4; Mango et al., 1994). The pharynx also needs to connect with the buccal cavity or mouth comprised of arcade cells (Figure 7; Mango, 2009; Portereiko and Mango, 2001; Portereiko et al., 2004). Polarization and cell movements aligns the pharyngeal and arcade cells, which then form adherens junctions with neighbouring epidermal cells to form a contiguous lumen (Figure 7; Portereiko and Mango, 2001). As was mentioned previously, an epithelialization event must occur between the pharynx and the epidermis in order for the anterior lumen to form. However, it is not known if morphogenesis of the pharynx is required for anterior migration of the epidermal cells, or vice-versa. Determining what role pharyngeal development plays in epidermal cell migration is crucial to gaining a better understanding of anterior morphogenesis.

The lumen is formed by epithelial cells which have apicobasal polarity, where the apical surface has secretory functions and the basement membrane connects to the extracellular matrix for tissue integrity (Nance et al., 2003; Achilleos et al., 2010). During development, apicobasal polarity requires the localization of distinct complexes to form and maintain the different domains, as well as the asymmetric distribution of actomyosin filaments, and adherens and tight junctions. In *C. elegans*, the PAR complex regulates apicobasal polarity for the developing pharyngeal and intestinal lumen during embryogenesis (Leung et al., 1999; Portereiko and Mango, 2001;

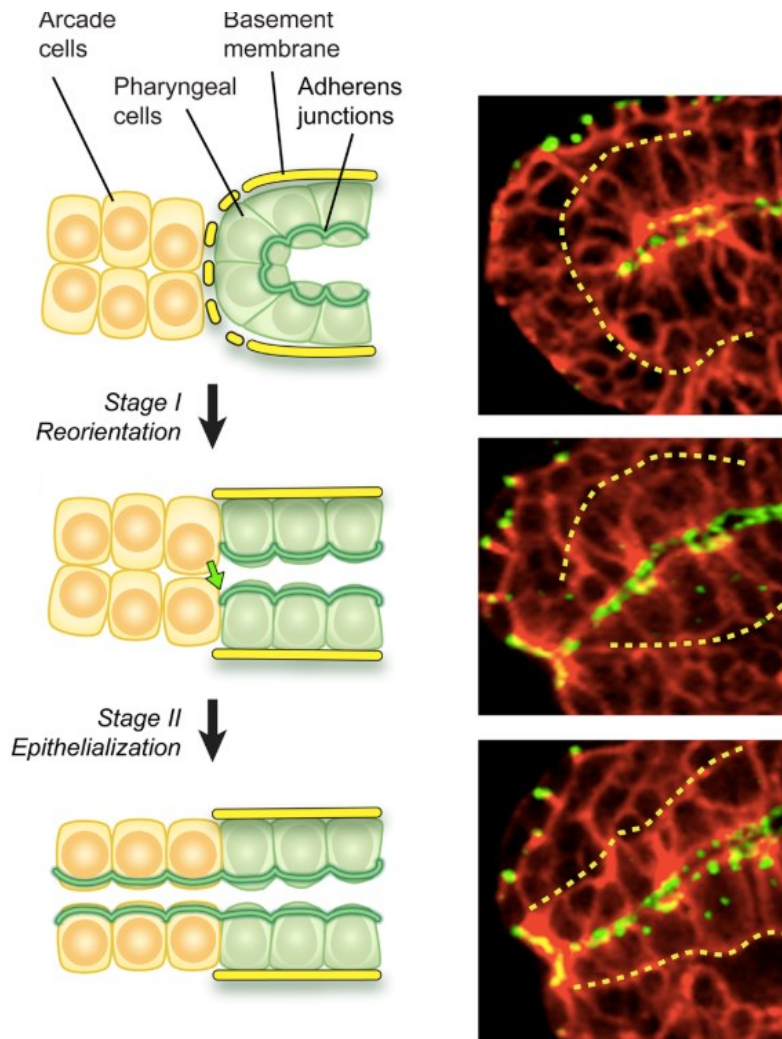


Figure 7. Pharyngeal morphogenesis. Left panel schematically shows the various stages of pharyngeal morphogenesis. Arcade cells are shown in yellow while pharyngeal cells are shown in green. Right panel shows the basement membrane of the pharynx outlined by the yellow dotted line through the various stages of development. Figure adapted from Mango 2009.

Rasmussen et al, 2012). In particular, the highly conserved PAR-3/PAR-6/PKC-3 complex accumulates near the apical region and mutually excludes basally localized complexes (Etemad-Moghadam et al., 1995; Hung and Kemphues, 1999; McMahon et al., 2001). Junctions that help define the apical and basolateral boundaries are comprised of at least two partially redundant complexes; the catenin-cadherin complex (CCC) and the DLG-1/AJM-1 complex (DAC) (Figure 8; Labouesse, 2006). The CCC is a multi-subunit complex containing E-cadherin (HMR-1), α -catenin (HMP-1) and β -catenin (HMP-2) (Costa et al., 1998; Labouesse, 2006). HMR-1 is a transmembrane protein with both extra- and intracellular domains. The extracellular domain homodimerizes with HMR-1 on an adjacent cell, while the intracellular domain forms a complex with F-actin, HMP-1 and HMP-2 (Figure 8; Costa et al., 1998; Labouesse, 2006). The CCC and the DAC, as well as tight junction components, such as occludins, are referred to as CeAJs, to distinguish them from other organisms where the adhesion and tight junctions are distinct structures (Suzuki et al., 2002; Labouesse, 2006). CeAJs are also found in epidermal cells, which keep them connected for the morphogenetic events described earlier such as for collective migration of the ventral epidermal cells, or for transmission of force during elongation of the lateral epidermal cells (Raich et al., 1999; Labouesse, 2006; Vuong-brender, 2016). While CCC and DAC components localize subapically, LET-413 (only Scribble homologue in *C. elegans*) is restricted to the basolateral membrane (Bossinger et al., 2004; Labouesse, 2006).

Other components help to establish epithelial cell polarity in *C. elegans* including PAR-3 (i.e. intestinal lumen) or the ZEN-4/CYK-4 complex (i.e. arcade cells of the pharynx) which was previously only thought to function as a complex to bundle microtubules at the spindle midzone during cytokinesis (Glotzer, 2001; Mishima et al., 2002; Portereiko et al., 2004; Labouesse, 2006). Polarized epithelial cells adhere to each other at apical junctions that associate with F-actin through

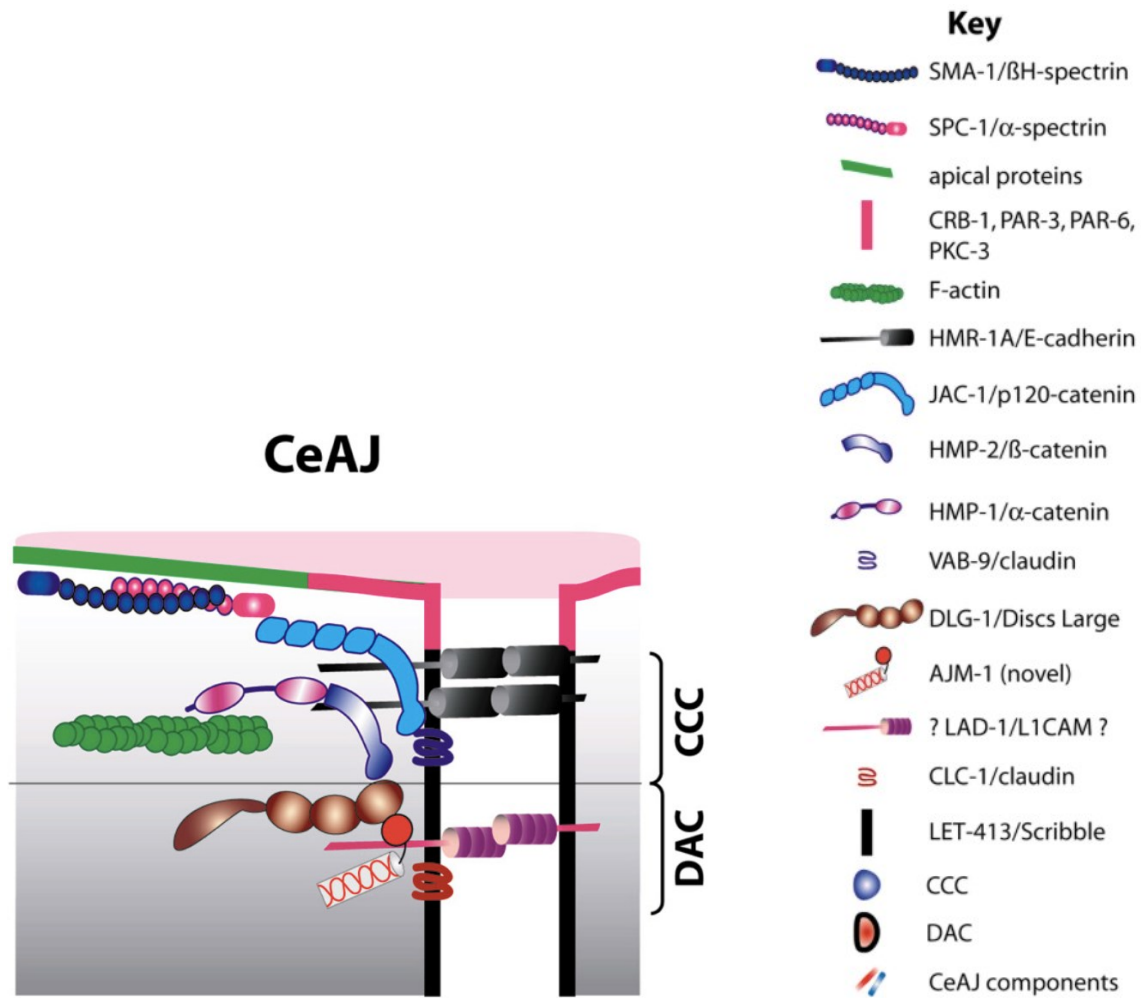


Figure 8. Schematic of the *C. elegans* adherens junction. Cartoon schematic shows the general architecture of adhesion junctions in *C. elegans* epidermal cells. The CCC consists of Ecadherin/HMR-1 (black) that homotypically binds to HMR-1 on adjacent cells via its extracellular domain. Intracellularly, HMR-1 binds to a complex of α -catenin/HMP-1 (pink) and β -catenin/HMP-2 (dark blue), which associates with F-actin (green) and helps tether the cytoskeleton to the junction. The DAC consists of DLG-1/Discs Large (brown) and AJM-1 and tethers to adjacent cells via a transmembrane protein with an extracellular domain, possibly LAD-1/L1CAM (purple). Other proteins are also found in the junction as indicated in the figure legend. This figure is adapted from Labouesse, 2006.

alpha/beta-catenin (Curdova-Burgos et al., 2021). Recent studies have shown that WAVE-dependent branched F-actin also may contribute to apical junctions, during both their establishment, and maintenance (Sasidharan et al., 2018).

1.4.4. Neuroblast morphogenesis

During epidermal morphogenesis and ventral enclosure in particular, the neuroblasts (neuronal precursor cells) provide chemical and mechanical cues that mediate ventral epidermal cell migration. For example, the VAB-2/EFN-1 ligand and its receptor, VAB-1 are expressed in distinct subsets of neuroblasts, and both are required to sort neuroblasts into separate locations with EFN-1-expressing cells in the middle of the embryo (Chin-Sang et al., 1999; Chin-Sang et al., 2002). Interestingly, *efn-1* or *vab-1* mutants also have ventral enclosure defects, suggesting that these pathways could also signal to the overlying epidermal cells. However, neither the ligand nor receptor are expressed in the epidermal cells, and tissue-specific rescue studies remain inconclusive. Two models have emerged from this work. One model is that even though it is not detectable, VAB-1 could be required in the ventral epidermal cells to help mediate their migration, by controlling the direction and formation of F-actin projections (Patel et al., 2008; Bernadskaya et al., 2012). Another model is that the position of the neuroblasts provides other cues that chemically or mechanically signal to the epidermal cells. In support of this, other receptors have also been shown to mediate epidermal cell migration for ventral enclosure, including UNC-40 (DCC – netrin receptor) and SAX-3/Robo (SLIT receptor), but their tissue-specific requirements remain unknown and their ligands have not been studied for roles in ventral enclosure (Bernadskaya et al., 2012). Another study showed that a subset of pocket epidermal cells relies on the formation of a neuroblast bridge to migrate successfully, which is mediated by

semaphorin/plexin signaling (Figure 9; Roy et al., 2000; Ikegami et al., 2012). Five pairs of neuroblasts expressing PLX-2, a semaphorin receptor, arrange themselves with bilateral symmetry to direct pocket cell migration toward the ventral midline during ventral enclosure (Figure 9; Ikegami et al., 2012). Interestingly, these neuroblasts make protrusions towards their neighbouring cells, which overlap and help to maintain cohesion via this “bridge” (Figure 9; Ikegami et al., 2012). It is not clear where the ligand is expressed or required, and how this bridge controls migration of the overlying epidermal cells. In support of mechanical signaling influencing epidermal cell migration, our lab and others found that subsets of neuroblasts form transient multicellular rosettes, which are required to mediate closure of the pocket and elongation of the embryo as they resolve (Fotopoulos et al., 2013; Wernike et al., 2016; Shah et al., 2017). Rosettes, which are cellular patterns required for the morphogenesis of a wide array of tissues, may mechanically influence migration of the overlying epidermal cells (Blankenship et al., 2006; Harding et al., 2014; Wernike et al., 2016). In support of this depletion of *ani-1*, which is required for neuroblast cell division caused ventral pocket closure defects where the cells closed more erratically (Fotopoulos et al., 2013; Wernike et al., 2016). A recent study showed that the amphid neuronal precursors form lateral rosettes, and their dendrites form attachments to the most anterior positioned epidermal cells which they use to co-migrate in a retrograde fashion (Fan et al., 2019). One aspect of neuroblast morphogenesis in particular has not been very well studied, and that is if and how the neuroblasts participate in the epithelialization of the anterior and formation of the future mouth of the worm.

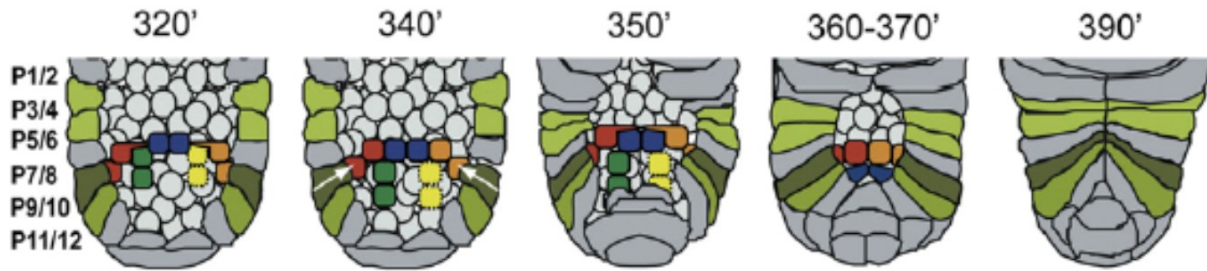


Figure 9. Schematics show neuroblast bridge formation during *C. elegans* ventral enclosure. Cartoon schematics show the different stages of pocket closure as indicated in minutes after first cell division. Five pairs of PLX-2-expressing neuroblasts (red, green, blue, yellow and orange) span across the open ventral pocket to form a bridge. Plexin-bands of cells of the same color are sisters (daughters from the preceding cell division). Laterally oriented sisters on either side of the embryo (red and orange) form protrusions (at 320 and 350 minutes) that overlap with neighboring cells (in blue). The neuroblast bridge enables the overlying epidermal pocket cells (P9/10) to migrate toward the ventral midline. This figure is adapted from Ikegami et al, 2012.

1.5. Cytoskeletal regulators

All cell divisions, cell shape changes, migration and adhesion require the spatiotemporal regulation of F-actin and myosin. Some of the master regulators of actomyosin cytoskeletal dynamics include the small GTPases RhoA, Rac1 and Cdc42. These molecular switches undergo conformational changes depending on their nucleotide-bound state and are activated by guanine nucleotide exchange factors (GEFs) which exchange GDP to GTP and inactivated by guanine nucleotide activating proteins (GAPs) which promote the hydrolysis of GTP to GDP (Lundquist, 2006; Bos et al., 2007). RhoA binds to effectors that regulate the assembly of unbranched F-actin and that assemble active bipolar nonmuscle myosin filaments, while Rac and Cdc42 tend to regulate the assembly of branched F-actin. These can generate different types of behaviors such as contractility underlying shape change, or the formation of lamellipodia for cell migration.

1.5.1. Rho-GTPases

Active RhoA is required for the assembly of actomyosin that regulates contractility for polarity and cell-shape changes. During cytokinesis, RhoA-GTP promotes the formation of an actomyosin contractile ring which ingresses to physically separate the daughter cells (Dechant and Glotzer, 2003; Piekny et al., 2005; Motegi et al. 2006; Green et al., 2012; Glotzer, 2017). Anillin and septins are also recruited to the ring and function to crosslink the ring to the overlying membrane (Oegema and Hyman, 2006; Green et al., 2012; Glotzer, 2017). As described earlier, RhoA is activated by Ect2 at the equatorial cortex which is recruited to the division plane by binding to the centralspindlin complex (Yuce et al., 2005; Bement et al., 2005). Active RhoA binds to downstream effectors, including formins and profilins that nucleate long, unbranched F-actin (*discussed in detail later*). Actomyosin filaments contract to ingress and shorten the cytoplasmic

bridge between two daughter cells, thereby separating them. Similarly, cell shape changes for morphogenesis require the formation and contraction of actomyosin filaments and as an upstream regulator of actomyosin contractility, RhoA is also required for these processes. In *C. elegans* embryos, RHO-1 is required for elongation and ventral enclosure, whereby LET-502 (Rho kinase) phosphorylates the non-muscle myosin light chain (MLC-4) to promote contractility and is negatively regulated by MEL-11 (myosin phosphatase regulatory subunit) (Piekny and Mains, 2002; Matsumura, 2005; Matsumura and Hartshorne, 2008; Heisenberg and Bellaïche, 2013).

The cytoskeleton is also tightly regulated to drive cell migration during morphogenesis. In migrating cells, Rac and Cdc42 are active at the leading edge to form filopodial/lamellipodial extensions at the front of migrating cells (Ridley, 2011). While Cdc42-GTP regulates the WASp complex, Rac1-GTP regulates the WAVE complex, leading to the nucleation of short, branched F-actin via Arp2/3 (Soto et al., 2002; Patel et al., 2008). In *C. elegans* embryos, Rac-1/CED-10 and the WAVE/SCAR complex, its effector, regulate ventral enclosure by promoting the protrusions that drive enclosure through the branch actin regulator Arp2/3 (Soto et al., 2002; Patel et al., 2008; Bernadskaya et al., 2011). Cdc42 has also been implicated in the formation of tight junctions and in the polarized vesicular trafficking required for polarized protein distribution (Rojas et al., 2001; Etienne-Manneville, 2004). In *C. elegans* embryos, CDC-42 and RHO-1 are essential for division of the one-cell embryo. RHO-1 activity is required for actomyosin contractility and organization of the myosin/NMY-2 foci and filaments. This NMY-2 meshwork is, in turn, responsible for localizing CDC-42 to the anterior of the embryo. The anterior localization of CDC-42 is then required to stabilize the actomyosin network and to localize anterior polarity proteins (Schonegg and Hyman, 2006).

1.5.2. Actin

Actin polymerization is essential for the contractile and migratory events necessary for cytokinesis and the morphogenesis of tissues. Different Rho GTPases regulate the nucleation of long, unbranched or short, branched F-actin filaments. RhoA-GTP is able to regulate long, unbranched F-actin through the Rho effector, formin (mDia/CYK-1). Formins help to elongate actin filaments by associating with profilin in order to polymerize actin filaments from their barbed end in an ATP-dependent manner (Pantaloni and Carlier, 1993; Watanabe et al., 1997; Paul et al., 2008). The branching of actin filaments is achieved by the activity of Arp2/3, a seven-subunit protein complex that mimics the core actin complex required to nucleate F-actin, and templates the growth of F-actin from pre-existing filaments at a 70° angle (Pollard et al., 2000; Amann and Pollard, 2000; Goley and Welch, 2006). Arp2 and Arp3, however, possess little activity on their own and require activation by the WASp (Wiskott-Aldrich syndrome protein) and WAVE/SCAR (WASp family verprolin homology proteins/suppressor of cAMP receptor) complexes, which bind to the Arp2/3 complex to promote actin nucleation. This subsequently results in branching followed by cell movement (Figure 10).

1.5.3. Myosin

Non-muscle myosin II (hereafter called myosin) motors associate with actin filaments and generate tensile force by crosslinking and/or sliding past one another. Non-muscle myosin II is comprised of a pair of heavy chains, a pair of regulatory light chains (RLC) and a pair of essential light chains (ELC). Each heavy chain possesses a catalytic motor head domain in its N-terminus, which has highly conserved actin-binding and ATP-binding sites. Both the RLC and ELC associate with the neck region of the heavy chain, which lies adjacent to the motor (Figure 11; Vincente-

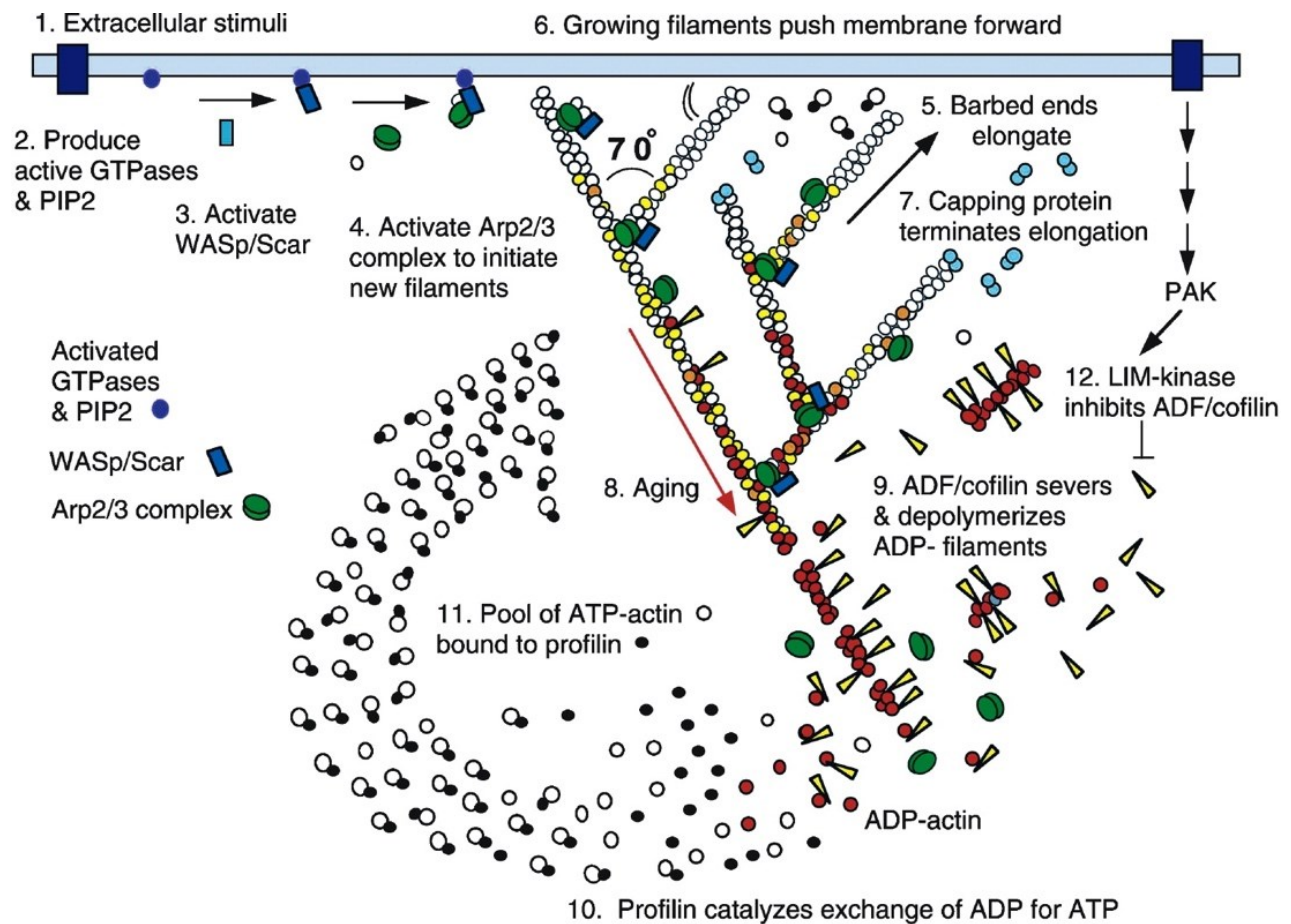


Figure 10. F-actin formation in lamellipodia/filopodia. The cartoon schematic depicts how F-actin is regulated in response to stimuli. **(1)** An external stimulus is translated into changes in F-actin by **(2)** triggering Rho GTPase activity, **(3)** promoting WASp or WAVE/SCAR function, and **(4)** bringing together the Arp2/3 complex with monomeric actin. **(5)** The addition of monomeric actin to the barbed end of actin filaments **(6)** facilitates their growth to push out the membrane **(7)** until actin-capping proteins terminate this process. **(12)** Rho GTPase-induced activation of kinases such as PAK or ROCK promote LIMK activation to prevent **(9)** actin depolymerization via the inhibition of cofilin. The dimerized FH2 domains of formins take on donut-like structures that surround the barbed end of actin filaments. The FH1 domains of formins tether profilin-actin to the barbed end, thereby elongating the filament (bottom left). Figure adapted from Pollard, 2007.

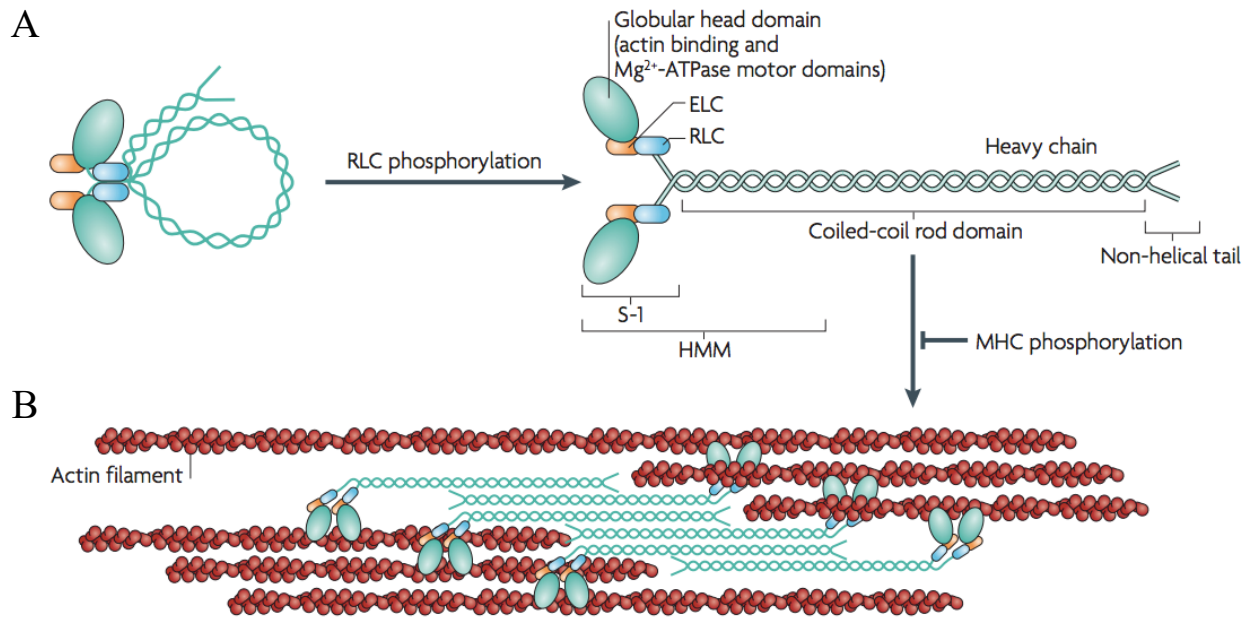


Figure 11. Structure and function of non-muscle myosin. Cartoon schematics show how myosin assembles into filaments. **A)** When the RLCs are dephosphorylated, myosin is folded (left), and upon their phosphorylation, myosin unfolds (right) and is able to form multimeric filaments (**B**). **B)** Each of the two heavy chains consists of a globular head motor domain in the N-terminus and a coiled-coil domain including a non-helical tail domain in the C-terminus. The ELCs and the RLCs wind around the heavy chains between the head motor domain and the coiled-coil domain. Myosin molecules assemble into bipolar structures through the interactions of their coiled-coil domain along the heavy chains. Myosin binds to actin filaments via its head motor domains. ATP hydrolysis, which is stimulated by RLC, enables myosin to move actin filaments past each other in an anti-parallel manner. Figure adapted from Vicente-Manzanares et al., 2009.

Manzanares et al., 2009). Non-muscle myosin activity is regulated by phosphorylation of the RLC, which promotes dimerization of the heavy chains and stimulates ATPase activity in the motor (Vincente-Manzanares et al., 2009). Interestingly, Rho kinase can phosphorylate and inactivate the regulatory subunit of myosin phosphatase causing an increase in myosin contractility (Vincente-Manzanares et al., 2009).

1.5.4. Anillin

Anillin is a highly conserved protein that is part of the contractile ring during cytokinesis. Active RhoA directly binds to and recruits anillin to the equatorial cortex where it also binds to actin, myosin, and phospholipids among other components (Piekny and Maddox, 2010). In cultured human cells, the loss of anillin causes the ring to oscillate, supporting its role in crosslinking the ring to the overlying membrane (Figure 12A; Piekny and Glotzer, 2008; Piekny and Maddox, 2010). Similar phenotypes have been observed in *Drosophila* S2 cells and *Xenopus* cells (Straight et al., 2005; Hickson and O'Farrell, 2008, Reyes et al., 2014).

There are three distinct anillin isoforms in *C. elegans*: *ani-1*, which shares the highest homology with both human and *Drosophila* anillin, and *ani-2* and *ani-3*, which encode truncated forms that lack the characteristic actin and myosin binding sites (Figure 12B; Maddox et al., 2005). *ani-2* is required for germline development (Maddox et al., 2005, Amini et al., 2014).

In the early embryo, *ani-1* depletion results in symmetric vs. asymmetric constriction of the contractile ring, although cytokinesis still succeeds (Maddox et al., 2007). As described earlier, our lab found that during mid-embryogenesis *ani-1* is primarily expressed in the neuroblasts and is required for neuroblast cytokinesis (Fotopoulos et al., 2013). In *ani-1*-depleted embryos, neuroblasts are misshapen and are often multinucleate. This also causes ventral enclosure

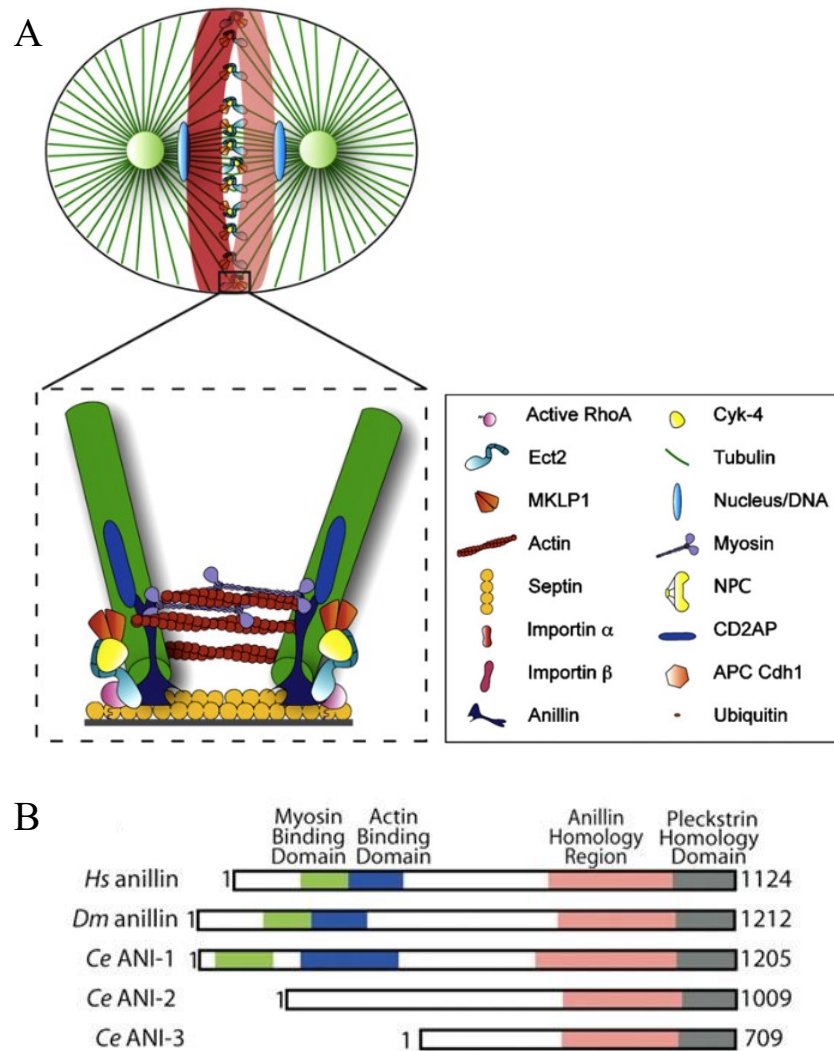


Figure 12. The structure and location of anillin during cytokinesis. **A)** Cartoon schematic shows the localization of anillin during mammalian cytokinesis. During anaphase, anillin is recruited to the equatorial cortex by RhoA-GTP where it tethers the contractile ring to the plasma membrane (red ring in the cell). A detailed view depicts anillin at the equatorial cortex with other contractile ring components. **B)** Cartoon schematic shows anillin's structure in human, *Drosophila* (scraps) and *C. elegans*. Human anillin, scraps and *ani-1* share high homology in their myosin (green) and actin (blue)-binding domains in the N-terminus, and the Anillin Homology (red) and Pleckstrin Homology (grey) domains in the C-terminus. Figures adapted from Piekny and Maddox, 2010 (A) and Maddox et al., 2005 (B).

phenotypes as the ventral epidermal cells were often misaligned and the embryos were prone to rupture during elongation (Fotopoulos et al., 2013). Interestingly, we also found that *ani-1* lethality is partially suppressed by over-expressing α -catenin. Since α -catenin tethers to intracellular F-actin, ANI-1 could also be required to tether F-actin to generate tension in the neuroblasts for ventral enclosure (Fotopoulos et al., 2013).

1.6. Thesis summary

C. elegans epidermal morphogenesis has been well-characterized, yet, how the head/anterior of the embryo gets encased in epidermis and forms the anterior lumen (stage between ventral enclosure and elongation) has been largely ignored. This is likely due to the difficulty of studying this process due to issues with imaging head-on, the number of tissue-types involved, as well as challenges in interpreting gene requirement when there is an upregulation of zygotic gene expression that occurs during mid-embryogenesis. Anterior morphogenesis involves the coordination of several tissues including epidermal cells, pharyngeal cells and neuronal precursor cells, and Chapter 2 of this thesis will provide the first in-depth description of anterior morphogenesis. Namely, a detailed characterization of the entire process, the contribution of various tissues as well as speculation on how these tissues are coordinated at the molecular level.

While we have extensive knowledge regarding the core machinery that regulates cytokinesis, the mechanisms that regulate this machinery are much less understood. Additionally, the mechanisms that govern cytokinesis can vary depending on cell type or cell fate. As cytokinesis is such an important process, the concerted action of multiple pathways ensures that it proceeds in a robust and efficient manner. Several mitotic spindle-dependent pathways provide spatiotemporal signals that regulate the cytokinetic machinery. However, a number of studies have shown that

spindle-independent pathways also regulate cytokinesis. Our lab has found that one microtubule-independent pathway in particular, the Ran pathway, spatially regulates the contractile ring in response to chromatin position in mammalian cells (Beaudet et al, 2017; Beaudet et al., 2020). Chapter 3 of this thesis will consider the implication of Ran-dependent regulation in the early *C. elegans* embryo, more specifically, the first three cell divisions, P0, AB and P1, respectively. These cells have varying sizes and cell-fates and we propose that the Ran pathway could play an important role in regulating cytokinesis in these cells.

Chapter 2: Multi-tissue patterning drives anterior morphogenesis of the *C. elegans* embryo

Adapted from: *Grimbert S, *Mastronardi K, Richard V, Christensen R, Law C, Zardoui K, Fay D, Piekny A. (2021). Multi-tissue patterning drives anterior morphogenesis of the *C. elegans* embryo. *Dev Biol.* Mar; 471:49-64. *Co-first author, equal contribution.

2.1. Abstract

Complex structures derived from multiple tissue types are challenging to study *in vivo*, and our knowledge of how cells from different tissues are coordinated is limited. Model organisms have proven invaluable for improving our understanding of how chemical and mechanical cues between cells from two different tissues can govern specific morphogenetic events. Here we used *Caenorhabditis elegans* as a model system to show how cells from three different tissues are coordinated to give rise to the anterior lumen. While some aspects of pharyngeal morphogenesis have been well-described, it is less clear how cells from the pharynx, epidermis and neuroblasts coordinate to define the location of the anterior lumen and supporting structures. Using various microscopy and software approaches, we define the movements and patterns of these cells during anterior morphogenesis. Projections from the anterior-most pharyngeal cells (arcade cells) provide the first visible markers for the location of the future lumen and facilitate patterning of the surrounding neuroblasts. These neuroblast patterns control the rate of migration of the anterior epidermal cells, whereas the epidermal cells ultimately reinforce and control the position of the future lumen, as they must join with the pharyngeal cells for their epithelialization. Our studies are the first to characterize anterior morphogenesis in *C. elegans* in detail and should lay the framework for identifying how these different patterns are controlled at the molecular level.

2.2. Introduction

Our knowledge of how complex structures form in the developing embryo is limited due to challenges in studying the morphogenesis of multiple tissues simultaneously *in vivo*. *C. elegans* is an extremely powerful organism to use for studies of development at the cellular and subcellular level, as they have multiple tissues with a defined number of cells. They are also a powerful genetic model, and the development of transgenic and microscopy tools makes them ideal for studying complex events *in vivo*. As the mechanisms regulating cell polarity and migration are highly conserved, studies of tissue morphogenesis in *C. elegans* have provided insight into how tissues develop in more complex organisms (Jacinto et al., 2001; Muller and Bossinger, 2003; Campanale et al., 2017).

Anterior morphogenesis is required for development of the anterior lumen, and involves the coordination of epidermal cells, pharyngeal cells and neuroblasts (neuronal precursor cells). Due to this complexity, it is not known how all three tissues form the anterior lumen but revealing this could provide fundamental knowledge that is relevant for other complex developmental processes. The timing of anterior morphogenesis coincides with epidermal and pharyngeal morphogenesis, which are outlined below. The anterior-most epidermal cells migrate toward the anterior of the embryo after the epidermal cells meet at the ventral midline. Similarly, a large subset of pharyngeal cells polarizes and forms a cyst to define a lumen that aligns with the intestinal cells (Rasmussen et al., 2012). Anterior to the cyst are the arcade cells, which migrate anteriorly before moving back inward as development progresses (Portereiko and Mango, 2001; Portereiko et al., 2004; Mango 2009). They also polarize and coordinate with the epidermal cells for epithelialization of the anterior pharynx, but it is not clear how this occurs (Von Stetina and Mango, 2015). During anterior morphogenesis, the neuroblasts presumably also undergo specific

movements and patterning, but with the exception of the amphid neurons this has not been extensively studied (Fan et al., 2019). Importantly, how all of these cell types are coordinated to give rise to a properly positioned anterior lumen remains poorly understood.

Epidermal morphogenesis has been relatively well-characterized and requires chemical and mechanical signaling between different cell types. During mid-embryogenesis, the dorsal epidermal cells intercalate, followed by migration of the ventral epidermal cells toward the ventral midline to enclose the embryo through a process called ventral enclosure (Williams-Masson et al., 1997; Chisholm and Hardin, 2005). Ventral epidermal cell migration relies on precisely positioned neuroblasts for chemical and/or mechanical signaling (Bernadskaya et al., 2012; Ikegami et al., 2012; Wernike et al., 2016). EFN-VAB signaling is required for neuroblast positioning and for ventral enclosure, although it is not clear if the ligands and/or receptors are required in the neuroblasts or epidermal cells (George et al., 1998; Chin-Sang et al., 1999; Bernadskaya et al., 2012). Other signaling pathways implicated in controlling ventral epidermal cell migration include semaphorin (MAB-20) and plexin (PLX-2; Roy et al., 2000; Nakao et al., 2007; Ikegami et al., 2012). One model is that the receptors are expressed in the epidermal cells and receive cues from the neuroblasts or neighbouring epidermal cells to regulate branched F-actin assembly for their migration (Withee et al., 2004; Chisholm and Hardin, 2005; Patel et al., 2008; Bernadskaya et al., 2012; Patel and Soto, 2013; Wallace et al., 2018). In addition, subsets of neuroblasts in the middle-posterior of the embryo form rosettes, likely via planar cell polarity, to elongate the tissue in preparation for epidermal elongation (Wernike et al., 2016; Shah et al., 2017). Rosettes are patterns required for the morphogenesis of different metazoan tissues, and form by apical-basal polarity or planar cell polarity, the latter of which are often associated with transient rosettes that facilitate tissue re-organization (Blankenship et al., 2006; Harding et al., 2014). The neuroblast rosettes that

form in the ventral pocket may mechanically influence migration of the overlying epidermal cells during ventral enclosure (Wernike et al., 2016). Non-muscle myosin (NMY-2) is required in both the underlying neuroblasts and the epidermal cells for ventral enclosure, suggesting that these two tissues are mechanically connected (Wernike et al., 2016). Mechanical signaling also occurs between the epidermal and muscle cells to drive later stages of elongation, the subsequent step in epidermal morphogenesis (Zhang et al., 2011). A recent study showed that the amphid neuronal precursors form lateral rosettes and maintain their organization as they co-migrate anteriorly with the epidermal cells (Fan et al., 2019). The authors proposed that there is chemical and/or mechanical feedback between these cell-types (Fan et al., 2019). Other neuroblast-epidermal cell interactions presumably also guide the anterior migration of epidermal cells for anterior morphogenesis, although this is not known.

Coincident with ventral epidermal morphogenesis, a large subset of pharyngeal cells polarizes to form a cyst to define the pharyngeal lumen. These cells apically constrict with PAR-3 accumulated apically and laminin basally to form a cyst (rosette) with a central lumen (Rasmussen et al. 2012). Apical rosettes are formed by cells that apically constrict as a result of actomyosin activity, which is coordinated at the intercellular level via adhesion junctions (Sawyer et al., 2010; Martin and Goldstein, 2014). This gives rise to a bulb-like organization of cells with their narrow tips coming together to form a small hole apically (Harding et al., 2014). Apically formed rosettes are typically highly stable and ultimately give rise to lumens (Lecaudey et al., 2008; Nechiporuk and Raible, 2008). Interestingly, the anterior arcade cells remain distinct from the large pharyngeal cyst, yet must polarize to form a contiguous lumen (Portereiko and Mango, 2001; Portereiko et al., 2004; Mango 2009; Von Stetina and Mango, 2015). These cells need to be

precisely positioned in line with the more posterior pharyngeal cells and the anterior epidermal cells, but as indicated earlier, it is not clear how they do this.

In metazoans, apicobasal polarity occurs due to the recruitment and maintenance of apical complexes (*e.g.* Par3, Par6, aPKC; Etemad-Moghadam et al., 1995; Hung and Kemphues, 1999; McMahon et al., 2001). Many factors contribute to the onset and establishment of this asymmetric segregation of proteins, including the trafficking and turnover of active Cdc42, actomyosin organization, asymmetric distribution of specific phospholipids, adhesion junctions and mutual antagonism (Jiang et al., 2015; Campanale et al., 2017; Jewett and Prekeris, 2018; Motegi et al., 2020). In *C. elegans*, intestinal cells acquire apicobasal polarity, which is crucial for formation of the interior lumen (Leung et al., 1999; Bernadskaya et al., 2012; Shafaq-Zadah et al., 2012; Rasmussen et al., 2012; Bossinger et al. 2015; Asan et al., 2016). Epidermal cells also have apicobasal polarity, which is reinforced by adhesion junction components that connect neighboring cells (Patel et al., 2008; Patel and Soto, 2013). These include the DAC (DLG-1 and AJM-1 Complex) and the CCC (Catenin Cadherin Complex; E-cadherin [HMR-1], α -catenin [HMP-1] and β -catenin [HMP-2]) which are located sub-apically (Costa et al., 1998; Labouesse, 2006; Totong et al., 2007; Armenti and Nance, 2012; Pasti and Labouesse, 2015; Gillard et al., 2015; Sasidharan et al., 2018). Adhesion junctions connect actomyosin filaments intercellularly to coordinate cell movements and patterning. The CCC, but not the DAC, is also expressed in neuroblasts (Wernike et al., 2016) and the function of the CCC in these cells is not clear. The expression of different adhesion junction components in different cell types could influence adhesion and how mechanical forces are transmitted between cells.

Here we provide the first detailed description of *C. elegans* anterior morphogenesis, which involves the coordination of neuronal precursors and their support cells, epidermal and pharyngeal

cells. Using diSPIM (dual-view inverted selective plane illumination microscopy) and confocal imaging, we observed that subsets of neuroblasts form concentric patterns around the site of the future lumen and that some of these neuroblasts ingress as the epidermal cells migrate anteriorly. We also observed that a subset of pharyngeal arcade cells forms a stable rosette, which aligns with the previously described pharyngeal cyst. The projections from these cells initially are enriched in PAR-6, NMY-2 and HMP-1 (CCC), which mark the site of the future lumen. Additionally, subsets of neuroblasts form specific patterns of foci around this location, which contain ANI-1, PAR-6, NMY-2 and CCC components. Other foci are closely associated with both the neuroblasts and the migrating epidermal cells and contain PAR-6, NMY-2, CCC and DAC components. All of the foci mature over time to also include the DAC, coincident with when the epidermal cells reach the anterior. The arcade cells regulate the patterning of neuroblasts, while the neuroblasts are required for epidermal cell migration and the timing of lumen formation, and the number of epidermal cells influences the position of the lumen. This is to our knowledge, the first in-depth description of anterior morphogenesis in *C. elegans* embryos.

2.3. Materials and Methods

2.3.1. Strains

Strains were maintained on nematode growth medium (NGM) agar plates with a lawn of *Escherichia coli* (OP50) according to standard procedures (Brenner, 1974). The list of *C. elegans* strains used in this study is presented in Table 1. All strains were maintained at 20°C unless indicated otherwise. Genetic crosses were performed using standard protocols (for review, see Fay, 2005).

Strain	Genotype
UM463	<i>cpIs42[mex-5p::mNeonGreen::PLCδ-PH::tbb-2 3'UTR, unc-119(+)] II; ItIs37[unc-119(+), Ppie-1::mCherry::HIS-58] IV</i>
SM481	<i>pxIs10 [pha-4::GFP::CAAX + (pRF4) rol-6(su1006)]</i>
UM456	<i>cpSi20[Pmex-5::TAGRFPT::PH::tbb-2 3'UTR; unc-119 (+)] I; unc-119(ed3) III</i>
SU159	<i>ajm-1(ok160) X; jcEx44 [ajm-1::GFP + rol-6(su1006)]</i>
SU265	<i>jcIs17 [hmp-1p::hmp-1::GFP + dlg-1p::dlg-1::DsRed + rol-6(su1006)]</i>
ML916	<i>mcls40 [lin-26p::ABDvab-10::mCherry+myo-2p::GFP]</i>
FT1197	<i>unc-119(ed3) III; xnIs449 [lin-26::LifeAct::GFP + unc-119(+)]</i>
LP216	<i>par-6(cp45[par-6::mNeonGreen::3xFlag + LoxP unc-119(+) LoxP]) I; unc-119(ed3) III</i>
LP162	<i>nmy-2(cp13[nmy-2::GFP + LoxP]) I</i>
MDX29	<i>ani-1(mon7[mNeonGreen[^]3xFlag::ani-1]) III</i>
AJP100	<i>mcls40 [lin-26p::ABDvab-10::mCherry+myo-2p::GFP]; par-6(cp45[par-6::mNeonGreen::3xFlag + LoxP unc-119(+) LoxP]) I; unc-119(ed3) III</i>
AJP101	<i>nmy-2(cp13[nmy-2::GFP + LoxP]) I; cpIs56 [mex-5p::TagRFPT::PLC(delta)-PH::tbb-2 3'UTR + unc-119 (+)] II</i>

AJP102	<i>cpIs56 [mex-5p::TagRFP-T::PLC(delta)-PH::tbb-2 3'UTR + unc-119 (+)] II; ani-1(mon7[mNeonGreen^3xFlag::ani-1]) III</i>
AJP103	<i>cpIs56 [mex-5p::TagRFP-T::PLC(delta)-PH::tbb-2 3'UTR + unc-119 (+)] II; par-6(cp45[par-6::mNeonGreen::3xFlag + LoxP unc-119(+) LoxP]) I; unc-119(ed3) III</i>
AJP104	<i>pxIs10 [pha-4::GFP::CAAX + (pRF4) rol-6(su1006)]; unc-119(ed3) III; xnIs449 [lin-26::LifeAct::GFP + unc-119(+)]; cpIs56 [mex-5p::TagRFP-T::PLC(delta)-PH::tbb-2 3'UTR + unc-119 (+)] II</i>
TU3335	<i>uls57[unc-119p::YFP + unc-119p::sid-1 + mec-6p::mec-6]</i>
LP244	<i>par-6(cp60[par-6::mKate2::3xMyc + LoxP unc-119(+) LoxP]) I; unc-119(ed3) III</i>
AJP105	<i>uls57[unc-119p::YFP + unc-119p::sid-1 + mec-6p::mec-6]; par-6(cp60[par-6::mKate2::3xMyc + LoxP unc-119(+) LoxP]) I; unc-119(ed3) III</i>
AJP106	<i>pxIs10 [pha-4::GFP::CAAX + (pRF4) rol-6(su1006)]; par-6(cp60[par-6::mKate2::3xMyc + LoxP unc-119(+) LoxP]) I; unc-119(ed3) III</i>
pGR71	<i>hsls391[Pmir-228::myristoylated-GFP; lin-15(+)]</i>
OH9729	<i>otls302[Ppsy-6::GFP; Pelt-2::RFP]</i>
	<i>lin-15(n744); nsEx4011[Phlh-16::GFP::myristoylated-GFP::UTR (pGR133); lin-15(+)]</i>
AJP107	<i>lin-15(n744); nsEx4011[Phlh-16::GFP::myristoylated-GFP::UTR (pGR133); lin-15(+)]; par-6(cp60[par-6::mKate2::3xMyc + LoxP unc-119(+) LoxP]) I; unc-119(ed3) III</i>
AJP108	<i>hsls391[Pmir-228::myristoylated-GFP; lin-15(+)]; par-6(cp60[par-6::mKate2::3xMyc + LoxP unc-119(+) LoxP]) I; unc-119(ed3) III</i>

2.3.2. RNAi

RNA-mediated interference (RNAi) by bacterial feeding was performed as described (Kamath et al., 2001; Timmons et al., 2001). Briefly, RNAi plates were made from NGM as above, with 50 mg/ml ampicillin and 1 mM IPTG. After growth to OD 0.6-1.0 (~6-12 hours), the cells were pelleted from their initial 5 mL volume and resuspended in varying amounts of LB to control the RNAi strength (e.g., in 100-400 μ L). Third and fourth larval stage (L3/L4) hermaphrodites

were transferred to plates with *E. coli* (HT115) transformed with dsRNA constructs; the animals were incubated for 24 hours, and then transferred to fresh RNAi plates, and progeny from these second plates were assessed for phenotype after 48 hours (Kamath et al., 2001). For the analysis of phenotypes after *pha-4* RNAi, worms were incubated for 24 hours, while they were only incubated for 3 hours for the analysis of phenotypes after *zen-4* RNAi. The Y49E10.19 (*ani-1* RNAi), W09C2.1 (*elt-1* RNAi), M03D4.1 (*zen-4* RNAi) and F38A6 (*pha-4* RNAi) clones used in this study were generously provided by J. C. Labbe, IRIC, Montreal and Michael Glotzer, University of Chicago).

2.3.3. Microscopy

Imaging was performed on embryos collected as described (Sulston et al., 1983; Wernike et al., 2016). Images were acquired using a Nikon Eclipse Ti inverted microscope with a NIDAQ/Piezo stage, a 100xPlanApo lens (NA, 1.4), sweptfield confocal illumination (livescan; Bruker), an Ixon3 EMCCD camera (Andor) and NIS-Elements acquisition software. Fluorophores were excited using 488 nm and 561 nm lasers and a dual bandpass emission filter (520/20 nm + 630/30 nm). Z-stacks were collected every 0.5 μm , and embryos were imaged every 2 minutes for up to 2 hours. To limit phototoxicity and photobleaching, exposure times were kept below 300 milliseconds. For RNAi-treated embryos, z-stacks were captured at 0.5 μm intervals every 4 minutes. For *en face* views, 0.2 μm z-stacks were collected and acquired at intervals of 2-4 minutes. To image embryos *en face*, they were manipulated to be positioned vertically (upright) in small holes made in the agarose pads.

Images were also acquired using a fiber-coupled diSPIM (parts list and construction detailed in Kumar et al., 2014) with MicroManager software (Open-Source, Vale Lab UCSF). C.

elegans embryos were mounted in an open-well chamber as described (Duncan et al., 2019). Image volumes were acquired in either single- or dual-view mode. Z-stacks were collected at 0.5 μm intervals with single-slice acquisition times of 12.75 milliseconds, leading to total volume acquisition times of 1.25 seconds for single-view volumes and 2.76 seconds for dual-view volumes. For single-view datasets, embryos were exposed simultaneously to 488 nm and 561 nm excitation with the emission optically split using a Hamamtsu W-View Gemini image splitter. Multi-point mode was used to capture multiple, spatially separated embryos per imaging session. For dual-view datasets, images were acquired sequentially, although within each path excitation at 488 nm and 561 nm was simultaneous and was again optically split with the Hamamtsu W-View Gemini image splitter. Dual-view data were also acquired using multi-point mode with multiple embryos captured per imaging run.

HILO, modified total internal reflection fluorescence (TIRF) imaging, was performed using an inverted Nikon Ti-E microscope outfitted with a NI-DAQ piezo Z stage (National Instruments), an Evolve (EMCCD) camera, with Elements 4.0 acquisition software (Nikon), filters for 488 and 561 laser diodes, and a 100x CFI Apo TIRF objective. Images were exported as TIFFs and opened in Image J (NIH Image) to create Z-stack projections, perform image rotation and to crop desired regions.

2.3.4. Image analysis

Data files obtained by sweptfield confocal imaging were deconvolved using AutoQuant X3 (MediaCybernetics) with adaptive point-spread function (PSF) and blind deconvolution. The total number of iterations was set to 10 and the noise level was set to medium. All measurements were performed in FIJI (Fiji Is Just ImageJ; NIH) using the deconvolved images. The datasets

were transferred to FIJI to generate hyperstacks and/or maximum-intensity projections and exported as TIFF files.

Single-view data obtained from diSPIM were exported as TIFF stacks through MicroManager software, and are shown in Figure 13C. Dual-view data were deconvolved after export from MicroManager using custom fusion and deconvolution software (Guo et al., 2019). All datasets were then screened and subsequently analyzed.

The circumference of the arcade-cell rosette and cell length measurements were performed on Z-stack projections from 1.5-fold embryos expressing *pha-4p::GFP::CAAX* using FIJI as shown in Figure 14D. To measure the rosette diameter, *en-face* images were used, and three lines drawn across the diameter were measured for each embryo and averaged together. To measure cell length, lateral-view images were used, and the length of the most in-focus cell was measured from top to bottom. All measurements were converted from pixels to micrometers.

To determine the effects of *ani-1* RNAi on epidermal cell migration, we used NIS-Elements Viewer (Nikon) to measure the time needed for the amphid dendrites to reach their anterior location as a read-out for epidermal cell migration. The ‘start’ of anterior morphogenesis ($t = 0$ minutes) was when the leading pair of ventral epidermal cells met at the ventral midline (Figure 13A). Control and *ani-1* RNAi embryos were analyzed, and the phenotypes were categorized based on the time required for the amphid dendrites to reach an anterior position (Figure 18). A chi-square test was used to determine statistical significance ($p < 0.001$) between control and *ani-1* RNAi phenotypes, as well as the proportion of phenotypes in each category with pharyngeal epithelialization ($p < 0.01$). Epithelialization was determined based on the accumulation of PAR-6 in the pharyngeal cells.

We quantified the number of actin-rich projections using FIJI (NIH). The image files were opened and staged to be 10 minutes after the start of anterior morphogenesis ($t = 0$). Then the number of projections were counted at this time point, and subsequently at 2-minute intervals for 6 minutes. The average number of projections were measured for each time point and averaged together. Then the control and *ani-1* RNAi conditions were compared using a two-tailed t test for significance, which we found was $p < 0.0005$ for each time point.

We determined the effects of *elt-1* RNAi on lumen position using deconvolved movie files that were analyzed with FIJI. Embryos were measured at $t = 20$ minutes after the leading pair of ventral epidermal cells met at the midline. The ratio of the distance between the Z2/Z3 cells (germline precursor cells) and the bright focal point (subset of PAR-6 positive cells) and the total length of the embryo was determined for each embryo. Although there was no difference in the average ratio per se, an F-test revealed that the variability was significantly higher in the *elt-1* RNAi embryos ($p < 0.01$).

All figures were generated using Adobe Photoshop and Illustrator, after generating 8-bit format images using FIJI. In figures where Fire LUTs were used, which is a pseudocolor that converts the signal into different colors based on intensity levels, where white or red is high, and blue or violet is low.

2.4. Results

2.4.1. Dynamic cell movements and patterning occur during anterior morphogenesis

We set out to characterize the cell movements and patterns that occur during anterior morphogenesis of *C. elegans* embryos. Anterior morphogenesis initiates during ventral enclosure when the leading pair of ventral epidermal cells meet at the ventral midline (Figure 13A) and continues until the 1.7-fold stage of embryogenesis when the muscles start twitching (Chisholm and Hardin, 2005). Initially the anterior-most part of the embryo is composed primarily of neuroblasts, and the epidermal cells migrate anteriorly to cover the head in epidermal tissue (Chisholm and Hardin, 2005). To visualize the cell patterns and movements during anterior morphogenesis, we imaged embryos co-expressing mNeonGreen-tagged pleckstrin homology (PH) domain, which localizes to membranes and mCherry-tagged histone H2B to visualize nuclei (Figure 13B-D). We used two types of imaging methods—sweptfield confocal microscopy ($n = 37$; Figure 13B) and diSPIM (Figure 13C; $n = 8$; Movie S1) to visualize changes in cell movements and patterns at different resolutions. diSPIM captures two orthogonal image volumes for two different views of the sample at each time point, allowing computational processing to create a single isotropic volume with better resolution than traditional imaging systems. Single-view images are shown here (Figure 13C). At 10-15 minutes after the start of anterior morphogenesis, rings of neuroblasts formed around the site of the future lumen (Figure 13B, C; Figure S1). As the epidermal cells migrated toward the anterior, a subset of these neuroblasts underwent ingression (Figure 13B, C). To better visualize the cell movements occurring during anterior morphogenesis, we imaged embryos *en face* (Figure 13B; see Methods). Using this approach, we were able to more clearly observe the ring-like patterns formed by the neuroblasts during anterior morphogenesis. The forces generated by cell movements and resistance of the rigid eggshell could facilitate the

ingression and/or inward direction of neuroblasts prior to elongation (Figure 13D). Since a large proportion of the neuroblasts will differentiate into neurons that form the nerve ring, which encircles the pharynx, this inward movement likely helps position these neuronal precursors appropriately (Hobert, 2010). When the epidermal cells reached the anterior region, the membrane marker revealed a star-like pattern. Since this marker contains a domain that binds to phospholipids, this pattern likely corresponds to the growing axons, with the central point corresponding to the site of the future lumen (Figure 13B, C). Thus, several distinct cell movements occurred during anterior morphogenesis that require further characterization.

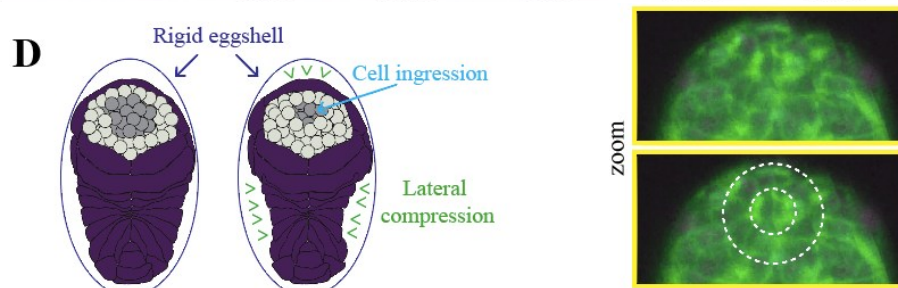
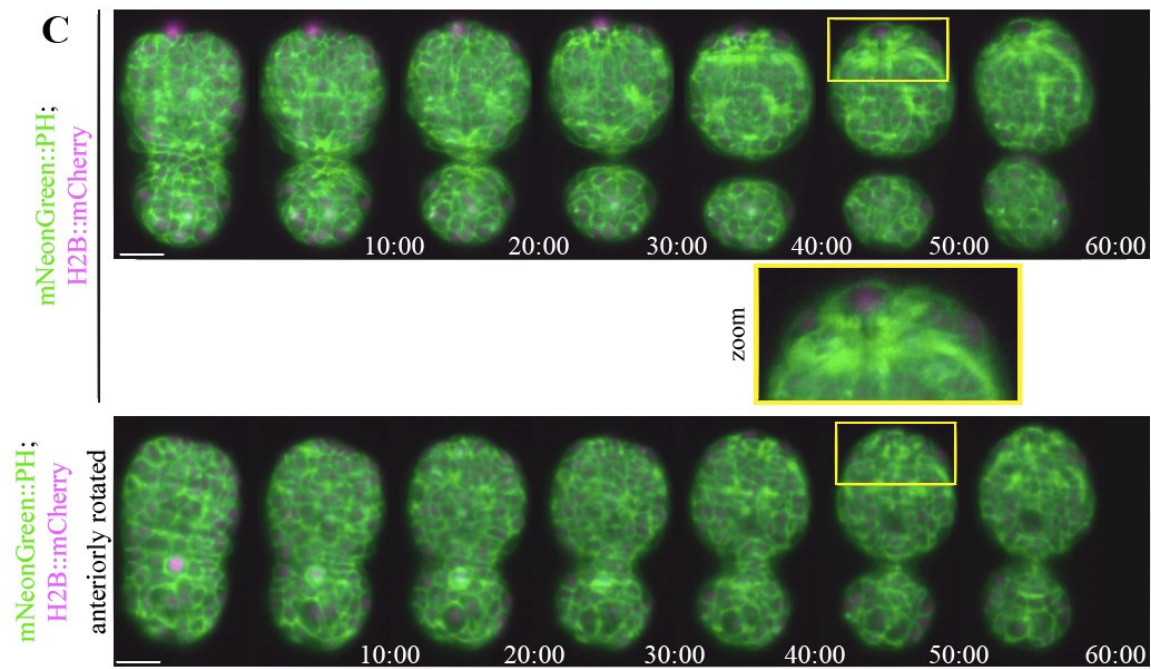
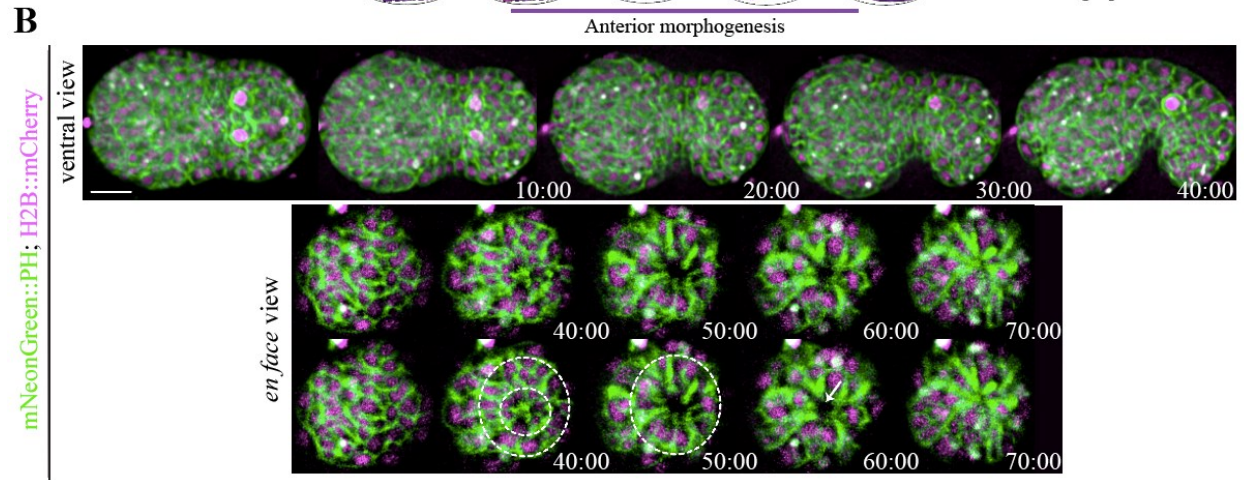
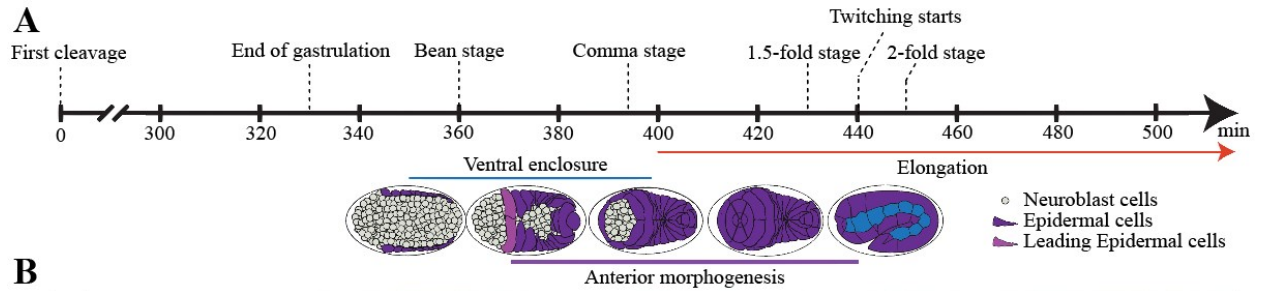


Figure 13. Cells ingress during anterior morphogenesis. **A)** The timeline (in minutes) shows the key morphogenetic events that occur during *C. elegans* embryogenesis. Anterior morphogenesis begins when the leading pair of migrating epidermal cells meet at the ventral midline ($t = \sim 380$) and continues throughout ventral enclosure and part of elongation (~ 440 minutes/twitching stage). **B)** Time-lapse images obtained by sweptfield microscopy (ventral view; anterior to the left) show an embryo co-expressing mNeonGreen::PH to visualize membranes (green) and H2B::mCherry to visualize nuclei (magenta) through anterior morphogenesis (time in minutes). The *en face* view shows cell organization at the anterior of the embryo, which results in the formation of a ‘ring in a ring’ (white dashed circles). The star-like pattern in the center marks the site of the future lumen, which forms after cells ingress into the embryo. Times are shown in minutes, and the scale bar is 10 μm . **C)** Raw time-lapse single-view images (ventral view; anterior pointing up) acquired using diSPIM show embryos as in B during anterior morphogenesis. The top panels show cell ingression at the anterior, whereas the bottom panels are tilted (anterior towards the reader) to show cell patterns (zoom, white dashed circles). Times are shown in minutes, and the scale bar is 10 μm . Zoom images have been magnified by 200%. **D)** Cartoon schematics show the embryo inside the eggshell. The epidermal cells are shown in purple, the ingressing cells are shown in grey, and arrowheads (green) point to the forces generated laterally to cause ingression anteriorly.

2.4.2. The arcade cells of the pharynx form a stable rosette

While we were imaging embryos using the membrane marker, we observed a rosette that formed at a depth of $\sim 4\text{-}5\ \mu\text{m}$ and aligned with the site of the future lumen (Figure 14A-C). This rosette formed anteriorly to the larger, previously described cyst formed by pharyngeal cells (Figure 14B; Rasmussen et al. 2012). This rosette contained six cells and persisted for an extended period of time, which is characteristic of apical polarity-derived rosettes known to give rise to lumens (Figure 14C; Sawyer et al., 2010; Harding et al., 2014; Martin and Goldstein, 2014). To determine if these cells are pharyngeal and to follow their patterning more specifically, we imaged embryos co-expressing *pha-4p::GFP::CAAX* ($n = 18$). This probe localizes to the membranes of pharyngeal cells, as *pha-4* encodes a forkhead box A (FOXA) transcription factor required for pharyngeal cell fate, and CAAX is post-translationally farnesylated (farnesyl is a lipid moiety; Horner et al., 1998; Kalb et al., 1998; Gaudet & Mango 2002; Roberts et al., 2008; Manolaridis et al., 2013). At the start of anterior morphogenesis, the most anterior *pha-4* positive cells moved toward the anterior of the embryo, but subsequently moved posteriorly within the embryo while retaining a narrow region of signal that aligned with the center of the rosette (Figure 14A). Approximately 40-50 minutes after the start of anterior morphogenesis, these cells adopted a teardrop shape (Figure 14A, C). Imaging *pha-4p::GFP::CAAX* and TagRFP::PH 1.5-fold embryos *en face* revealed the rosette more clearly. Consistent with what we had observed earlier, the rosette was positioned at a depth of $5 \pm 0.40\ \mu\text{m}$ from the anterior tip of the embryo (Figure 14B, middle panel), whereas the previously characterized, larger pharyngeal rosette was at $11 \pm 0.40\ \mu\text{m}$ ($n = 13$ embryos; Portereiko & Mango, 2001; Figure 2B, bottom panel). To better characterize the small *pha-4* positive rosette, we measured its diameter along three axes per rosette, as well as the length

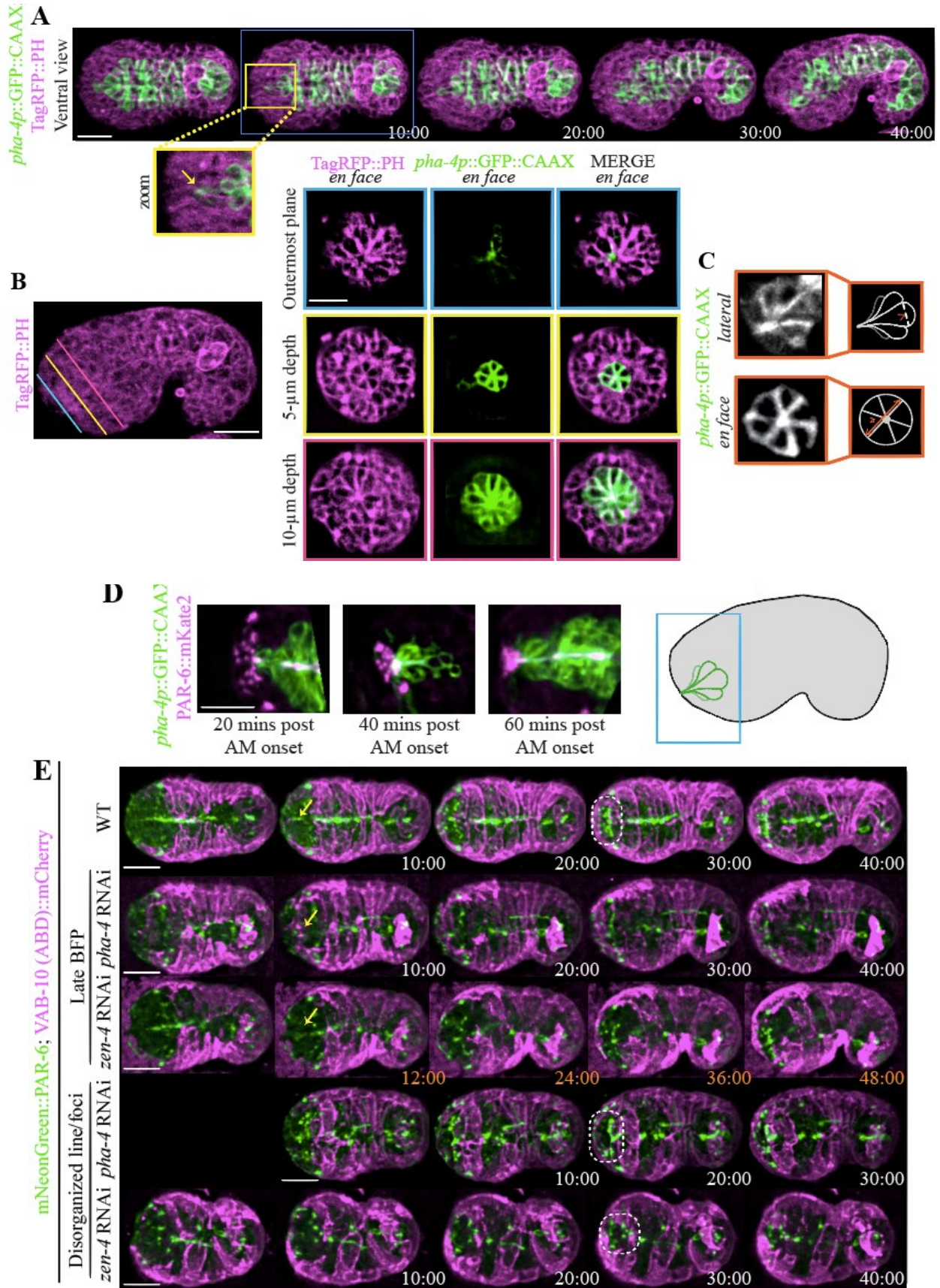


Figure 14. The pharyngeal arcade cells form a rosette. **A)** Time-lapse images acquired using sweptfield microscopy show an embryo co-expressing *pha-4p::GFP::CAAX* to visualize the pharyngeal cells in green and Tag-RFP::PH to visualize membranes in magenta during anterior morphogenesis. The anterior-most pharyngeal cells (arcade cells) form apical constrictions (yellow box) which coalesce (zoom; yellow arrow). Times are shown in minutes. **B)** The image shows a comma-staged embryo expressing Tag-RFP::PH to visualize membranes (magenta). The colored lines indicate the three depths in the embryo corresponding to the images to the right. Images show separate and merged channels from an embryo co-expressing Tag-RFP::PH (magenta) and *pha-4p::GFP::CAAX* to visualize pharyngeal cells (green) at ~40 min. Three *en face* views are shown, which correspond to the depths (colored lines). The outermost plane (blue) shows the coalescence of the arcade-cell projections at the anterior of the embryo. At a 5 μm depth into the embryo (yellow) a small multicellular pharyngeal rosette is visible. The larger, previously characterized pharyngeal rosette is visible at a depth of 10 μm (pink). **C)** Images show *en face* or lateral views of *pha-4p::GFP::CAAX* outlining the anterior rosette. The cartoon schematics to the right show the regions used to determine the diameter and length of individual cells. **D)** Shown are images from excerpts of different time-lapse movies from embryos co-expressing PAR-6::mKate2 (magenta) and *pha-4p::GFP::CAAX* (green) acquired using sweptfield microscopy during anterior morphogenesis. The embryo in the panel on the left is ~20 minutes after the onset of anterior morphogenesis (when the leading epidermal cells meet at the ventral midline), while the middle is at ~30 minutes, and the right is at ~40 minutes. A cartoon on the right shows the relative position of the images in the embryo. **E)** Time-lapse images acquired using sweptfield microscopy show control (top panels), *pha-4* or *zen-4* RNAi embryos expressing mNeonGreen::PAR-6 (green) and *lin-26p::VAB-10 (ABD)::mCherry* (magenta) during anterior morphogenesis. Yellow arrows point to the position of the bright focal point (BFP), which demarcates the site of the future lumen, while the dotted circles highlight the location of the pentagon and semi-circle of foci. Times are indicated in minutes. For all images, the scale bar is 10 μm .

of individual cells in the rosette (Figure 14C). We found that the average diameter was 6.9 ± 0.13 μm ($n = 13$ embryos), whereas the average cell length was 4.9 ± 0.04 μm ($n = 16$ cells), consistent with what we had observed for depth. Given the location and number of these cells, the anterior rosette is likely composed of a subset of arcade cells. The arcade cells formed projections that extended anteriorly and remained in place as the arcade cells moved back inside the embryo.

As the arcade cell projections were aligned with the center of the rosette, this polarized structure could be one of the first anterior-positioned markers that defines the site of the future lumen. To determine if a marker of apical polarity is enriched at this location, we co-imaged embryos expressing PAR-6::mKate2 and *pha-4p*::GFP::CAAX during anterior morphogenesis. After ~10 minutes, we observed the appearance of a bright focal point (BFP) that corresponded to the tip of the arcade cell projections as they grew toward the anterior ($n = 18$; Figure 14D; Movie S2). We also observed the emergence of other distinct PAR-6 foci, which likely correspond to other cell types.

2.4.3. Distinct patterns of PAR-6 foci form in the anterior region of the embryo

Next, we characterized the patterns of PAR-6 foci during anterior morphogenesis. We speculated that these correspond to subsets of neuroblasts and/or epidermal cells. We imaged embryos co-expressing mNeonGreen::PAR-6 and mCherry-tagged actin-binding domain (ABD) from VAB-10 driven by the epidermal region of the *lin-26* promoter (Landmann et al., 2004; Gally et al., 2009; Zilberman et al., 2017) to visualize epidermal F-actin ($n = 15$). As reported recently by the Bao lab, we observed that PAR-6 was enriched at the vertex of the amphid dendrite tips (Figure 15A; Fan et al., 2019). As embryos progressed through morphogenesis, we saw PAR-6 localize to foci that formed two pentagons on either side of the BFP, and to a semi-circle of foci

that moved toward the BFP (Figure 15A, S2A; Movie S3). The BFP first appeared on the ventral side of the embryo ~10 minutes after the start of anterior morphogenesis. At ~20 minutes, we observed a semi-circle of foci that aligned with the leading edge of the migrating epidermal cells (Figure 15A, zoom; S2A; Movie S3). The two pentagon patterns initiated at a more dorsal position and then moved more ventrally to meet with the semi-circle (Figures 15A; S2A; Movie S3). The most dorsal foci of the pentagons aligned with the leading edge of epidermal cells migrating from more dorsal positions (Figures 15A; S2B). By 40 minutes, the foci formed a rectangular pattern with the semi-circle and the three ventral foci from each pentagon marking one side and the two dorsal foci marking the other, which subsequently resolved into a circular pattern around the lumen (Figure 15A, zoom; S2A; Movie S3).

To determine if the pentagons or semi-circle of foci correspond to neuroblasts, we imaged embryos expressing mNeonGreen::ANI-1 (anillin) during anterior morphogenesis. We previously found that ANI-1 is specifically enriched in subsets of neuroblasts (Wernike et al., 2016), and is an indicator of polarity during cell division as it binds to actomyosin. ANI-1 localized to the pentagon foci, but not to the BFP as expected, or the (majority of) foci that form the semi-circle ($n = 29$; Figure 15B). This suggests that the pentagon foci originate in the neuroblasts (Figure 15B). To further show this, we imaged embryos co-expressing a pan-neuronal marker, UNC-119::YFP, and PAR-6::mKate2. As embryos progressed through anterior morphogenesis, we observed neuroblast projections aligned with the PAR-6 foci in the pentagons, and to the outermost foci of the semi-circle ($n = 35$; Figure 15C zoom; Movie S4). Since this expression could reflect neuronal precursors or their support cells, we imaged markers that are known to be expressed in these tissues during embryogenesis (Rapti et al., 2017). Myristoylated (post-translational modification that targets proteins to the membrane) MIR-228::GFP, which is a pan-glial cell

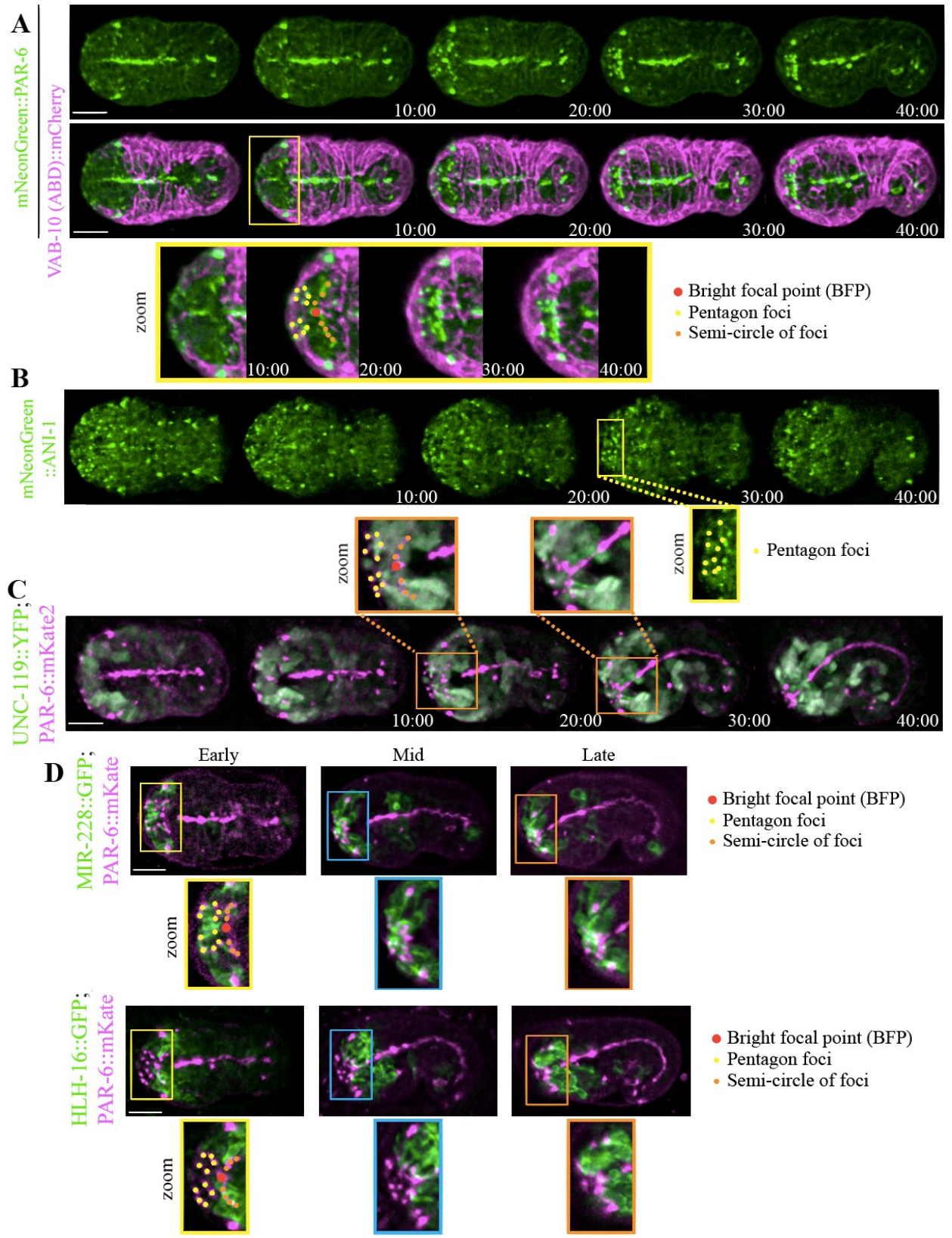


Figure 15. Distinct patterns formed by PAR-6 foci correlate with the migrating anterior epidermal cells. **A)** Time-lapse images acquired using sweptfield microscopy show ventral views (anterior to the left) of an embryo expressing mNeonGreen::PAR-6 (green; top panel) and epidermal VAB-10 (ABD)::mCherry (magenta; middle panel) during anterior morphogenesis. Times are indicated in minutes. Zoomed-in regions (bottom panel; 200%) show the patterns formed by PAR-6 more clearly (yellow box). PAR-6 localizes to the BFP (red), the pentagon foci (yellow), and the semi-circle of foci (orange) that corresponds to the anterior-most boundary of ventral epidermal cells. **B)** Time-lapse images acquired using sweptfield microscopy show ventral views of embryos expressing mNeonGreen::ANI-1 (green). Times are indicated in minutes. A zoomed-in region (yellow box; 150%) shows the pentagon foci highlighted by yellow dots. **C)** Time-lapse images acquired using sweptfield microscopy show embryos expressing UNC-119::YFP (green) and PAR-6::mKate2 (magenta). Times are indicated in minutes. Zoomed-in regions (orange boxes; 150%) show the neuronal projections in the anterior region with the pentagons, BFP and semi-circle of foci marked in yellow, red and orange, respectively. **D)** Images show embryos expressing MIR-228::GFP (green) and PAR-6::mKate2 (magenta), or HLH-16::GFP (green) with PAR-6::mKate2 (magenta). Zoomed-in regions (150%) are indicated by yellow, blue or orange boxes and reflect early (10-20 minutes), mid (30-35 minutes) and later (>40 minutes) stages of anterior morphogenesis. As above, the pentagons, BFP and semi-circle of foci are indicated in yellow, red and orange, respectively. For all images, the scale bar is 10 μm .

Marker (CEPsh, labial sh and amphid sh), localized to projections that aligned with the PAR-6 pentagon foci (early; $n = 6$ MIR-228::GFP; PAR-6::mKate2; Figure 15D; Movie S5; $n = 6$ MIR-228::GFP; Figure S2C; Movie S6; Rapti et al., 2017).

Myristoylated HLH-16::GFP, which is expressed in the SMDD/AIY and SIAD/SIBV lineages, localized to some of the semi-circle of foci early, and to most foci by mid stages of anterior morphogenesis ($n = 20$ HLH-16::GFP; PAR-6::mKate; Figure 15D; Movie S7; $n = 9$ HLH-16::GFP; Figure S2C; Movie S8; Bertrand et al., 2011; Rapti et al., 2017). We also imaged embryos expressing LSY-6::GFP, which is expressed in a small subset of neurons including the ASEL neuron, but these projections did not reach the anterior ($n = 7$; Figure S2C; Rapti et al., 2017). Therefore, this data demonstrates that subsets of glial and neuronal precursor cells form polarized projections with distinct patterns during anterior morphogenesis. The proximity of a subset of these foci with the leading edge of the epidermal cells suggests that these cells are in close association during epidermal migration.

2.4.4. Junction proteins are enriched in foci at the anterior of the embryo

To characterize foci in the epidermal cells, we imaged embryos expressing different adhesion components in the DAC (DLG-1 and AJM-1 complex) and CCC (cadherin/HMR-1 and α -catenin/HMP-1 complex; Costa et al., 1998; McMahon et al., 2001; Chisholm and Hardin, 2004; McMahon et al., 2001). AJM-1::GFP is enriched in epidermal cells, and we used Fire LUTs to better visualize changes in AJM-1 intensity to reveal more detailed localization patterns during anterior morphogenesis (Figure 16A). As anterior morphogenesis progressed, AJM-1 foci appeared at the leading edge of the anterior ventral epidermal cells ($n = 15$; Figure 16A). While AJM-1 was not apparent in the BFP and only weakly visible in anterior foci initially

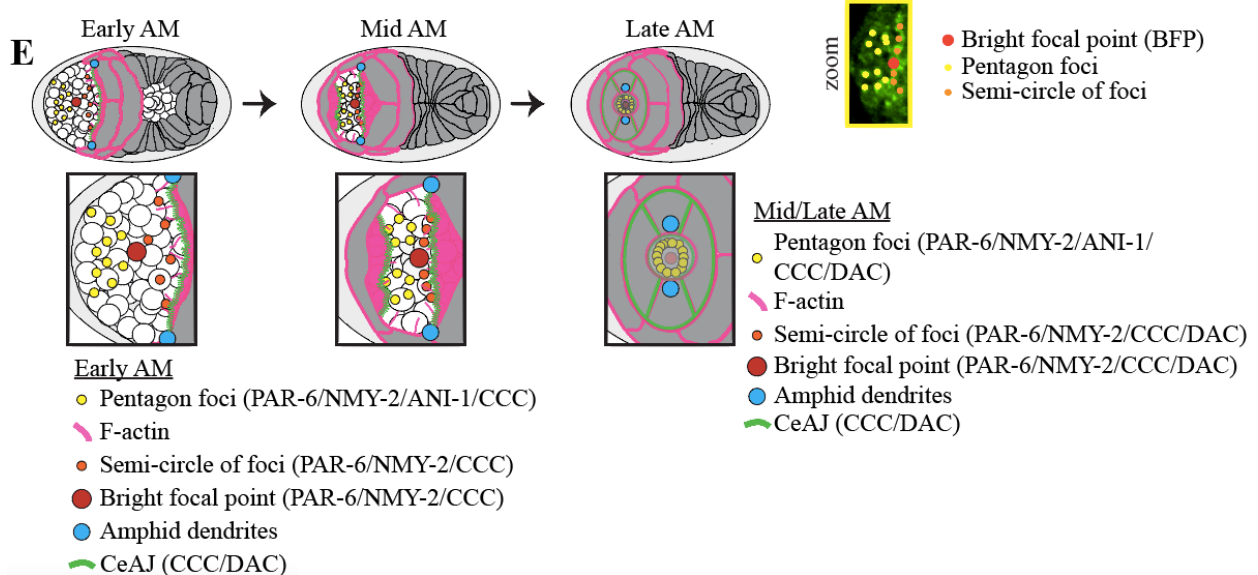
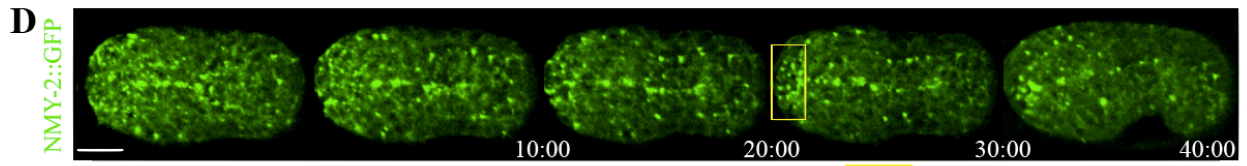
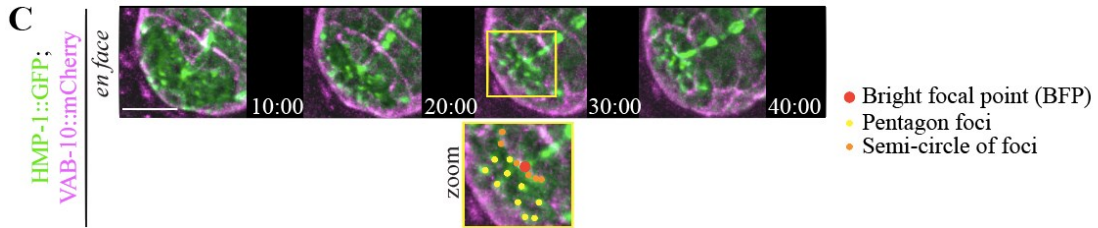
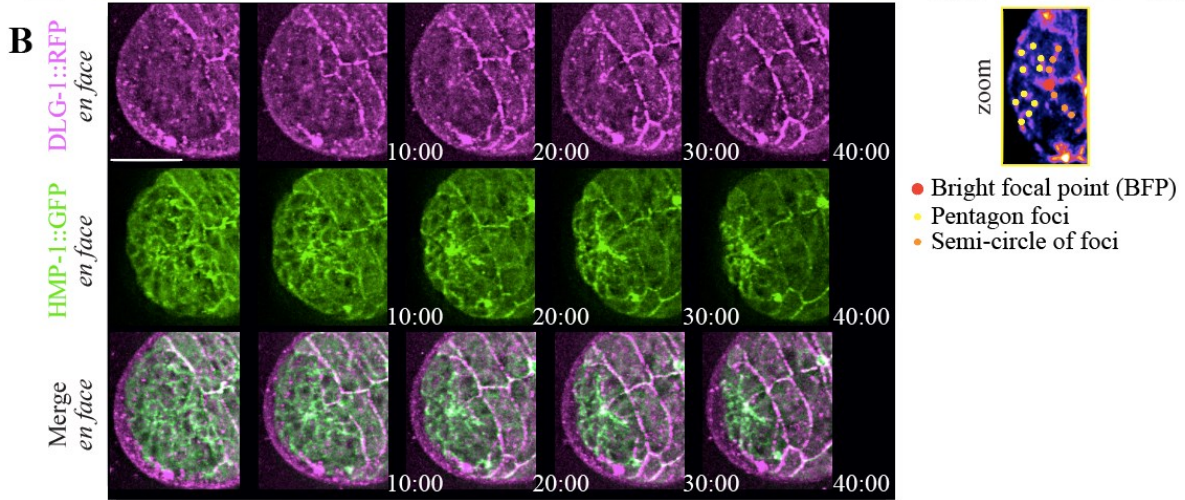
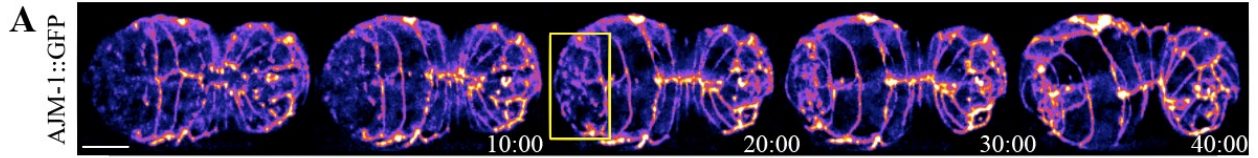


Figure 16. Adhesion junctions are enriched in subsets of cells during anterior morphogenesis.

A) Time-lapse images acquired using sweptfield microscopy show ventral views (anterior to the left) of an embryo expressing AJM-1::GFP (Fire LUTs). A zoomed-in region (150%) is shown underneath (yellow box; bottom right) with the pentagon foci, BFP and semi-circle of foci labeled in yellow, red and orange as indicated. Times are shown in minutes and the scale bar is 10 μ m. **B)** Time-lapse images show ventral, *en face* views of an embryo expressing HMP-1::GFP (green) and DLG-1::RFP (magenta) during anterior morphogenesis. Times are shown in minutes, and the scale bar is 10 μ m. **C)** Time-lapse images show ventral, *en face* views of an embryo expressing HMP-1::GFP (green) and *lin-26p*::VAB-10(ABD)::mCherry (magenta) during anterior morphogenesis. One of the images is duplicated below and labeled as in A). Times are shown in minutes, and the scale bar is 10 μ m. **D)** Time-lapse images show ventral views of embryos expressing NMY-2::GFP (green). Zoomed-in regions (yellow box; 150%) show the anterior foci as labeled in A). Times are shown in minutes, and the scale bar is 10 μ m. **E)** Cartoon schematics show the patterns of foci and associated proteins during anterior morphogenesis. The pentagon foci are in yellow, the BFP is in red, and the semi-circle of foci are in orange. Also shown are adhesion junctions (green) formed by the DAC and CCC, F-actin projections (pink) and amphid foci (blue). At early stages of anterior morphogenesis, the pentagon foci contain PAR-6, ANI-1, HMP-1 (CCC) and NMY-2, while the BFP contains PAR-6, HMP-1 (CCC) and NMY-2, and the semi-circle of foci contains PAR-6, HMP-1 (CCC), DAC and NMY-2. During mid and late stages of anterior morphogenesis, the pentagon foci and BFP also contain the DAC.

(e.g. at 10 minutes), it increased in intensity in these locations as anterior morphogenesis progressed (Figure 16A). This likely reflects the maturation of adhesion junctions as the epidermal cells contact neighboring cells at the anterior. Ultimately, the epidermal cells arranged themselves to form two bilateral rings, which fused and joined the pharynx, with another ring forming around it (Figure S3A). Imaging embryos co-expressing DLG-1::RFP and HMP-1::GFP revealed that DLG-1 had a similar pattern of localization to AJM-1, albeit weaker ($n = 8$; Figures 16B; S3B). We previously showed that the CCC, but not the DAC, is enriched in the mid-posterior neuroblasts that forms transient rosettes for tissue re-organization during ventral enclosure (Wernike et al., 2016). The CCC component HMP-1 localized to the BFP by 10 minutes, and was enriched in the pentagons and semi-circle of foci ($n = 8$; Figure 16A). Imaging embryos co-expressing HMP-1::GFP and *lin-26p*::VAB-10(ABD)::mCherry revealed that the anterior-most epidermal cells were in close contact with the HMP-1-rich semi-circle of foci ($n = 8$; Figure 16C). As actomyosin is typically enriched at junctions, we also imaged embryos expressing GFP::NMY-2 (non-muscle myosin) and observed patterns similar to PAR-6 and HMP-1 ($n = 23$; Figure 16D). Therefore, the enrichment of PAR-6, HMP-1 and NMY-2 within subsets of cells reflects their polarity and adhesion with neighboring cells.

2.4.5. Ventral and dorsal epidermal cells migrate to an anterior-ventral position

Next, we characterized anterior epidermal cell migration. To do this, we monitored the localization of F-actin expressed in epidermal cells during anterior morphogenesis in embryos expressing either *lin-26p*::VAB-10(ABD)::mCherry ($n = 32$) or *lin-26p*::GFP-tagged LifeAct ($n = 12$; Figure 17A). As the anterior ventral epidermal cells migrated anteriorly, we observed the formation of actin-rich projections (Figure 17A, zoom). The dorsal epidermal cells also migrated

anteriorly during this time, which need to move a greater distance to reach the site where the ventrally positioned lumen will form (Figure 17A, zoom).

To follow epidermal cell migration with a higher temporal resolution, we imaged F-actin in embryos using HILO (highly inclined and laminated optical sheet) microscopy (Wernike et al., 2016). With this method, TIRF (total internal reflection fluorescence) objectives are used and the illumination beam is angled to obtain a thicker z plane (*e.g.*, in this case to a depth of $\sim 1 \mu\text{m}$) emerging obliquely from the sample. In Figure 5B, the top panel shows images of LifeAct taken every 30 seconds (anterior is pointing down; $n = 8$; Movie S9). Projections from the anterior ventral epidermal cells were dynamic, extending anteriorly for several microns. However, they did not extend far past the leading edge of the cell, and aligned with mNeonGreen::PAR-6 foci (Figure 17C).

The bottom panel of Figure 17B shows the migrating epidermal cells positioned more dorsally in an embryo expressing VAB-10(ABD)::mCherry (see arrow; anterior pointing down; $n = 9$; Movie S10). The extensions at the leading edge were more uniform and smaller in length compared to the ventral epidermal cells (Figure 17B). It is striking how epidermal cells positioned ventrally and dorsally coordinated their movements to reach the location of the future lumen at the same time, suggesting that their movements are controlled by cues associated with other cells in this location.

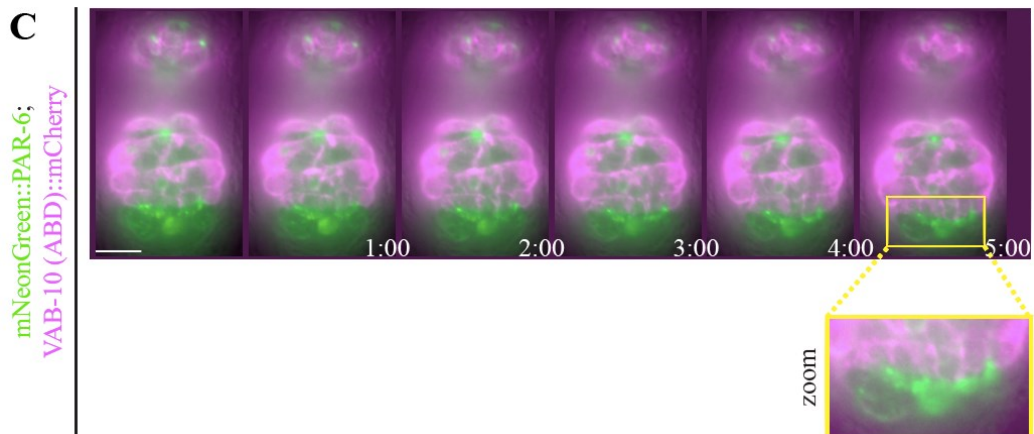
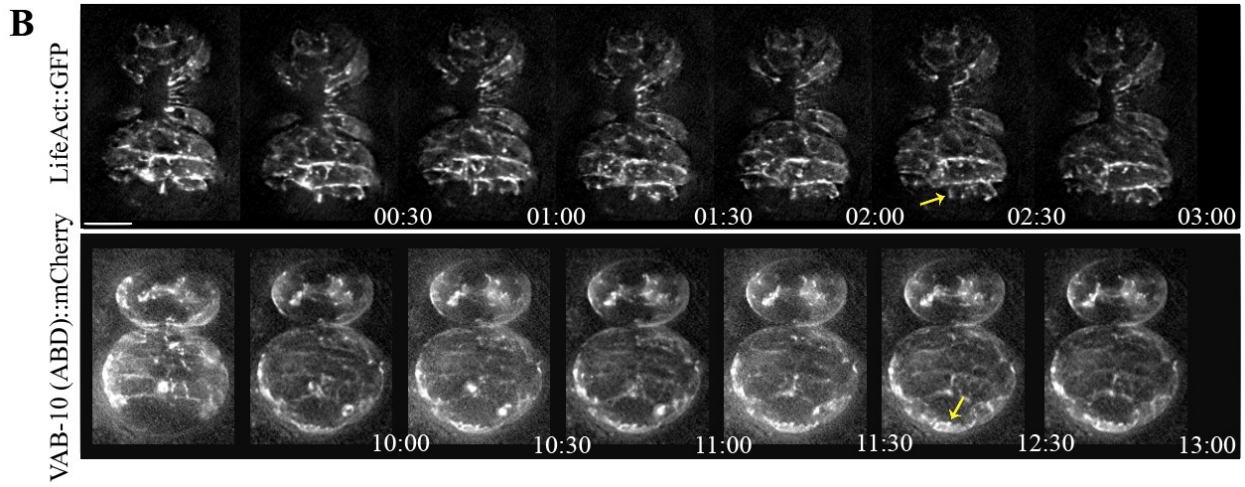
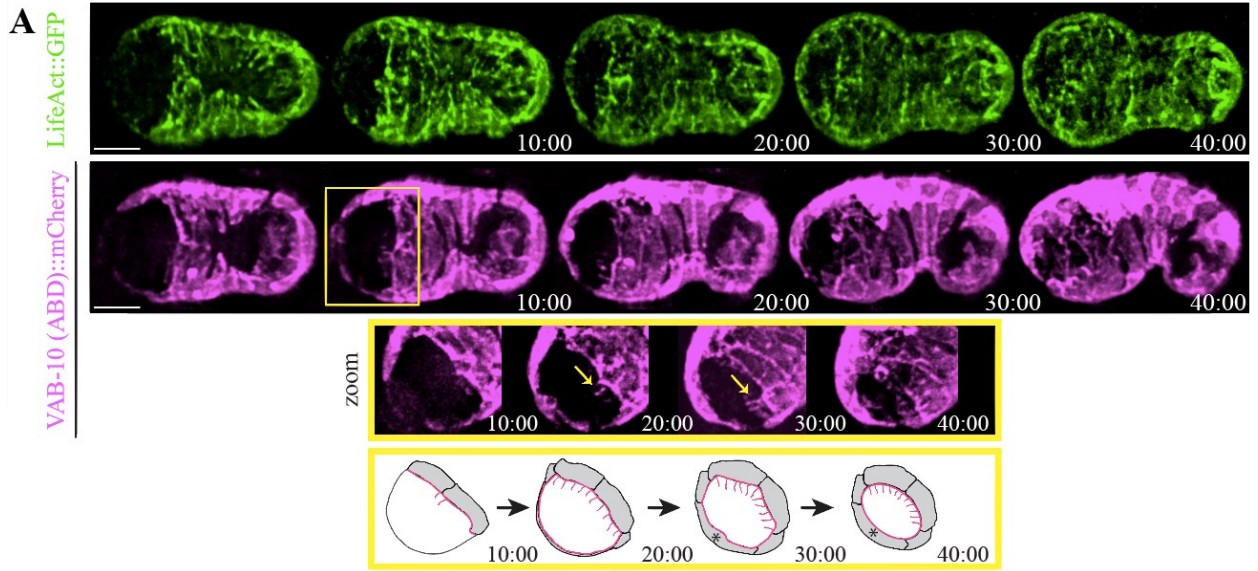


Figure 17. Projections form at the leading edge of the migrating anterior ventral epidermal cells. A) Time-lapse images acquired using sweptfield microscopy show ventral views (anterior to the left) of embryos expressing *lin-26p::LifeAct::GFP* (green) or *lin-26p::VAB-10(ABD)::mCherry* (magenta) during anterior morphogenesis. Times are shown in minutes, and the scale bar is 10 μm . At the onset of anterior morphogenesis, the anterior of the embryo is devoid of epidermal cells, which subsequently migrate into this space. The ventral cells migrate a shorter distance compared to the dorsal cells. The yellow box highlights a region that has been tilted to better visualize the F-actin projections (yellow arrows). The bottom row shows cartoon schematics that indicate the orientation of the projections in pink. **B)** Time-lapse images acquired by HILO microscopy show ventral views (anterior pointing down) of embryos expressing epidermal *lin-26p::LifeAct::GFP* (top panel) or *lin-26p::VAB-10(ABD)::mCherry* (bottom panel). Times are shown in minutes, and the scale bar is 10 μm . The projections are dynamic and longer at the leading edge of the ventral epidermal cells (top panel; yellow arrow), whereas the dorsal epidermal cells have smaller, more uniform projections (bottom panel; yellow arrow). **C)** Time-lapse images acquired by HILO microscopy show a ventral view of an embryo co-expressing mNeonGreen::PAR-6 (green) and *lin-26p::VAB-10(ABD)::mCherry* (magenta). Times are shown in minutes, and the scale bar is 10 μm . A zoomed in region (yellow box) shows the alignment of projections with the foci.

2.4.6. Anterior epidermal cell migration depends on the arcade cells and subsets of anterior neuroblasts

We propose that the patterns formed by the arcade cells and neuroblasts influence epidermal cell migration. Given the timing of the BFP appearance, the arcade cells may provide the first signal to coordinate the surrounding neuroblasts, which in turn provide a substrate and/or cues for the epidermal cells. First, we perturbed the arcade cells to determine the effect on anterior morphogenesis by depleting *pha-4*, which is required for pharyngeal cell fate (Kalb et al., 1998), or *zen-4*, which is required for their polarization (Portereiko et al., 2004). Since *zen-4* is also required for cytokinesis and ventral enclosure (Raich et al., 1998; Hardin et al., 2008), embryos were only treated with *zen-4* RNAi for a short period of time. In *pha-4* or *zen-4* RNAi embryos co-expressing mNeonGreen::PAR-6 and *lin-26p*::VAB-10(ABD)::mCherry, we observed that the BFP was delayed in its formation ($n = 7/9$ for *pha-4*, and $14/15$ for *zen-4*; Figure 14E), and the other foci were disorganized ($n = 6/14$ for *pha-4*, and $8/16$ for *zen-4*; Figure 14E). The majority of embryos from both treatments showed defects in anterior morphogenesis, ranging from mild to more severe ($n = 14/18$ for *pha-4*, and $21/21$ for *zen-4*). We also noticed that a BFP-like signal appeared later in development, although dimmer in appearance, and we speculate that this comes from neuronal or support cell projections (e.g. Figure 15C). This data suggests that the arcade cells provide early cues to organize the surrounding neuroblasts.

Next, we determined how perturbing the neuroblasts impacts epidermal cell migration. We previously showed that *ani-1* is required for neuroblast cell division (Fotopoulos et al., 2013; Wernike et al., 2016). Depleting *ani-1* in embryos co-expressing mNeonGreen::PAR-6 and *lin-26p*::VAB-10(ABD)::mCherry caused changes in PAR-6 localization and delayed anterior epidermal cell migration ($n = 34$; Figure S4). We observed a correlation in the severity of anterior

morphogenesis phenotypes with higher degrees of perturbed PAR-6 localization and delayed migration, including failed polarization of the anterior pharynx (Figure S4).

We quantified the different anterior morphogenesis phenotypes caused by *ani-1* RNAi in embryos co-expressing mNeonGreen-tagged PAR-6 and a Tag-RFP membrane marker ($n = 15$ control and $n = 28$ *ani-1* RNAi embryos; PH domain; Figure 18A). To measure the duration of anterior epidermal cell migration, we determined the time it took for the amphid dendrites to reach the anterior region. The Bao lab recently showed that the amphid dendrites extend with epidermal cells, and we used this as a marker for epidermal migration (Fan et al., 2019). We observed embryos with a range in delay phenotypes that we categorized as mild (50-69 minutes; 45%), moderate (70-89 minutes; 30%) and severe (≥ 90 minutes; 10%), based on the amphid dendrite extension time relative to that of control embryos (40-49 minutes; 15%; Figure 18B). We also observed that PAR-6 failed to localize within the anterior pharynx in a subset of the *ani-1* RNAi embryos. Of the embryos that displayed a mild delay phenotype, 33% failed to polarize, whereas 67% of embryos with moderate delays failed and 100% of the severely delayed embryos failed (Figure 18B). We correlated the changes in neuroblast/foci patterns with the observed phenotypes and found that more of the foci that form the semi-circle or pentagons were lost or severely disorganized as the delay worsened from mild to severe (Figure 18C).

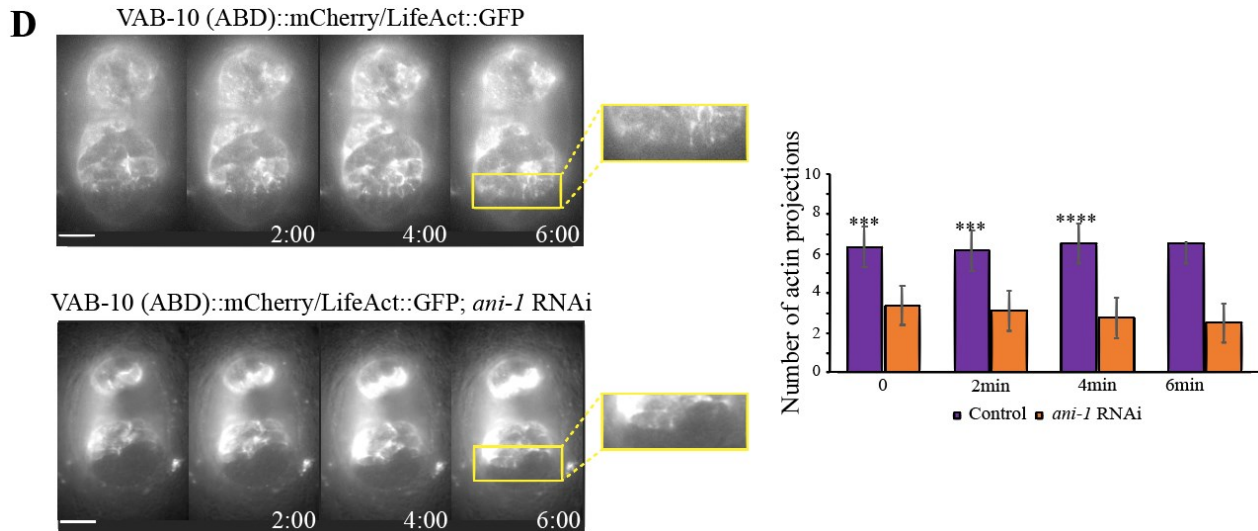
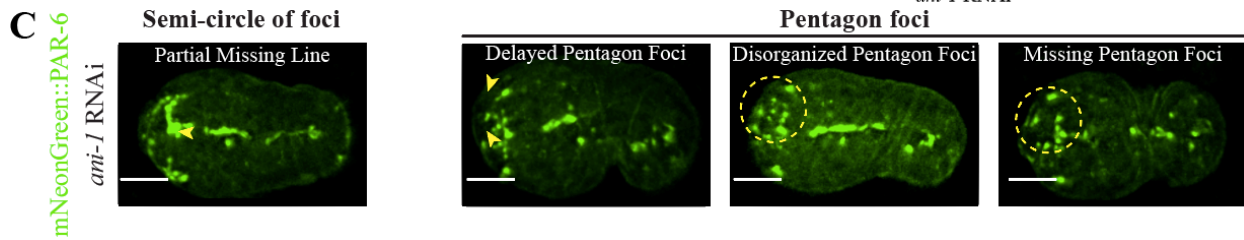
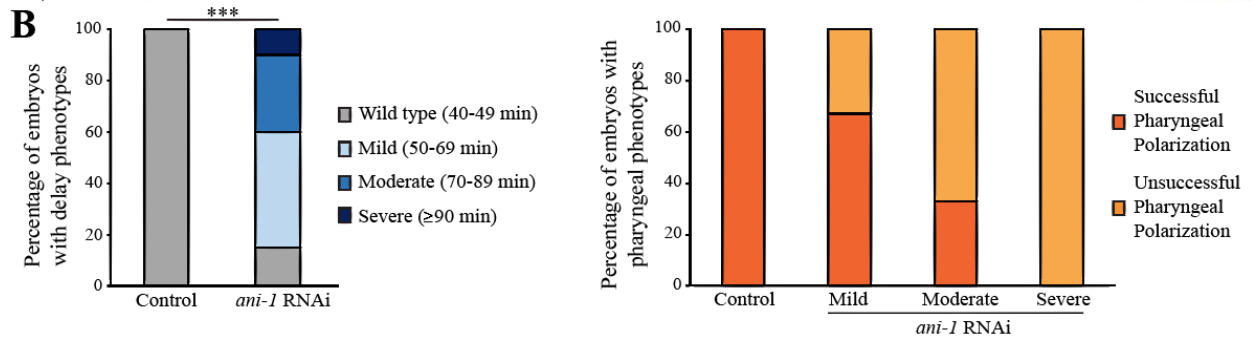
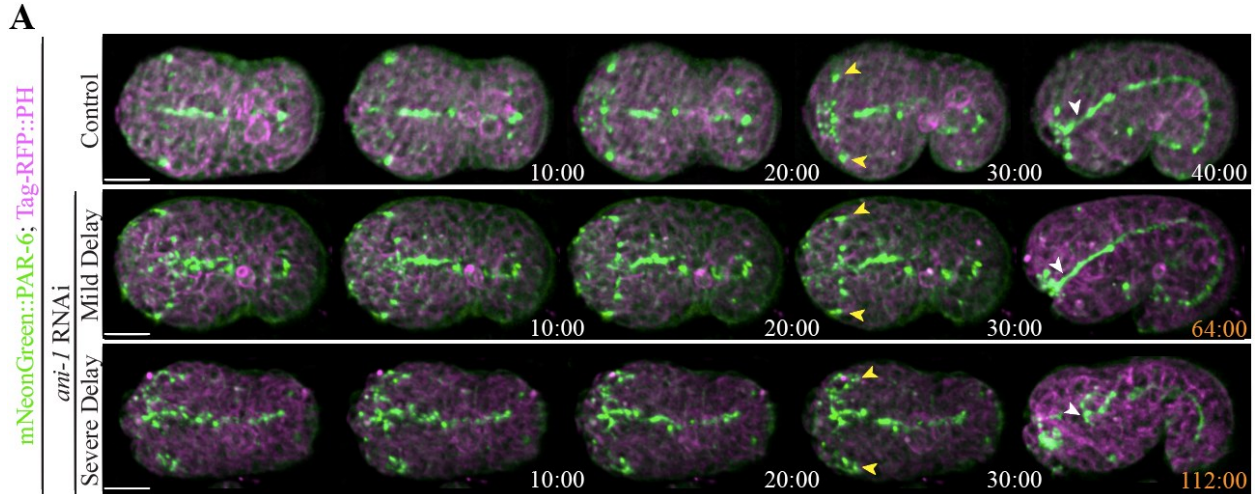


Figure 18. Disrupting neuroblast division causes delays in anterior epidermal cell migration.

A) Time-lapse images acquired using sweptfield microscopy show ventral views of embryos (anterior to the left) expressing mNeonGreen::PAR-6 (green); Tag-RFP::PH (magenta) in control (top panel) and after *ani-1* RNAi to disrupt neuroblast cell division (middle and bottom panels). Delays in epidermal cell migration, marked by the amphid dendrites (yellow arrowheads), correlated with changes in the number or position of PAR-6 foci and/or failure of the anterior pharynx to polarize (white arrowheads) in *ani-1*-depleted embryos compared to control embryos. Times are shown in minutes and the scale bars are 10 μ m. **B)** Epidermal cell migration was monitored by measuring the time it took for the amphid dendrites to reach the anterior region. The bar graph on the left shows the proportion of embryos with different delays in epidermal cell migration after *ani-1* RNAi when compared with control embryos. The bar graph on the right shows the proportion of control and *ani-1* RNAi embryos with delay phenotypes in which the anterior pharynx failed to polarize. **C)** Images show changes in the patterns of PAR-6 foci observed in mNeonGreen::PAR-6 (green) embryos with epidermal cell migration delays after *ani-1* RNAi. The scale bar for all embryos is 10 μ m. **D)** Time-lapse images acquired by HILO microscopy show ventral views of control or *ani-1* RNAi embryos expressing *lin-26p*::LifeAct::GFP or *lin-26*::VAB-10 (ABD)::mCherry in greyscale. Zoomed in regions (yellow box) show the projections more clearly. To the right, the bar graph shows the average number of projections for each time point as indicated. The asterisks indicate $p < 0.0005$.

The delays in epidermal migration in *ani-1* RNAi embryos likely are due to cytoskeletal changes that impact their ability to migrate. As described earlier, we observed F-actin projections at the leading edges of the anterior ventral epidermal cells. We performed HILO imaging on control and *ani-1* RNAi embryos expressing *lin-26p::LifeAct::GFP* or *lin-26p::VAB-10(ABD)::mCherry*, and quantified the length and number of projections from the onset of anterior morphogenesis over several time points ($n = 6$ for control, and 8 for *ani-1* RNAi; Fig. 18D). While there was no change in the length of the projections ($0.6 \mu\text{m}$ in both conditions), there was a significant decrease in the number of projections at each time point, which correlated with their delayed migration (Figure 18D).

It is important to note that we did not observe changes in the position of lumen formation (e.g., in embryos with a less-severe delay) in *ani-1* RNAi embryos, nor was the BFP altered in intensity or appearance. Therefore, neuroblasts are required for controlling the speed of epidermal cell migration, but not their direction. Also, the failure to polarize the pharynx in the more severely delayed embryos reflects a threshold requirement for the timing of cell-cell contacts to complete lumen formation.

2.4.7. Epidermal cells determine the position of the lumen

Next, we determined how mild perturbation of epidermal cell fate affects anterior morphogenesis. To accomplish this, we partially depleted *elt-1* in embryos co-expressing mNeonGreen::PAR-6 and Tag-RFP::PH ($n = 15$ control vs. $n = 35$ *elt-1* RNAi). *elt-1* encodes a GATA-like transcription factor and is essential for determining epidermal cell fate (Figure 19A; Page et al. 1997). After partial *elt-1* depletion, there was no significant delay in the migration of anterior epidermal cells. However, we observed a ventral shift in the position of the anterior lumen

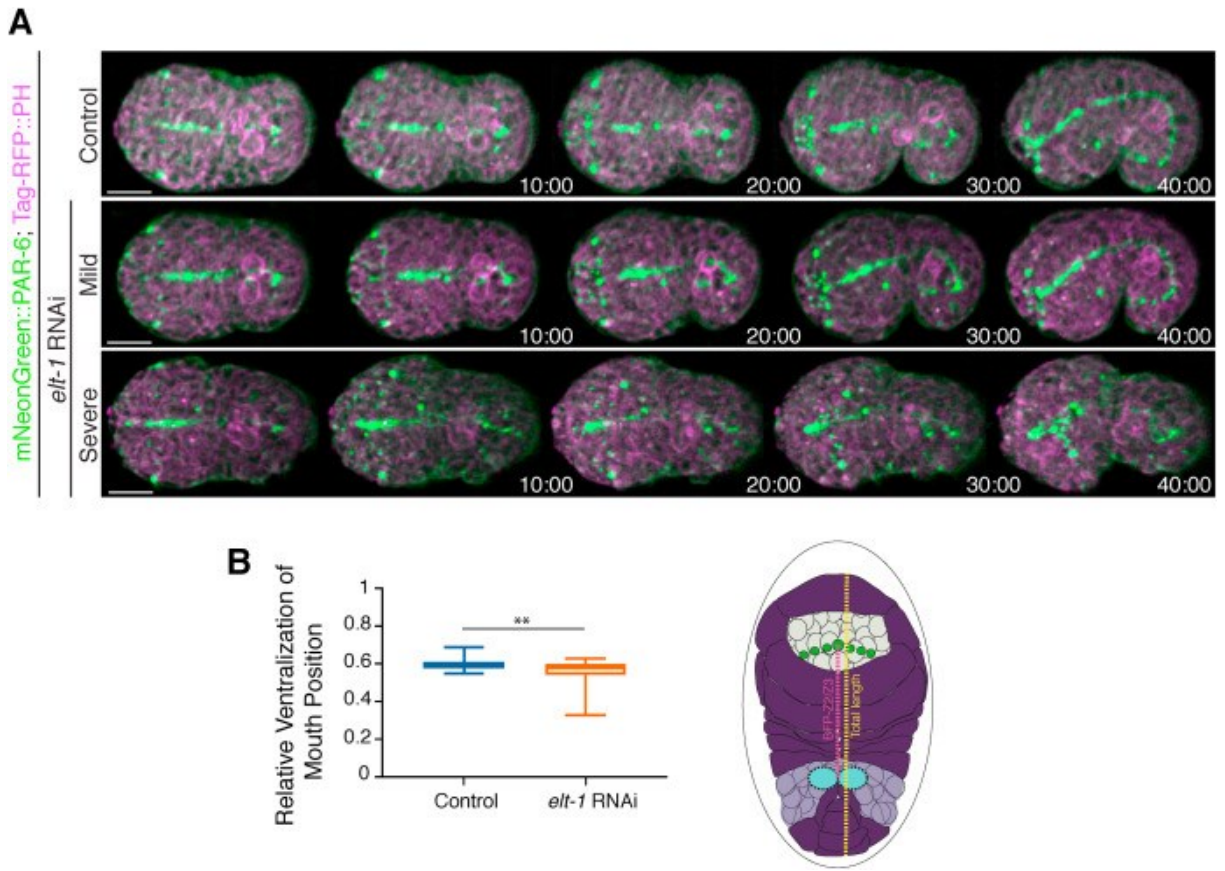


Figure 19. Altering epidermal cell fate causes a change in lumen position. A) Time-lapse images acquired using sweptfield microscopy show ventral views (anterior to the left) of embryos expressing mNeonGreen::PAR-6 (green); Tag-RFP::PH (magenta) in control (top panel) and *elt-1* RNAi embryos (middle and bottom panels). Times are shown in minutes, and the scale bar is 10 μ m. A range of phenotypes was observed: 1) mild, in which PAR-6 foci patterns were similar to those of control embryos, although there was a shift toward a more ventrally positioned lumen, and 2) severe, in which foci failed to coalesce into patterns, and the lumen was extremely displaced. **B)** A graph shows the average ratio of the distance between the lumen and Z2/Z3 cells (magenta in the cartoon schematic; future germline) to the total length of the embryo (yellow in the cartoon schematic). Only mildly perturbed embryos were measured, and the variability of the ratio was significantly increased in *elt-1* RNAi (orange) as compared with control (blue) embryos. The asterisks indicate $p < 0.01$.

formation (Fig. 19A, B). To quantify this, we measured the ratio of the distance between the lumen (marked by PAR-6) and the Z2/Z3 cells (germline precursors) to the total length of the embryo. Whereas the average ratio was not significantly different, the variability was significantly higher in mildly perturbed *elt-1* RNAi embryos ($n = 19$) as compared with control embryos ($n = 10$; Figure 19B). In a subset of the more severely affected embryos we saw that the PAR-6 foci formed patterns that were initially similar to those of control embryos, but these foci failed to coalesce and shifted more ventrally as compared to control embryos (Figure 19A). The BFP also underwent a more ventral shift in severely affected embryos, and the pharynx failed to epithelialize. Therefore, the position of the anterior lumen was determined by the epidermal cells. Although it is not clear why the lumen tended to shift more ventrally, this could be because there are two rows of dorsal cells that intercalate and fuse, and perhaps the loss of one/more of these cells has less of an impact vs. the loss of ventrally positioned cells. These cells also migrate over a longer distance and may interpret cues differently as compared with the ventrally positioned cells.

2.5. Discussion

We characterized anterior morphogenesis of the *C. elegans* embryo. This developmental process is crucial for giving rise to a properly formed anterior lumen, which must align precisely with the pharynx and intestine. Cells from three different tissues are coordinated for anterior morphogenesis: neuroblasts, pharynx and epidermis. But how they did this was not known, largely due to the complexity of studying multiple tissues simultaneously *in vivo*. We used various types of microscopy and post-acquisition software to define the patterns formed by different cell types during anterior morphogenesis. We observed the ingression of neuroblasts as epidermal cells migrated anteriorly to enclose the anterior surface of the embryo in a layer of epidermis. The

neuroblasts arranged into a circle-like pattern that likely facilitates their inward movement. We propose that their movement could in part be due to forces generated from cell movements and patterning during ventral enclosure. We also observed that the arcade cells, the anterior-most pharyngeal cells, formed a rosette positioned at a depth of $\sim 5 \mu\text{m}$. These cells formed projections that reached the anterior, marking the location of the future lumen. The ends of the projections accumulated markers of apical polarity including PAR-6, NMY-2 and HMP-1. Since the projections coalesce causing fluorophores detecting these proteins to be bright compared to other cellular locations, we referred to them as the ‘bright focal point’ (BFP; Figure 4E). While the BFP initially reflected signals associated with the arcade cells, neuronal and/or support cells also could join this location later in anterior morphogenesis. Soon after the appearance of the BFP, foci expressing PAR-6, HMP-1, NMY-2 and ANI-1 arranged themselves into two pentagons that formed on either side of the BFP and aligned with UNC-119 and MIR-228 neuronal and glial cell projections (Figure 16E). Another set of foci expressing PAR-6, HMP-1, NMY-2 and HLH-16 (in a subset) formed a semi-circle and corresponded to the leading edge of the ventral epidermal cells as they migrated anteriorly (Figure 16E). The majority of anterior foci also expressed AJM-1, which initially was weak, but strengthened with time. The ventral epidermal cells co-migrated with the semi-circle of foci and remained in a more ventral position, whereas the dorsal epidermal cells co-migrated with the dorsal foci of the pentagons and migrated over a longer distance. We observed F-actin-rich projections in the migrating epidermal cells, which appeared longer and more dynamic in the ventral cells than in the dorsal cells, where they were shorter and more uniform in appearance. We found that the neuroblasts were required for controlling the speed of epidermal migration, as reducing their numbers by *ani-1* RNAi caused delays. In contrast, mildly

perturbing epidermal cell fate caused a shift in the location of the future lumen but did not affect the timing of its formation.

We propose that the arcade cell projections provide cues that could influence the patterning of the surrounding neuroblasts, which in turn provide a substrate and/or cues to regulate epidermal cell migration. In support of this model, removing the arcade cells or disrupting their polarity caused anterior morphogenesis phenotypes, including the altered organization of neuroblast-associated foci. We also found that using *ani-1* RNAi to reduce the number of neuroblasts caused a range of anterior morphogenesis phenotypes, including delayed epidermal cell migration and failure to epithelialize the anterior lumen. During ventral enclosure, where the ventral surface of the embryo is covered by epidermal cells, several signaling pathways have been shown to regulate WSP-1 and WVE-1 to control the formation of branched F-actin in the migrating ventral epidermal cells (Sawa et al., 2003; Withee et al., 2004; Patel et al., 2008; Bernadskaya et al., 2012; Wallace et al., 2018). For ventral enclosure, it is not clear where the ligands for these pathways are located as rescue studies show that they could originate in the neuroblasts or epidermal cells (*e.g.*, Bernadskaya et al., 2012). It is likely that similar pathways influence the migration of anterior epidermal cells, and we propose that they originate from the subset of neuronal precursors and glial support cells that form the pentagons and semi-circle of foci around the arcade cell projections. In support of this hypothesis, we found that fewer actin projections formed in the anterior ventral epidermal cells that were delayed after *ani-1* RNAi, however, the length of the projections was not affected as expected if the signal was non-autonomous. The pathways controlling F-actin include those responding to ligands such as UNC-6 (netrin), SLT-1 (slit), EFN-1-4 (ephrins) and MAB-20 (semaphorin) and their receptors UNC-40 (DCC), SAX-3 (Robo), VAB-1 (Eph receptor) and PLX-2 (plexin), respectively (Chin-Sang et al., 1999; George et al.,

1998; Wang et al., 1999; Chin-Sang and Chisholm, 2000; Roy et al., 2000; Bernadskaya et al., 2012; Ikegami et al., 2012). We are testing this by perturbing components of these different pathways to determine their impact on anterior epidermal cell migration. As the dorsal cells migrate over a longer distance, they could be influenced by some of the same pathways but with different sensitivities and/or subsets of receptors to account for this distance.

While we saw ventral shifts in the position of the BFP when we perturbed epidermal cell fate, this only occurred at a later timepoint, during polarization of the anterior pharynx. Prior to this, it initiated in the correct position. This suggests that the epidermal cells are crucial for reinforcing lumen position, while the neuroblasts control the timing of lumen formation. We also observed shifts in the position of neuroblast foci just prior to polarization, suggesting that they also associate with and rely on the epidermal cells for late vs. early positioning. This was recently described by the Bao lab for amphid neuroblasts, which form rosettes and piggyback on the migrating epidermal cells for anterior-directed dendrite growth (Fan et al., 2019).

Our studies show how cells from different tissues are coordinated to give rise to the anterior lumen during development. These findings will facilitate more in-depth studies of how chemical cues organize and coordinate the patterning and movements of the different cell types. Given the challenges of studying tissues in more complex metazoans, our studies provide fundamental knowledge of how different cell types can be coordinated for the development of structures.

2.6. Conclusion and model

Here we provide the first detailed description of *C. elegans* anterior morphogenesis, which involves the coordination of neuronal precursors and their support cells, epidermal and pharyngeal cells. We observed that subsets of neuroblasts form concentric patterns around the site of the future

lumen and that some of these neuroblasts ingress as the epidermal cells migrate anteriorly. We also observed that a subset of pharyngeal arcade cells forms a stable rosette, which aligns with the previously described pharyngeal cyst. The projections from these cells initially are enriched in PAR-6, NMY-2 and HMP-1 (CCC), which mark the site of the future lumen. Additionally, subsets of neuroblasts form specific patterns of foci around this location, which contain ANI-1, PAR-6, NMY-2 and CCC components. Other foci are closely associated with both the neuroblasts and the migrating epidermal cells and contain PAR-6, NMY-2, CCC and DAC components. All of the foci mature over time to also include the DAC, coincident with when the epidermal cells reach the anterior. The arcade cells regulate the patterning of neuroblasts, while the neuroblasts are required for epidermal cell migration and the timing of lumen formation, and the number of epidermal cells influences the position of the lumen. This is, to our knowledge, the first in-depth description of anterior morphogenesis in *C. elegans* embryos.

Chapter 3: Cytokinesis is regulated differently in cells with different fates in the early *C. elegans* embryo

Part of this work is included in: Ozugergin I., Mastronardi K., Law C. and Piekny A. (2021) Diverse mechanisms regulate contractile ring assembly for cytokinesis in the two-cell *C. elegans* embryo. Article in revision.

3.1. Preface

Chapter 3 will describe mechanisms regulating cytokinesis in the early *C. elegans* embryo. Cytokinesis is a well-conserved process where one cell divides into two daughters, and must be tightly regulated to prevent aneuploidy and fate changes. Many of the cytoskeletal regulators that control cytokinesis also control polarity and cell migration for tissue morphogenesis, as described in Chapter 1. In particular, active RhoA regulates actomyosin contractility for polarity and migration, and to pinch in the membrane of the separating daughter cells during cytokinesis (Akhshi et al., 2014). The core machinery that regulates the contractile ring for cytokinesis is conserved, but the mechanisms that spatiotemporally control ring assembly is diverse and varies with cell type. The concerted action of multiple pathways likely ensures that cytokinesis occurs in a robust and efficient manner. Several mitotic spindle-dependent pathways provide spatiotemporal signals that regulate the cytokinetic machinery. However, a number of studies have shown that spindle-independent pathways also regulate cytokinesis. In particular, our lab has found that a chromatin-sensing pathway that involves Ran GTPase spatially regulates the contractile ring in response to chromatin position in mammalian cells (Beaudet et al, 2017; Beaudet et al., 2020). During mitosis, a Ran-GTP gradient forms near chromatin, since RCC1, the RanGEF that generates active Ran is tethered to chromatin, while RanGAP generates inactive Ran (Ran-GDP) in the cytosol (Clarke and Zhang, 2008). Since importins can bind to NLS-containing proteins,

which are released by active Ran, this creates an inverse gradient whereby importins can bind to NLS-containing proteins near the cortex, at positions away from chromatin (Ozugergin and Piekny, 2021). Our lab found that importin binding is required for the localization and function of anillin in the equatorial cortex during cytokinesis in HeLa cells (Beaudet et al, 2017; Beaudet et al., 2020). However, the Ran-dependent regulation of cytokinesis has not been studied *in vivo*, nor is it known whether its requirement differs in other cell types. In the early *C. elegans* embryo, the first division of the P0 zygote occurs asymmetrically to give rise to a larger AB daughter fated to become somatic tissue and a smaller P1 cell fated to become the germline. We compared cytokinesis between these three cell types to determine if ring assembly occurs differently in these cells, and how the requirement for the Ran-dependent regulation of cytokinesis varies with cell fate *in vivo*.

3.2. Abstract

Cytokinesis is a process that occurs at the end of mitosis to cleave a cell into two daughters and is crucial for development. Cytokinesis occurs due to the RhoA-mediated assembly and ingression of an actomyosin ring. Multiple mechanisms regulate ring assembly and ingression, but it is not known how their requirement varies with cell type. We recently found that active Ran is a chromatin-associated cue that coordinates the position of the contractile ring with segregating chromosomes. We hypothesized that the requirement for this pathway changes with parameters including size and fate. We tested this using the early *C. elegans* embryo as a model system. The P0 embryo (one-cell) divides asymmetrically to give rise to a larger AB cell (gives rise to multiple tissues) and a smaller P1 cell (future germline). We showed for the first time that these cells have distinct ring closure kinetics, which is reflected by differences in the levels of contractile ring proteins. Disrupting polarity equalized cytokinesis kinetics between the P0 daughter cells, which

ingressed similar to control AB cells. Depleting contractility regulators including ECT-2 (RhoA GEF) and LET-502 (Rho kinase) also equalized cytokinesis kinetics between AB and P1 cells, which had kinetics more like control P1 cells. Interestingly, in P1 cells depleted of LET-502, we observed a bimodal distribution of phenotypes, suggesting that there could be different threshold requirements, with a sharp threshold in P1 cells. Depleting RAN-3 or IMA-3 also equalized contractility in AB and P1 cells, which ingressed like control AB cells, and this was suppressed by co-depletion of ECT-2 or LET-502. Together, our data shows that AB and P1 cells have distinct cytokinesis kinetics and are regulated by the Ran pathway.

3.3. Introduction

Cytokinesis occurs at the end of mitosis to separate a cell into two daughters. Cytokinesis occurs due to the assembly and ingression of an actomyosin ring, which must be properly positioned to prevent aneuploidy or cell fate changes. Both spindle-dependent and -independent mechanisms are known to control the contractile ring, but the conservation and relative contribution of these mechanisms in different cell types is not well understood. We propose that the requirement for different mechanisms varies with parameters including cell fate and size.

C. elegans is an excellent model organism to study conserved cell biological processes, and extensive studies of the P0 zygote (one-cell) revealed how different pathways control ring assembly and ingression. The P0 cell divides asymmetrically in the anterior-posterior axis to give rise to AB and P1 daughter cells with different fates. The AB cell gives rise to multiple lineages that produce many tissues of the worm while the P1 cell is fated to give rise to the germline (Sulston et al., 1983; Guo and Kemphues, 1995). Despite our knowledge of P0 cell division, cytokinesis has not been extensively studied in AB and P1 cells.

Anterior-posterior polarity is established after sperm entry where the sperm-derived pronucleus/centrosome complex determines the posterior pole of the embryo (Goldstein and Hird, 1996; Bowerman and Shelton, 1999; Singh and Pohl, 2014; Kimura and Kimura, 2020). Prior to sperm entry, the oocyte cortex displays a uniform distribution of actomyosin foci and contractility. These foci move rapidly away from the sperm centrosome, leaving the posterior region devoid of contractility (Munro et al., 2004; Eweis and Plastino, 2020). Anterior contractility causes the internal cytoplasm to flow towards the posterior, while cortical cytoplasm flows back toward the anterior. These flows help position fate-determinants to the future AB and P1 cells including MEX-5 (AB), PIE-1 (P1) and P granules (P1) (Strome and Wood, 1982; Draper et al., 1996; Guedes and

Priess, 1996; Hird et al., 1996; Cuenca et al., 2003; Daniels et al., 2010; Wu et al., 2018). These flows also contribute to cortical polarity, which is established by the PAR proteins (partitioning defective) (Kemphues et al., 1988; Rose and Kemphues, 1998; Bowerman, 2000; Wu et al., 2018; Lim et al., 2021). In wild-type embryos, PAR-3, PAR-6 and PKC-3 localize to the anterior cortex, while PAR-1 and PAR-2 localize to the posterior cortex. Distinct domains are formed by these anterior and posterior complexes through mutual inhibition. Each complex has kinase activity that can phosphorylate and negatively regulate the cortical localization of components in the other complex (Kemphues and Strome, 1997; Bowerman, 2000; Wu et al., 2018; Lim et al., 2021). Polarity establishment requires Rho-dependent actomyosin contractility as embryos treated with actin depolymerizing drugs and/or depleted of myosin do not establish polarity (Guo and Kemphues, 1996; Shelton et al., 1999; Severson and Bowerman, 2003). CDC-42 is then required to maintain polarity, as active CDC-42 binds to PAR-6 and stabilizes localization of the anterior complex. Establishing and maintaining polarity is important for placement of the mitotic spindle, which is displaced toward the posterior due to pulling forces generated by dynein-dynactin on the astral microtubules (Sulston et al., 1983; Albertson, 1984; Goldstein and Hird, 1996; Labbe et al., 2004; Nance, 2005; Wang et al., 2017).

RhoA is also required for cytokinesis as it promotes assembly of the actomyosin contractile ring (Piekny et al., 2005; Green et al., 2012). Active RhoA activates the Rho kinase ROCK (LET-502), which induces myosin light chain phosphorylation, filament assembly, and motor activation (Kosako et al. 2000; Piekny and Mains, 2002). RhoA also directly activates formins, which nucleate assembly of unbranched actin filaments. RhoA recruits anillin (ANI-1), a scaffold protein that can interact with RhoA, F-actin, microtubules and myosin (Straight et al. 2005; Piekny and Glotzer, 2008; Piekny and Maddox, 2010; Sun et al. 2015; Pintard and Bowerman, 2019).

The site of ring assembly is determined through signaling between the anaphase spindle and overlying cortex which generates an equatorial zone of active RhoA (RHO-1). Experiments in multiple organisms, including *C. elegans*, revealed that both the central spindle and astral microtubules position the contractile ring (Dechant and Glotzer, 2003; Lewellyn et al., 2010; Tse et al., 2011; van Oostende Triplet et al., 2014). The central spindle, a narrow zone of bundled overlapping microtubules (MTs), forms by centralspindlin (a complex of MKLP1/ZEN-4 and Cyk4 (MgcRacGAP)/CYK-4) between the separating chromosomes in anaphase (Mishima et al. 2002; Glotzer, 2009). The central spindle stimulates ring assembly, because Cyk4-binding to Ect2 is required to generate active RhoA at the equatorial cortex (Mishima et al., 2002; Mishima et al., 2004; Bement et al., 2005; Yuce et al., 2005; Petronczki et al., 2007; Burkard et al., 2009; Wolfe et al., 2009). However, the role of the central spindle microtubules is not clear given that they are not required for ring assembly per se. In different cell types, PRC1/SPD-1 RNAi prevents central spindle assembly, but a ring still forms and ingresses, and lipid-binding is required for Ect2 function (Verbrugghe and White, 2004; Lewellyn et al., 2010; Frenette et al., 2012; Lekomtsev et al., 2012; Kotynkova et al., 2016). In *C. elegans*, ECT-2 does not localize to the central spindle, and only localizes to the P0 cell membrane (Motegi et al. 2006; Green et al., 2012). Recent findings suggest that membrane-localized centralspindlin is inhibited by 14-3-3 in the polar regions of the cell, while Aurora B kinase activity at the central spindle overrides this inhibition (Guse et al., 2005; Douglas et al., 2010; Basant et al., 2015). Polo-like kinase (Plk1) also phosphorylates Cyk4, which could release it from the midzone and permit formation of a complex with Ect2 (Yuce et al., 2005; Petronczki et al., 2007).

Astral microtubules also regulate the zone of active RhoA for contractile ring positioning during cytokinesis (Tse et al., 2011; van Oostende Triplet et al., 2014). Astral microtubules prevent

the accumulation of contractile proteins at the cell poles by promoting their removal or excluding them from the cortex. Treating mammalian cells with low doses of nocodazole, a microtubule-depolymerizing drug, causes a decrease in astral microtubules and a broader zone of active RhoA (van Oostende Triplet et al., 2014). Together, the central spindle and astral microtubule-dependent pathways ensure the spatiotemporal assembly and positioning of the contractile ring.

Microtubule-independent mechanisms also influence the division plane via signals from the cortex, centrosomes, kinetochores and chromatin (Deng et al., 2007; von Dassow et al., 2009; Cabernard et al., 2010; Sedzinski et al., 2011; Kiyomitsu and Cheeseman, 2013; Zanin et al., 2013; Rodrigues et al., 2015). Cortically, several pathways function to spatiotemporally regulate RhoA activity directly or indirectly. In both *C. elegans* and mammalian cells, the GTPase activating protein MPGAP (RGA-3/4) globally inhibits RhoA to dampen contractility, as its depletion causes hypercontractility and ectopic active RhoA (Zanin et al., 2013). Unique to *C. elegans*, a protein called NOP-1 functions redundantly with CYK-4 to regulate ECT-2 (Tse et al., 2012). NOP-1 regulates RhoA activity to promote cortical contractility during pseudocleavage, which occurs after sperm entry and before the first cell division (Tse et al., 2012). Subsequently, CYK-4 takes over (part) of this role in mitosis (Tse et al., 2012). Kinetochores also have an associated complex that can regulate cytokinesis in *Drosophila* S2 cells and HeLa cells (Rodrigues et al., 2015). The regulatory subunit Sds22 of the PP1 phosphatase recruits the complex to kinetochores and triggers relaxation of the polar cortex in anaphase cells (Rodrigues et al., 2015). Here, it dephosphorylates, thereby inactivating, the ERM proteins (Ezrin/Radixin/Moesin) by causing dissociation of F-actin at the cell poles (Roubinet et al., 2011; Rodrigues et al., 2015). This promotes local softening of the polar cortex which allows for elongation of the anaphase cells prior to cytokinesis. However,

this pathway is only functional for a short period of time and its requirement in different cell types during development is not known.

A chromatin-associated cue also spatially controls ring assembly. Active Ran (Ran-GTP) associated with chromatin can influence the localization of anillin, a contractile ring protein (Kiyomitsu and Cheeseman, 2013; Beaudet et al., 2017). Ran is better known for its role in interphase cells where it regulates the nuclear import of proteins with a nuclear localization signal (NLS) (Clarke and Zhang, 2008). High levels of Ran-GTP are generated in the nucleus by RCC1 (RanGEF), which is tethered to chromatin, while Ran-GDP is primarily found in the cytosol due to the enrichment of RanGAP (Clarke and Zhang, 2008). An importin alpha-beta complex binds to the NLS of a target protein and carries the protein through the nuclear pore complex into the nucleus (Clarke and Zhang, 2008). In the nucleus, Ran-GTP binds to importins and releases the protein (Clarke and Zhang, 2008). After nuclear envelope breakdown (NEBD) during mitosis, high levels of Ran-GTP are maintained around chromatin and decrease toward the cortex until early telophase when the envelope begins to reassemble (Kalab et al., 2006; Clarke and Zhang, 2008; Kalab and Heald, 2008). Prior studies found that importin-binding inhibits the function of spindle assembly factors, and the high levels of active Ran around chromatin relieves this inhibition to permit spindle assembly during mitosis (Kalab et al., 2006; Kalab and Heald, 2008). Recent findings from our group showed that importin-binding facilitates the function of human anillin for cytokinesis, leading us to propose that importin-binding could facilitate vs. inhibit the function of cortical proteins (Beaudet et al., 2017; Beaudet et al., 2020; Ozugergin and Piekny, 2021). Our model is that a reciprocal gradient of importins free to bind to NLS-containing cortical proteins forms in the equatorial plane of the cell to control their localization and function. This mechanism could ensure that the contractile ring does not form near chromatin to prevent aneuploidy (Beaudet

et al., 2017; Beaudet et al., 2020; Ozugergin and Piekny, 2021). However, it is not clear if the Ran pathway regulates the function of cortical proteins other than anillin, and how the requirement for this pathway varies with cell type, especially *in vivo*.

Here we used the early *C. elegans* embryo as a model system to determine if the Ran pathway differently regulates cytokinesis in cells with different fates. Our data shows that cytokinesis is differently regulated in cells with different fates; in particular, the phases of ingression kinetics differ greatly. We found that the Ran pathway does contribute to this regulation but does so differently in AB vs. P1 cells when compared to the P0 cell. Additionally, these cell-specific differences seem to be due to differences in the regulation of contractile proteins.

3.4. Materials and Methods

3.4.1. Strains

Strains were maintained on nematode growth medium (NGM) agar plates with a lawn of *Escherichia coli* (OP50) according to standard procedures (Brenner, 1974). The list of *C. elegans* strains used in this study is presented in Table 1. All strains were maintained at 20C unless indicated otherwise. Genetic crosses were performed using standard protocols (for review, see Fay, 2005).

Strain	Genotype
UM463	<i>cpIs42[mex-5p::mNeonGreen::PLCδ-PH::tbb-2 3'UTR, unc-119(+)] II;</i> <i>ItIs37[unc-119(+), Ppie-1::mCherry::HIS-58] IV</i>
UM456	<i>cpSi20[Pmex-5::TAGRFPT::PH::tbb-2 3'UTR; unc-119 (+)] I; unc-119(ed3)</i> <i>III</i>
LP162	<i>nmy-2(cp13[nmy-2::GFP + LoxP]) I</i>
MDX29	<i>ani-1(mon7[mNeonGreen^{3xFlag}::ani-1]) III</i>
OD95	<i>ItIs37 [(pAA64 Ppie-1::mCherry::HIS-58 + unc-119(+)); ItIs38 [pie-1p::GFP::PH(PLC1delta1) + unc-119(+)] III</i>
AJP102	<i>cpIs56 [mex-5p::TagRFP-T::PLC(delta)-PH::tbb-2 3'UTR + unc-119 (+)] II;</i> <i>ani-1(mon7[mNeonGreen^{3xFlag}::ani-1]) III</i>

3.4.2. RNAi

RNA-mediated interference (RNAi) by bacterial feeding was performed as described (Kamath et al., 2001; Timmons et al., 2001). Briefly, RNAi plates were made from NGM as above, with 50 mg/mL ampicillin and 1 mM IPTG. After growth to OD 0.6–1.0 (~6–12 h), the cells were pelleted from their initial 5 mL volume and resuspended in varying amounts of LB to control the RNAi strength (100 ul for *ran-3*, *par-1* and *par-3*, 300uL for *ani-1* and *ima-3*, 400ul for *ect-2* and 500ul for *let-502*). Third and fourth larval stage (L3/L4) hermaphrodites were transferred to plates

with *E. coli* (HT115) transformed with dsRNA constructs; the animals were incubated for 24 hours (*par-1*, *par-3*, *par-6*, *ran-3*, *ect-2*, *let-502* and *ani-1* RNAi) or 30 hours (*ima-3* RNAi) and then transferred to fresh RNAi plates, and progeny from these second plates were assessed for phenotype after 48 h (Kamath et al., 2001). The Y49E10.19 (*ani-1* RNAi) was generously provided by J. C. Labbe, IRIC, Montreal.

3.4.3. Microscopy

Imaging was performed on embryos collected as described (Sulston et al., 1983; Wernike et al., 2016). Images were acquired using a Nikon Eclipse Ti inverted microscope with a NIDAQ/Piezo stage, a 100x PlanApo lens (NA, 1.4), sweptfield confocal illumination (livescan; Bruker), an Ixon3 EMCCD camera (Andor) and NIS-Elements acquisition software. Embryos were imaged using 488 nm and 561 nm lasers and a dual bandpass emission filter (520/20 nm + 630/30 nm). Images of 0.7 μm z-stacks for a total range of 4 μm were collected at 5 second intervals for kymograph analysis. Images were exported as ND2 files.

3.4.4. Image analysis

Only cells that successfully completed cytokinesis, had correct DNA segregation and no gross morphological defects were used for analysis. All images were analysed and processed in FIJI (ImageJ, NIH).

To determine the kinetics of ring closure, ingresson measurements were made using a macro developed by Dr. Chris Law written for FIJI to generate kymographs. Time-lapse images were staged to anaphase onset based on DNA segregation using mCherry-tagged histone, which was subsequently removed to analyze the membrane (mNeonGreen or GFP-tagged PH domain

from PLC δ). A line was drawn manually over the ingression furrow at every time point starting from anaphase onset until furrow closure; 5 pixels on each side of the line were aligned parallel with each other, and placed in order by time, to produce kymographs. The distance between the two sides of the membrane were manually measured at each timepoint using the straight-line tool, and measurements were exported to Excel by Imge Ozugergin. The diameter of the cell at anaphase onset was set to a maximum value (100%) and used to normalize diameter throughout ingression. All n's within the condition were averaged, and the cut-off for the final value for the averaged data was when at least three cells had completed cytokinesis. The averaged values were then plotted against time (seconds).

3.4.5. Quantitative data analysis

The quantitative analysis of ingression was done by Imge Ozugergin. To characterize ingression and determine changes in velocity, data were plotted using GraphPad Prism. All data-points were used when possible, or until ~40% closure to improve the fit of tangents. A sigmoidal line of best fit was plotted using the averaged data for control AB and P₁ cells, then the second derivative of the best fit line with second order smoothing (4 neighbors averaged) was plotted. The x (time) values of the minimum and maximum values of this second derivative curve represent the time points at which there is a change of slope in the original data. The y (% ingression) value at the last time point of Phase 1 (ring assembly), 2 (furrow initiation) and 3 (ring constriction) was noted for each control cell. These values were used as a cut-off to define phase transitions in the RNAi treated embryos. These values were then verified in Excel, and the rate of each phase of ingression was determined by drawing tangents to the curve for each phase. To calculate tangents, data for each treatment were first separated into three phases, and the data points of each individual

phase were then plotted as a scatter graph. A linear trendline of best fit was then drawn through this subset of data to determine the slope of ingress (tangent) at that phase. If the tangent was parallel to the data between two time points, the latter was included in the phase, if not (i.e. the data sloped away from the tangent), it would indicate a phase transition and the beginning of the subsequent phase. If the first two tangents overlapped or were parallel to each other (for example in the case of curves missing the plateau of the first phase), the end of phase 2 was the last time point at which the curve was still parallel to the tangent. Phase duration for individual cells within a cell type of a given condition and their average was then plotted in groups on Prism.

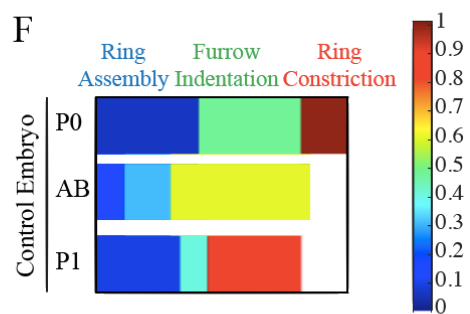
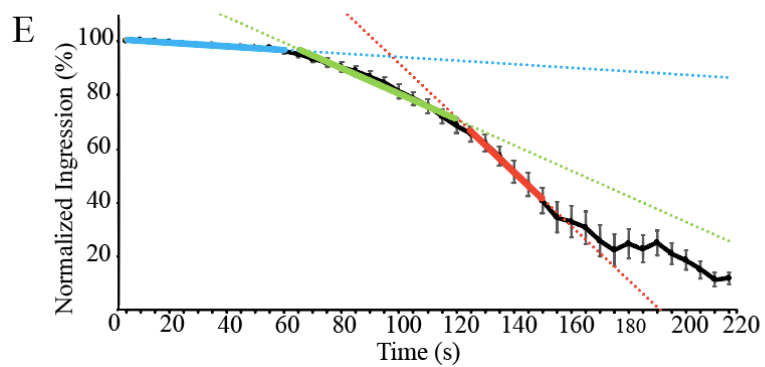
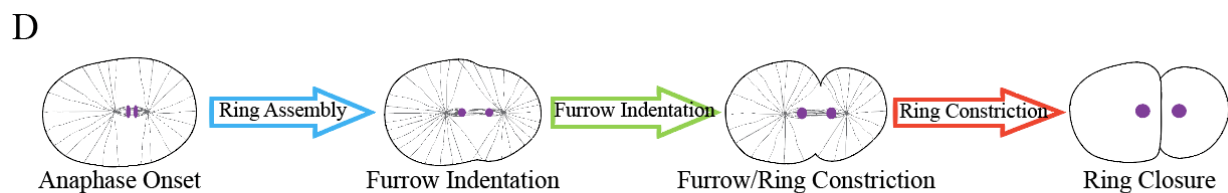
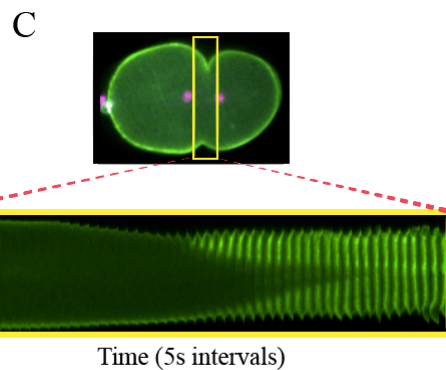
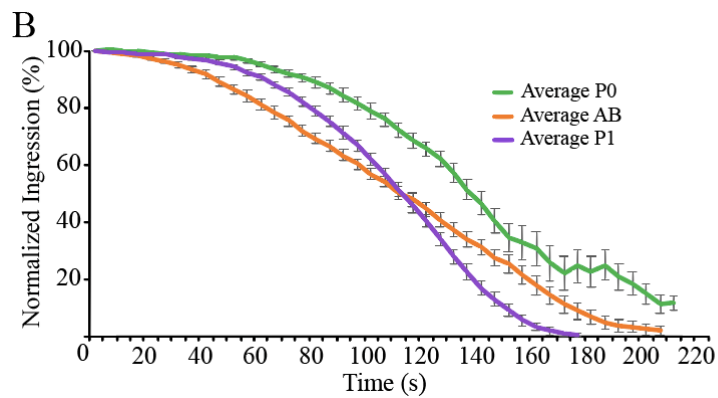
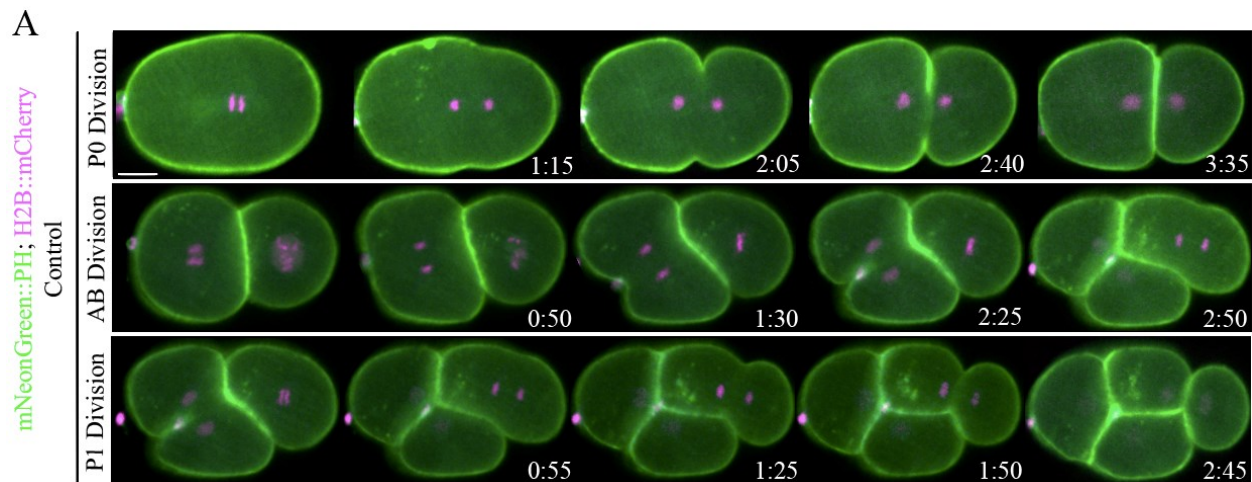
3.4.6. Statistical analysis

Statistical significance was determined using unpaired Student's t test in Graphpad Prism (version 8.4.3). Statistical significance was defined as: $p \geq 0.05$ not significant (ns). * $p = 0.01$ to 0.05, ** $p = 0.001-0.01$, *** $p = 0.001$ to 0.001, **** $p < 0.0001$.

3.5. Results

3.5.1. Cells with different fates have unique ring closure kinetics

We wanted to determine how mechanisms regulating cytokinesis vary with cell fate. We used the early *C. elegans* embryo as a model system, where the first cell (P0) division gives rise to cells of two different fates and sizes, a larger AB daughter fated to give rise to most tissues and a smaller P1 daughter fated to be the germline. Cytokinesis has not been extensively studied in AB or P1 cells before. First, we characterized ring closure kinetics in AB and P1 cells, and compared them to P0 cells. To accomplish this, we imaged embryos co-expressing mNeonGreen::PH (membrane marker) and mCherry::HIS-58 (chromatin marker) from anaphase onset until furrow closure with 5 second intervals (Figure 20A). Kymographs were created for all three cell types to measure the % change in the contractile ring (cell diameter at the furrow) over time from anaphase onset until the end of ingression. This data was used to plot the % change in diameter (ingression) over time (Figure 20B, C). As shown in the graphs, the cells did not ingress in a linear fashion; they had an initial plateau phase with no cortical/furrow indentation, followed by the onset of furrowing, and lastly more rapid ingression (Figure 20B). Since ring closure was not linear, we calculated the inflection points on the curves to measure the transition from one phase to the next. As reported previously for P0 cells, we observed three distinct stages: ring assembly, furrow indentation and ring constriction (Figure 20D, E; Osorio et al., 2018). We specifically compared the early phases for AB and P1 cells. Our results showed that while AB cells had short ring assembly and furrow initiation phases, these phases were prolonged in P1 cells (Figure 20F, G). This suggests that AB and P1 cells may require different mechanisms to control cytokinesis.



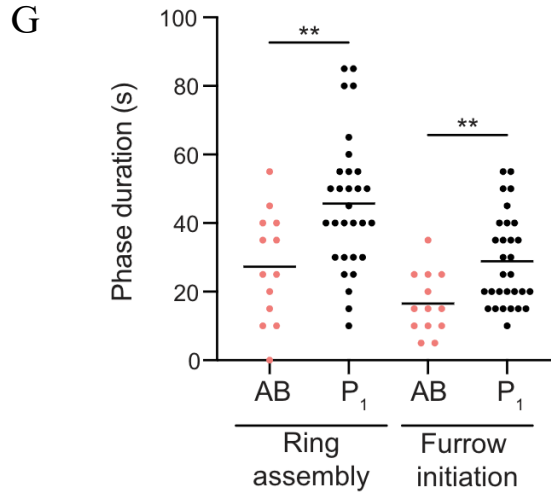


Figure 20. P0, AB and P1 cells have unique ring closure kinetics. **A)** Time-lapse images show P0, AB and P1 cell divisions in a *C. elegans* embryo expressing mCherry::HIS-58 (magenta) and GFP::PH (green). The times shown are after anaphase onset in seconds. The scale bar is 10 μm . **B)** The graph shows the % ingression of the membrane (ring closure) over time (in seconds), where each line represents a different cell division: P0 (green, n=10), AB (orange, n=16) and P1 (purple, n=35). The error bars show SEM. **C)** The yellow box depicts the region used to generate a kymograph used to measure changes in the membrane. The panel shows 5 second intervals from anaphase onset until closure. **D)** Cartoon schematics show the three phases of ingression; ring assembly (blue), furrow indentation (green) and ring constriction (red). DNA is in purple, central spindle microtubules, astral microtubules and centrosomes are in grey. **E)** The graph shows the average % ingression of P0 cell ring closure over time in seconds (n=10). Tangents are drawn to show the transition for each phase (blue for ring assembly, green for furrow indentation, red for ring constriction). Error bars show SEM. **F)** Colour heat map shows the extent of each phase of ring closure and corresponding rate (%/s) for that phase. The colours are shown in the scale bar to the right, with red being the fastest and blue being the slowest. Note that these were only measured until 40% closure. **G)** A plot shows the duration of ring assembly, furrow initiation and ring closure in individual cells (average indicated; ** $p < 0.01$; **** $p < 0.0001$). Done by Imge Ozugergin.

3.5.2. Differences in ring closure kinetics are cell fate-dependent

We hypothesized that the differences in ring closure kinetics between AB and P1 cells is fate-dependent. The first division occurs asymmetrically due to a posterior shift in spindle position caused by cortical flows and greater actomyosin contractility in the anterior vs. posterior cortex (Kemphues et al., 1988; Rose and Kemphues, 1998; Bowerman, 2000; Munro et al., 2004; Wu et al., 2018; Lim et al., 2021). As described in the introduction, anterior and posterior cortical boundaries are defined by distinct anterior (PAR-3, PKC-3 and PAR-6) and posterior (PAR-1 and PAR-2) complexes, respectively (Kemphues et al., 1988; Rose and Kemphues, 1998; Bowerman, 2000; Wu et al., 2018; Lim et al., 2021). The anterior AB daughter is fated to become multiple tissues of the body, while the P1 daughter is fated to be germline. Since the AB cell could inherit greater amounts of actomyosin and/or its regulators, this could influence its kinetics relative to the P1 cell. To test this, we disrupted cell fate by depleting PAR-1, which should result in an expanded anterior domain and contractility in P0 cells, as well as PAR-3 and PAR-6, which should cause the opposite phenotype. As expected, depletion of any of the *par* genes caused the P0 daughter cells to be similar in size and divide synchronously, unlike control embryos where AB cells are larger in size and complete mitosis before P1 cells (Figure 21A). Ring closure kinetics for *par-1*, *par-3* and *par-6* (*RNAi*) P0 daughter cells were similar to each other, and to AB cells, with *par-1* RNAi P0 daughter cells having slightly faster kinetics compared to the others (Figure 21B, C). In particular, the ring assembly phase was short, similar to AB cells, supporting that they could have increased levels of actomyosin compared to P1 daughters. Even though *par-3* or *par-6* RNAi P0 embryos have smaller anterior domains with less contractility, more actomyosin could be inherited compared to P1 cells. This data shows that differences in ring assembly between AB and P1 cells is cell-fate dependent.

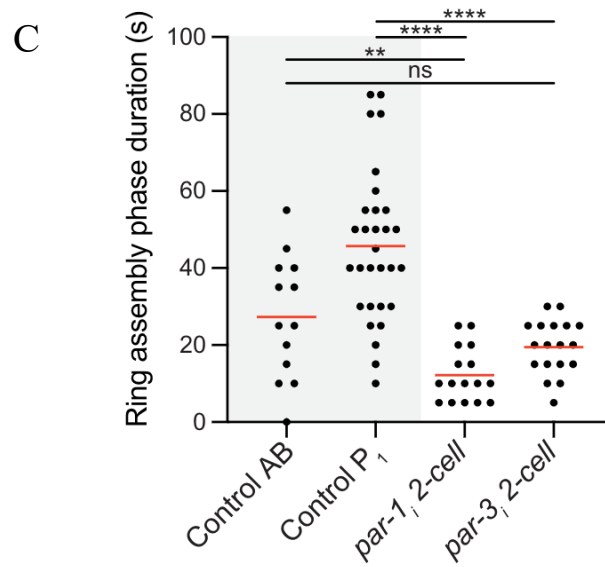
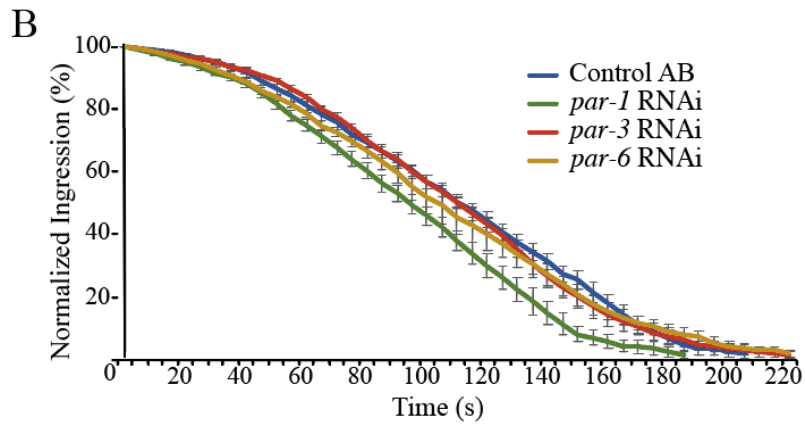
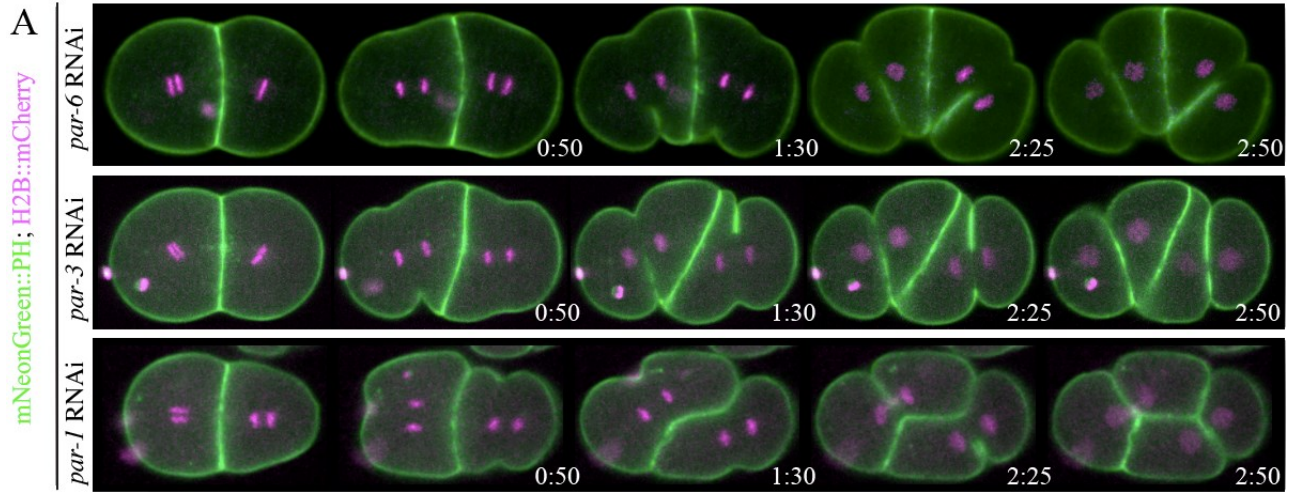


Figure 21. Altering cell fate affects ring closure kinetics. **A)** Time-lapse images show divisions of the P0 daughter cells after *par-1*, *par-3* or *par-6* RNAi in embryos co-expressing H2B::mCherry (magenta) and mNeonGreen::PH (green). The times shown are after anaphase onset ($t=0$) in seconds. The scale bar is 10 μm . **B)** A graph shows the normalized % ingression over time (s, seconds) for embryos as in (A) for control cells (blue; $n=16$), *par-1* RNAi cells (green; $n=10$), *par-3* RNAi cells (red; $n=12$) and *par-6* RNAi cells (yellow; $n=10$). **C)** A plot shows the duration of ring assembly for individual cells (average indicated; ** $p<0.01$; **** $p<0.0001$; ns, not significant). The error bars show SEM. Done by Imge Ozugergin.

3.5.3. Regulators of actomyosin contractility control ring kinetics in P0, AB and P1 cells

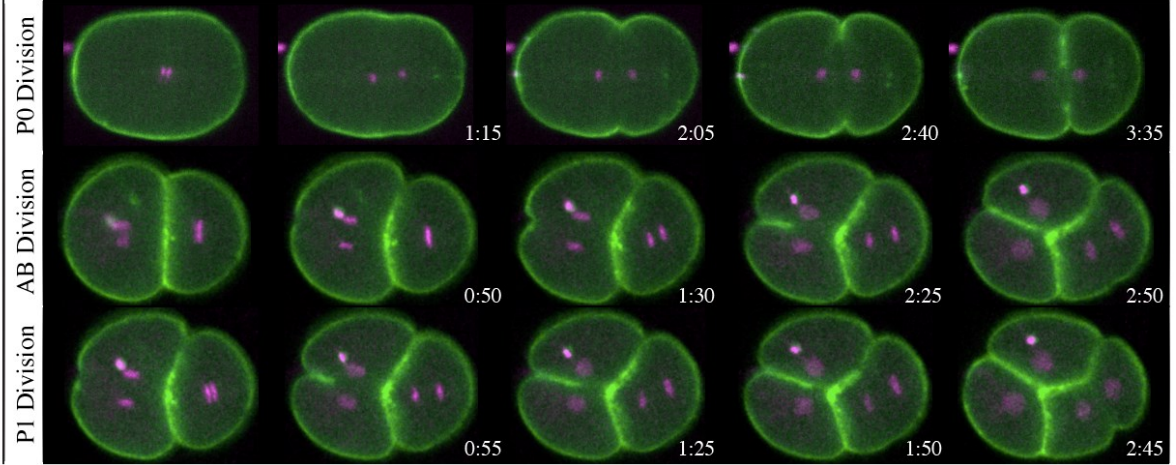
The cytokinetic machinery is heavily dependent on actomyosin and its regulators. We hypothesized that faster ring assembly in AB cells is due to greater amounts of actomyosin and/or its regulators. In this case, perturbing upstream regulators of actomyosin should equalize kinetics to be more similar to P1 cells. To test this, we knocked down *ect-2*, which encodes the GEF for RhoA (Yuce et al., 2005; Basant and Glotzer, 2018). Prior studies showed that ring closure is abolished in P0 cells after *ect-2* RNAi, and to prevent complete failure and permit AB and P1 cells to arise, we used partial RNAi (Prokopenko et al., 1999; Dechant & Glotzer, 2003; Yuce et al., 2005; Kotynkova et al., 2016). We saw that ingression was delayed in P0, AB and P1 cells after partial ECT-2 depletion compared to control cells (Figure 22A, B). Interestingly, while ring assembly was not different in control vs. *ect-2* RNAi AB cells, it was dramatically delayed in P1 cells (Figure 22D). Therefore, AB and P1 cells have different sensitivity to partial *ect-2* RNAi, and retain relative differences in the different phases, supporting different threshold requirements in the two cell types.

We also determined how depletion of another regulator of actomyosin contractility, Rho kinase (LET-502), affects ring closure kinetics. Depletion of *let-502* was previously shown to cause delays or failure in ingression in P0, AB and P1 cells, with P1 cells often completing cytokinesis before AB cells (Piekny and Mains, 2002). However, ring closure kinetics had not been measured in these earlier studies. Here, we found that as expected, *let-502* RNAi caused a delay in ring closure kinetics in P0 and AB cells (Figure 22A, C). There was a more dramatic effect in AB cells, which showed delays in ring assembly and ring closure kinetics similar to P0 cells (Figure 22D). Interestingly, *let-502* RNAi caused P1 cells to have two dramatically different ring

A

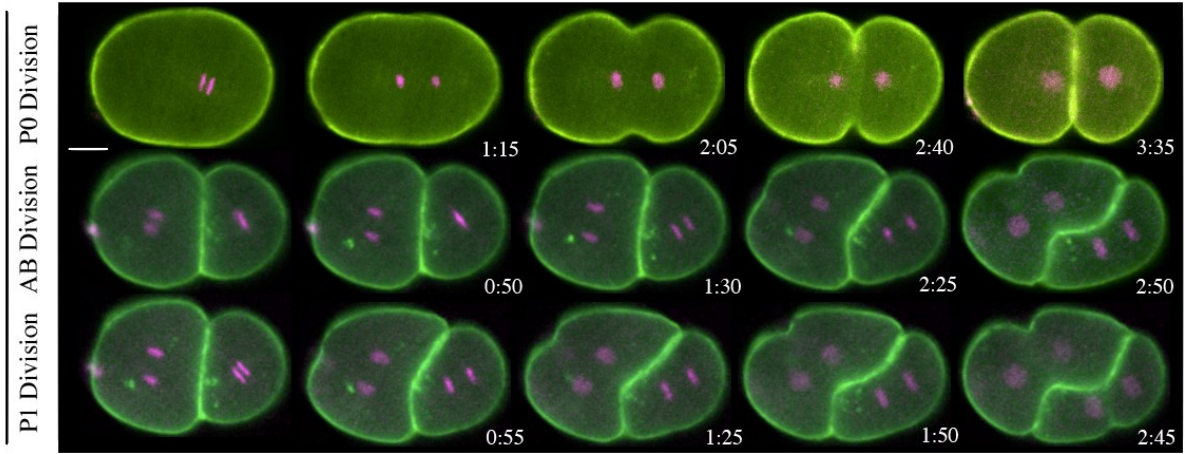
mNeonGreen::PH; H2B::mCherry

ect-2 RNAi

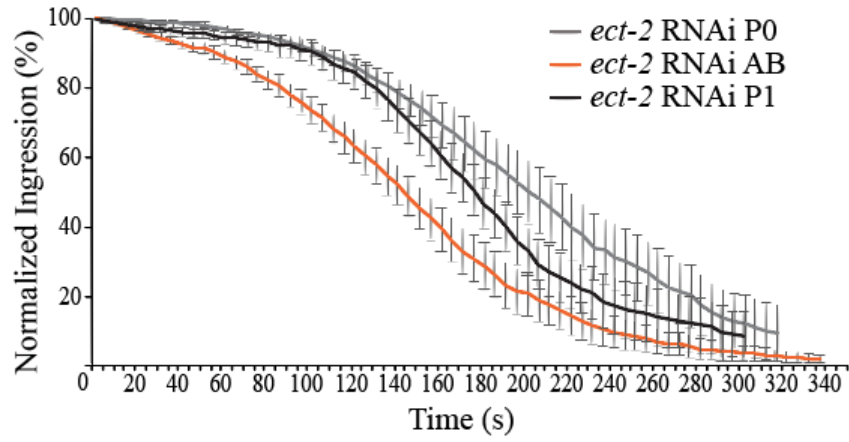
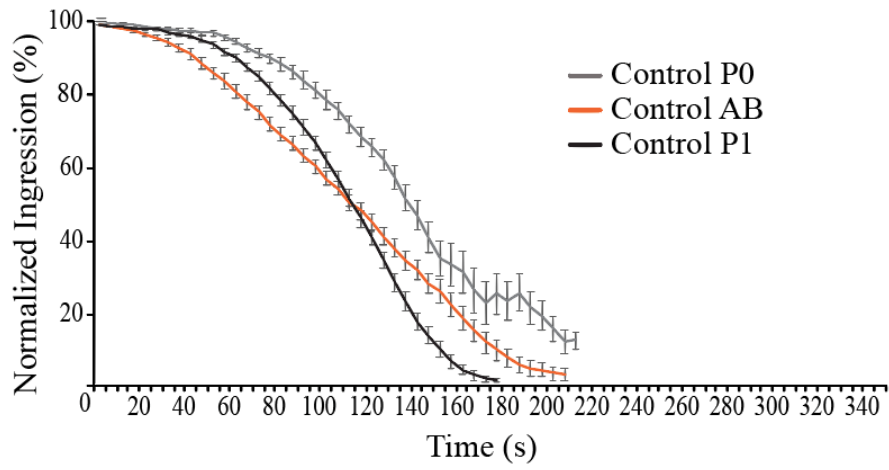


mNeonGreen::PH; H2B::mCherry

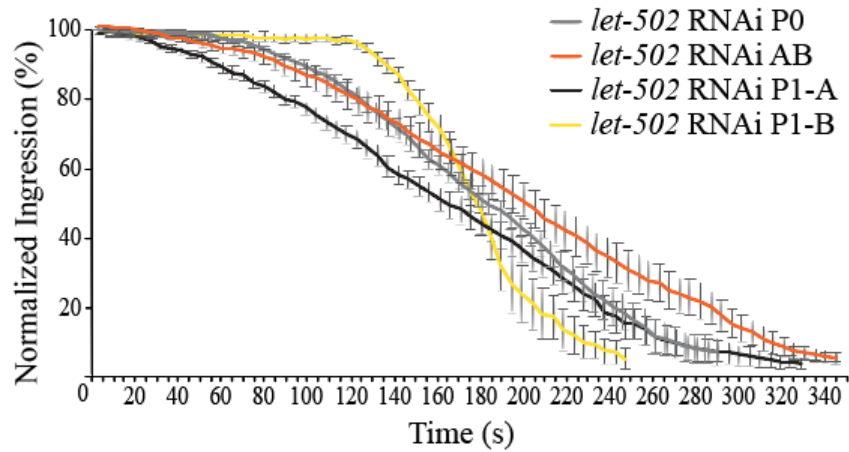
let-502 RNAi



B



C



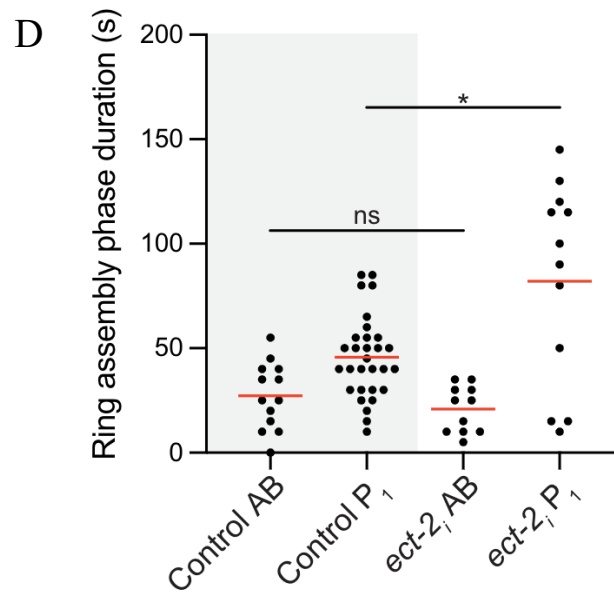


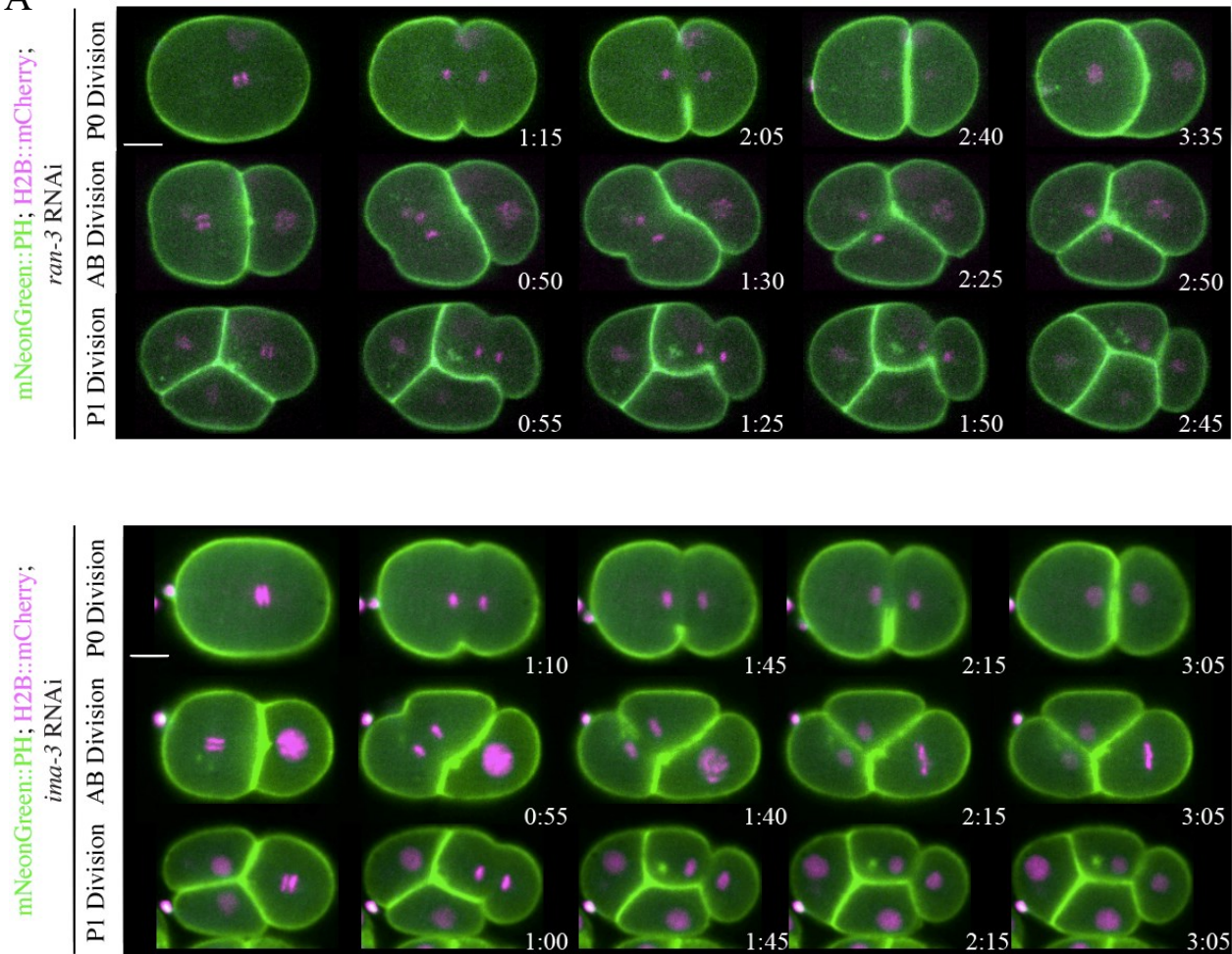
Figure 22. Ring closure kinetics in P0, AB and P1 cells are dependent on regulators of contractility. **A)** Time-lapse images show P0, AB and P1-cell divisions for *ect-2* RNAi embryos co-expressing H2B::mCherry (magenta) and mNeonGreen::PH (green). Time-lapse images show P0, AB and P1-cell divisions for *let-502* RNAi embryos co-expressing H2B::mCherry (magenta) and mNeonGreen::PH (green). The times shown are after anaphase onset in seconds. The scale bar is 10 μ m. **B)** The graph on the top shows the normalized % ingression over time (in seconds) in P0 (grey; n=10), AB (orange; n=16) and P1 (black; n=35) cells in control embryos. The graph in the middle shows the normalized % ingression over time (in seconds) in P0 (grey; n=10), AB (orange; n=11) and P1 (black; n=12) cells in *ect-2* RNAi embryos. **C)** The graph shows the normalized % ingression over time (in seconds) in P0 (grey; n=10), AB (orange; n=10), P1-A (black; n=9) and P1-B (yellow; n=6) cells in *let-502* RNAi embryos. Error bars show SEM. **D)** A plot shows the duration of ring assembly for individual cells in control and *ect-2* RNAi embryos (average indicated; * $p < 0.05$; ns, not significant). Done by Imge Ozugergin.

closure kinetics. In one set of cells (P1-B) there was a severely delayed plateau phase followed by rapid ingression that was comparable to control P1 cells, while the other set (P1-A) had kinetics that resembled P0 and AB cells (Figure 22C). This data helps explain why prior studies observed P1 cells completing cytokinesis before AB cells, and supports that there are unique threshold requirements for *let-502* and actomyosin regulation that depend on the cell type.

3.5.4. The Ran pathway uniquely regulates ring closure kinetics in AB vs. P1 cells

Our data shows that cell fate-dependent differences in ring closure kinetics may be due to differences in the amounts of inherited actomyosin, as well as upstream regulators. These regulators could be controlled by various spindle-dependent and -independent pathways. We recently discovered that the Ran pathway regulates cytokinesis in cultured human cells in response to chromatin position and our model is that importin-binding to cortical proteins that contain an NLS facilitates their localization to the equatorial cortex (Beaudet et al., 2017; Beaudet et al., 2020; Ozugergin and Piekny, 2021). Thus, we determined if the Ran pathway plays a role in regulating ring closure kinetics in P0, AB and/or P1 cells. Depleting *ran-3* (the Ran-GEF; RCC1) should cause a decrease in the levels of active Ran, with a concomitant increase in importin-binding to NLS-containing proteins. Indeed, in embryos depleted of *ran-3*, we observed faster ring assembly in P0, AB and P1 cells (Figure 23A, B). Excitingly, we observed equalized kinetics in *ran-3(RNAi)* AB and P₁ cells, which both had shorter ring assembly phases compared to control cells (Figure 4). To further test this hypothesis, we depleted embryos of *ima-3*, which encodes importin-alpha and is another component of the Ran pathway. We were surprised to see that ring assembly was also faster in all three cell types, with kinetics that resembled *ran-3* RNAi (Figure 23A, B).

A



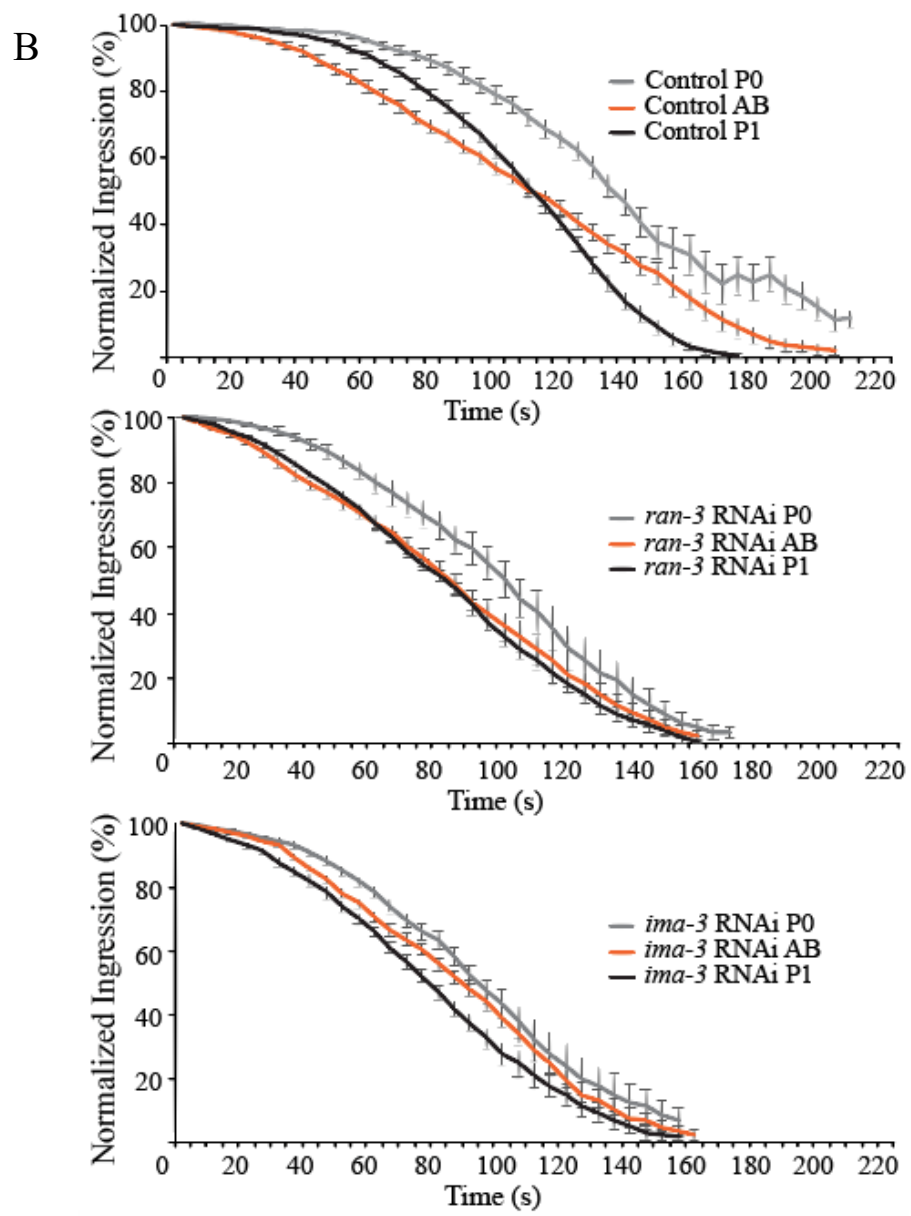


Figure 23. The Ran pathway regulates cytokinesis in early *C. elegans* embryos. **A)** Top panel shows time-lapse images show P0, AB and P1-cell divisions for *ran-3* RNAi embryos co-expressing H2B::mCherry (magenta) and mNeonGreen::PH (green). The times shown are after anaphase onset in seconds. The scale bar is 10 μ m. The bottom panel shows time-lapse images show P0, AB and P1-cell divisions for *ima-3* RNAi embryos co-expressing H2B::mCherry (magenta) and mNeonGreen::PH (green). The times shown are after anaphase onset in seconds. The scale bar is 10 μ m. **B)** The top graph shows the normalized % ingression over time (in seconds) in P0 (grey; n=10), AB (orange; n=16) and P1 (black; n=35) cells in control embryos. The middle graph shows the normalized % ingression over time (in seconds) in P0 (grey; n=10), AB (orange; n=11) and P1 (black; n=21) cells in *ran-3* RNAi embryos. The bottom graph shows the normalized % ingression over time (in seconds) in P0 (grey; n=10), AB (orange; n=12) and P1 (black; n=15) cells in *ima-3* RNAi embryos. Error bars show SEM.

We previously found that importin-beta binds directly to anillin in human cells to regulate its cortical localization (Beaudet et al., 2017; Beaudet et al., 2020). Since importin-alpha and -beta typically form heterodimers, we hypothesize that decreasing importin-alpha increases the levels of importin-beta that are free to bind to cortical proteins such as anillin.

Perturbing the Ran pathway could cause rapid ring assembly due to changes in the regulation of cortical proteins. However, the Ran pathway has been shown to affect bipolar spindle assembly during metaphase in cultured human cells (Kalab et al., 2006; Kalab and Heald, 2008). To determine if the spindle forms properly after *ran-3* RNAi, we imaged embryos expressing TBB-2::GFP (tubulin marker), GFP::PH (membrane marker) and mCherry::HIS-58 (chromatin marker). Indeed, in *ran-3* RNAi embryos, the spindle appeared similar to control embryos and progressed through anaphase and telophase as expected (Figure 24A). In addition, since altering cell fate also equalizes kinetics between the P0 daughter cells, another explanation for our data is that the Ran pathway controls cell fate. To determine if *ran-3* RNAi causes a change in polarity, we imaged embryos expressing a P-granule marker (PGL-1::RFP) and a membrane marker (GFP::PH). We previously found that importin-beta binds directly to anillin in human cells to regulate its cortical localization (Beaudet et al., 2017; Beaudet et al., 2020). Since importin-alpha and -beta typically P-granules in *ran-3* RNAi embryos were sequestered properly to the P-cell lineage which is indicative of the cells maintaining correct cell-fate (Figure 24B).

Thus, increasing Ran-GTP levels or increasing the proportion of importin-beta by removal of its binding partner, importin-alpha, causes ring assembly to occur more rapidly and similarly among the different cell types. We propose that this equalizing effect of Ran pathway perturbation occurs due to increased cortical contractility in the P lineage.

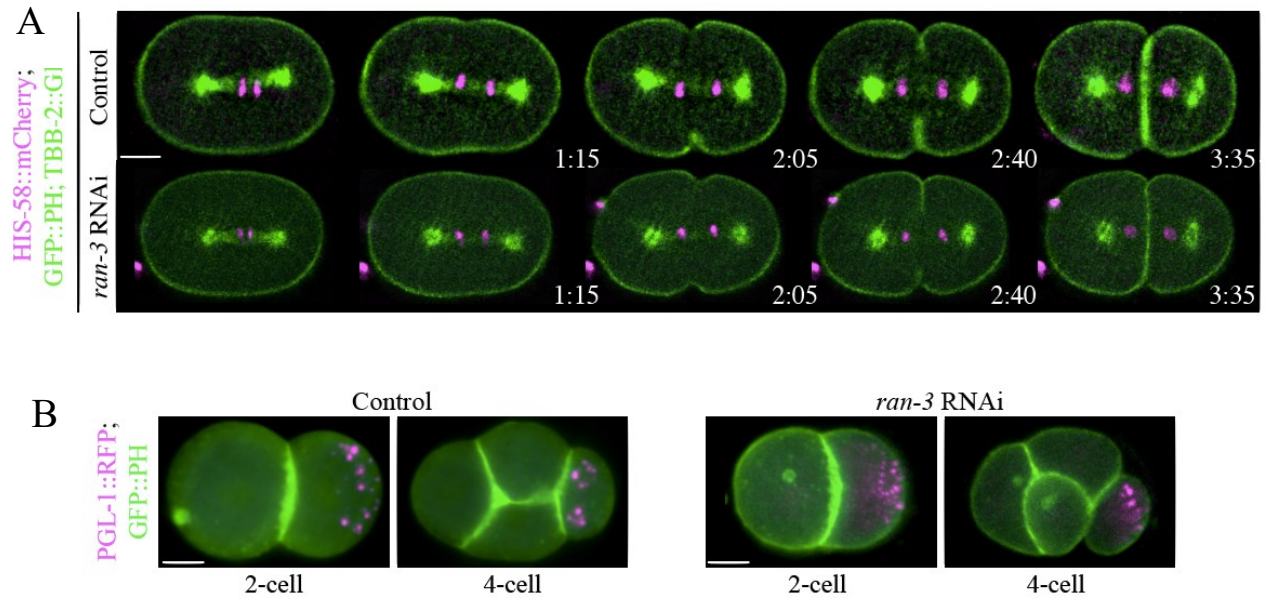


Figure 24. Ran-3/RCC1 is not required for polarity or spindle assembly in the early embryo.

A) Images show embryos co-expressing PGL-1::RFP (P granules; magenta) and GFP::PH (green) in control or *ran-3* RNAi conditions at the 2-cell and 4-cell stage. **B)** Time-lapse images show a control (top) and *ran-3* RNAi (bottom) P0 cell division in a *C. elegans* embryo expressing mCherry::HIS-58 (to visualize chromatin; magenta), GFP::PH (to visualize the membrane; green), and GFP::TBB-2 (to visualize microtubules; green). The times shown are after anaphase onset in seconds. The scale bar for all images is 10 μ m.

3.5.5. The regulation of ring closure kinetics by the Ran pathway is dependent on *ect-2*

We found that the Ran pathway controls differences in ring assembly kinetics in P0, AB and P1 cells. As shown earlier, since *ect-2* regulates actomyosin contractility in the early embryo, we determined if partial *ect-2* RNAi could suppress the faster ring assembly caused by *ran-3* RNAi. While *ect-2* RNAi caused delays in ring assembly in P0, AB and P1 cells, and *ran-3* RNAi caused ring assembly to go faster in all three cell types, their co-depletion restored kinetics back to control (Figure 25). Therefore, this suggests that the Ran pathway affects contractility regulators to influence ring assembly in the different cell types, although the direct targets of this pathway in *C. elegans* embryos are not known.

3.5.6. Anillin is differently regulated by the Ran pathway in AB and P1 cells

Our lab has previously shown that importin-beta binds to and facilitates anillin's recruitment to the equatorial cortex to function during cytokinesis in cultured human cells (Beaudet et al., 2017; Beaudet et al., 2020). Since the Ran pathway controls ring assembly in different cell types in the early embryo, we determined if anillin (ANI-1) is a target of this pathway. Similar to actomyosin, ANI-1 is enriched at the anterior cortex in P0 embryos, and greater levels are inherited by the AB vs P1 cell (Figure 26A). Next, we tested if co-depletion of *ani-1* could suppress the faster ring assembly kinetics caused by *ran-3* RNAi. As previously reported, *ani-1* RNAi caused mild delays in ring closure kinetics in P0 cells (Figure 26B, C; Maddox et al., 2007). We also observed mild delays in ring closure kinetics in AB and P1 cells after *ani-1* RNAi (Figure 26B, C). Interestingly, we saw that while co-depletion of *ani-1* and *ran-3* partially suppressed the rapid ring assembly kinetics caused by *ran-3* RNAi in P0 cells, and fully suppressed AB cells, but we did not observe suppression in P1 cells (Figure 26B, C). This suggests that while ANI-1 could be

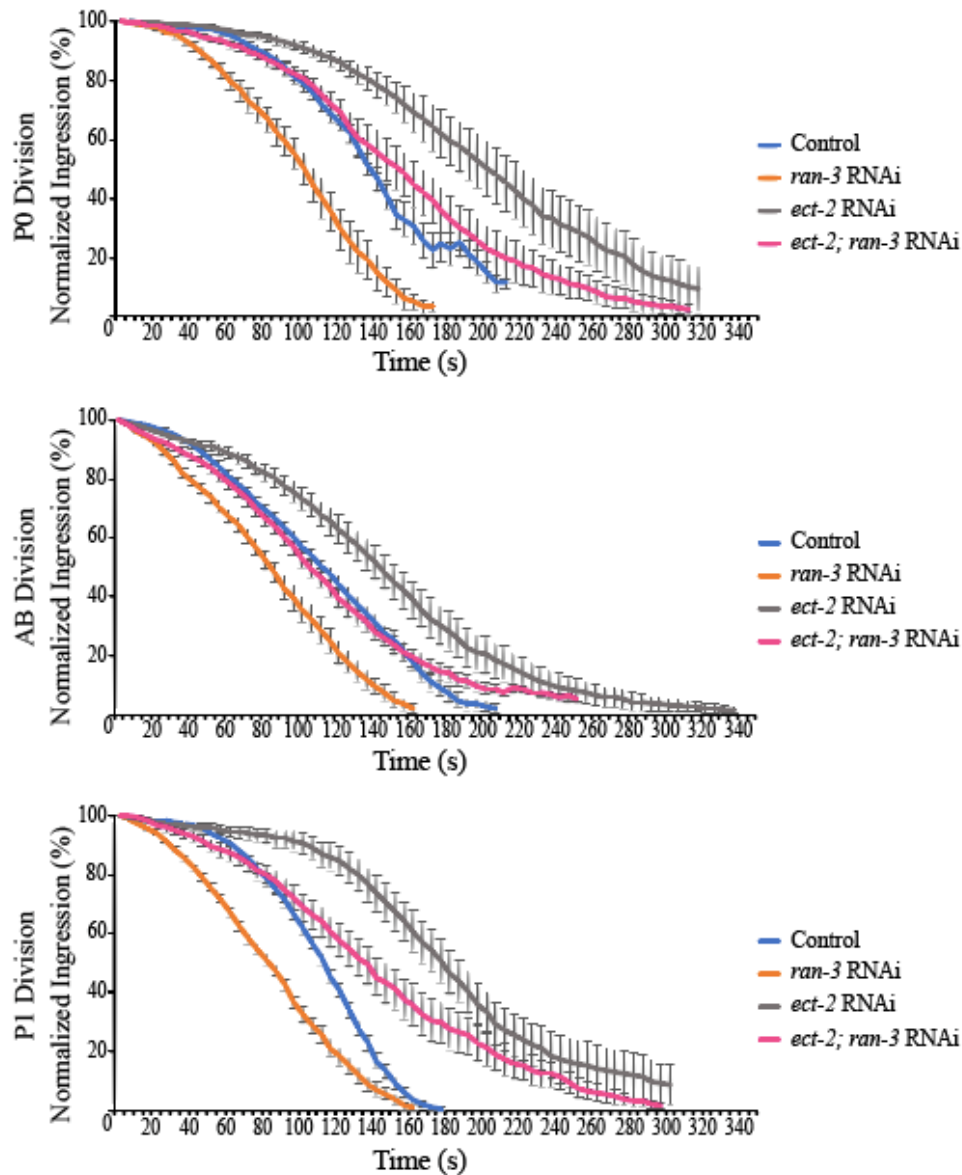
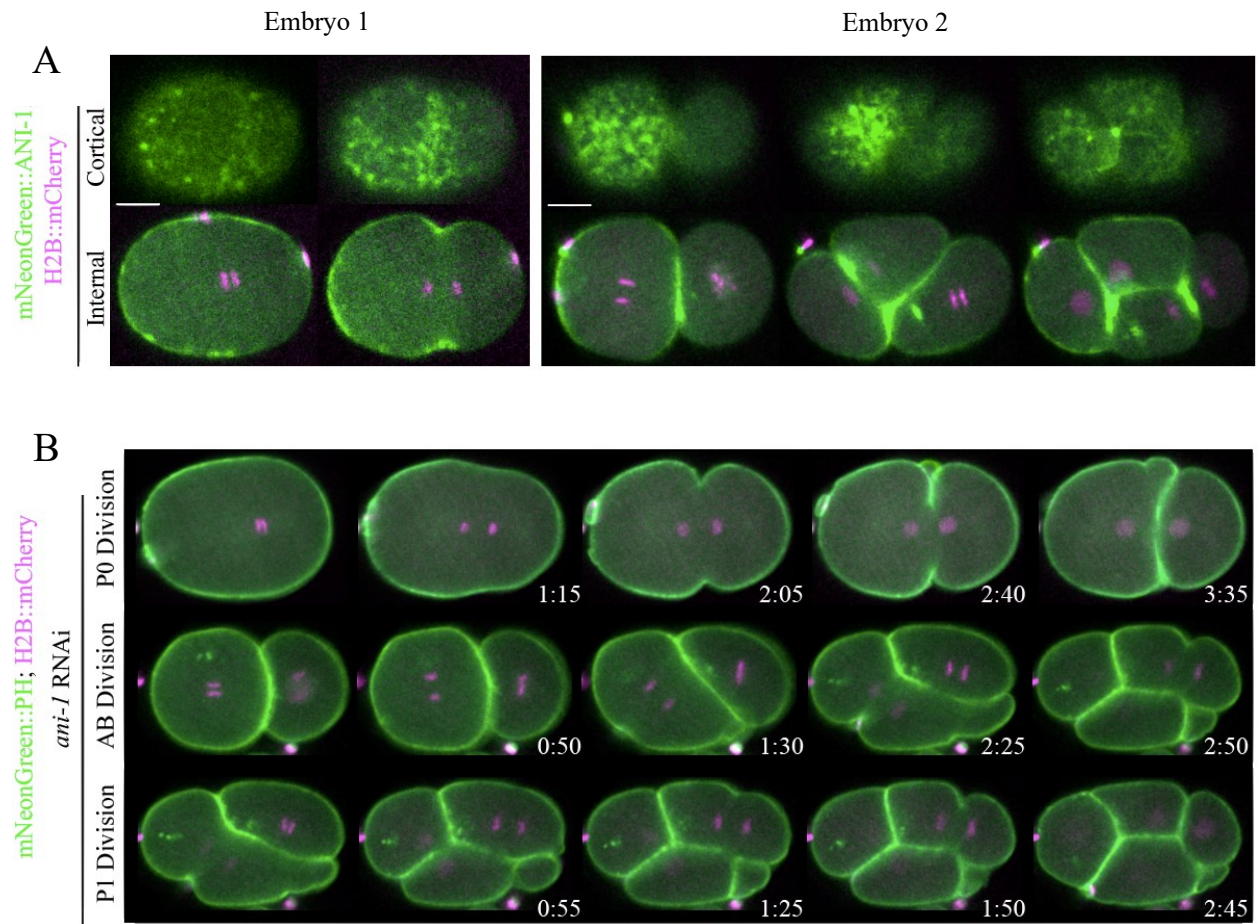


Figure 25. Depleting regulators of contractility suppresses the Ran-GEF/RCCI phenotype.

The top graph shows the normalized % ingressions over time (in seconds) in P0 control cells (blue, n=10); *ran-3* RNAi cells (orange, n=10); *ect-2* RNAi cells (grey, n=10) and *ran-3;ect-2* RNAi cells (pink, n=14). The middle graph shows the % ingressions over time in AB control cells (blue, n=16); *ran-3* RNAi cells (orange, n=11); *ect-2* RNAi cells (grey, n=11) and *ect-2;ran-3* RNAi cells (pink, n=10). The bottom graph shows the % ingressions over time in P1 control cells (blue, n=35); *ran-3* RNAi cells (orange, n=21); *ect-2* RNAi cells (grey, n=12) and *ect-2;ran-3* RNAi cells (pink, n=11). Error bars for all graphs show SEM.



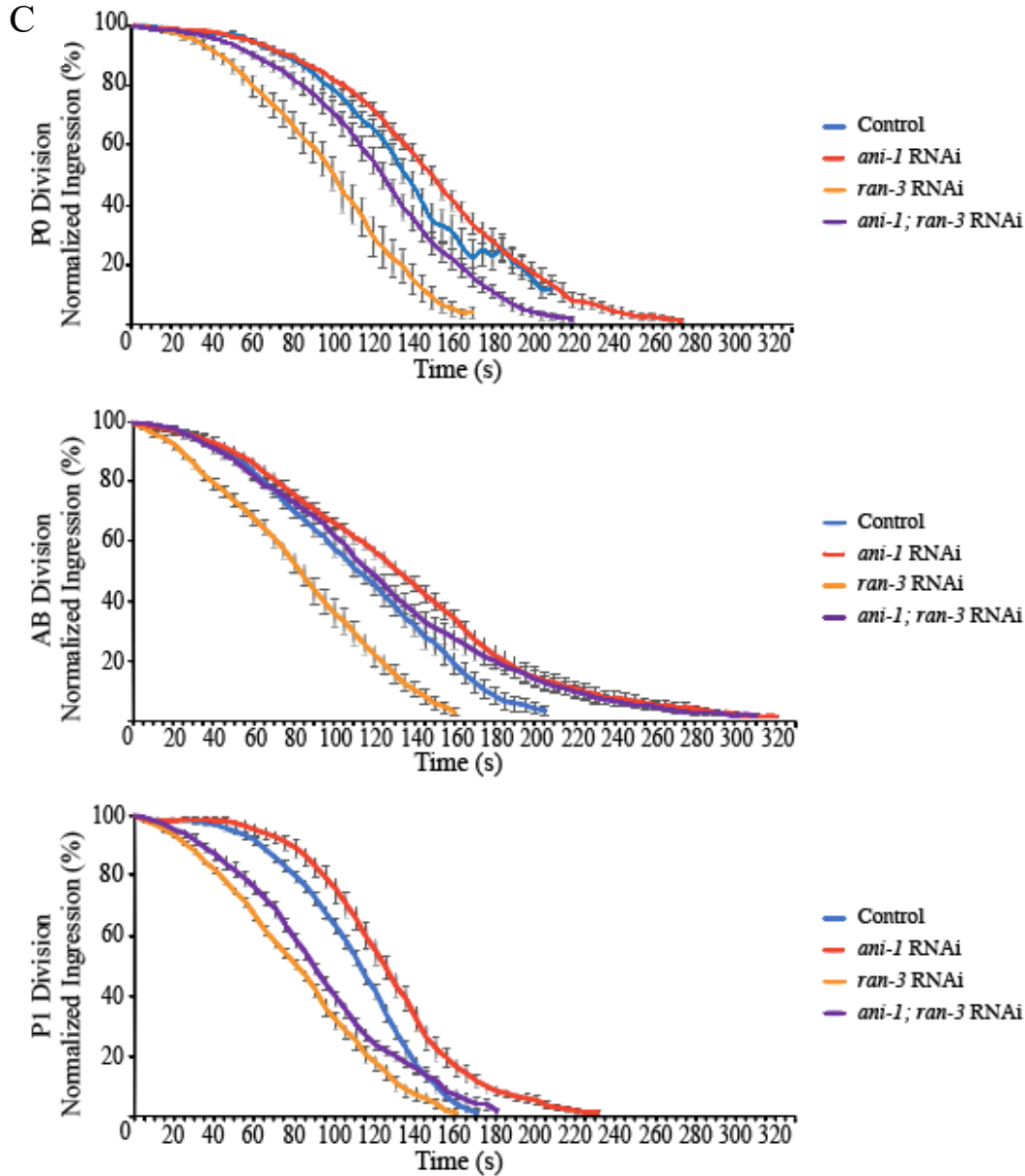


Figure 7. ANI-1 is differently regulated by the Ran pathway in AB vs. P1 cells. **A)** Time-lapse images show the P0 cell division (embryo 1) and the AB and P1-cell divisions (embryo 2) for *C. elegans* embryos expressing mCherry::HIS-58 (histone marker; magenta) and mNeonGreen::ANI-1 (anillin marker; green). Top row shows anillin localization at the cortex while bottom row shows anillin accumulation at the AB furrows in particular. The times shown are after anaphase onset in seconds. **B)** Time-lapse images show P0, AB and P1-cell divisions in *ani-1* RNAi embryos co-expressing H2B::mCherry (magenta) and mNeonGreen::PH (green). The times shown are after anaphase onset in seconds. The scale bar for all embryos is 10 μ m. **C)** The top graph shows the normalized % ingressions over time (in seconds) in P0 control cells (blue, n=10); *ran-3* RNAi cells (orange, n=10); *ani-1* RNAi cells (grey, n=10) and *ani-1; ran-3* RNAi cells (pink, n=12). The

middle graph shows the % ingression over time in AB control cells (blue, n=16); *ran-3* RNA cells (orange, n=11); *ani-1* RNAi cells (grey, n=10) and *ani-1;ran-3* RNAi cells (pink, n=12). The bottom graph shows the % ingression over time in P1 control cells (blue, n=35); *ran-3* RNAi cells (orange, n=21); *ani-1* RNAi cells (grey, n=14) and *ani-1;ran-3* RNAi cells (pink, n=11). Error bars for all graphs show SEM. The scale bar is 10 μ m.

a target of the Ran pathway in some cell types, it has different thresholds of regulation in other cell types.

3.6. Discussion

In this thesis, we demonstrated that cells with different fates in the early *C. elegans* embryo have different ring closure kinetics. First, we characterized cytokinesis in AB and P1 cells, and compared them to the well-studied P0 zygote. As described in the introduction, AB cells are fated to become different tissues of the adult, while the P1 cell is fated to give rise to the germline. We found that all three cell types have three distinct phases of ring closure, which have been previously described for the P0 zygote (Osorio et al., 2018). The first plateau phase corresponds to ring assembly, when actomyosin filaments accumulate in the equatorial plane, and in the second indentation/initiation phase, the filaments align and begin to pull in the membrane. In the third and final phase, the actomyosin filaments constrict to shorten the ring as the opposing sides of the membrane are brought together (Osorio et al., 2018). We measured changes in the velocity of the ingressing membrane to precisely define the phases. Interestingly, the ring assembly phase took longer, and constriction was faster in P0 and P1 cells compared to AB cells (Figure 20). This data suggests that cells fated for the germline have distinctive ring closure kinetics compared to their somatic cell counterparts. One hypothesis is that this is due to actomyosin contractility being enriched in the anterior cortex in dividing P0 zygotes (Munro et al., 2004; Tse et al., 2012) which could lead to the inheritance of higher levels of actomyosin and/or regulators in AB vs. P1 cells. In support of this, depletion of *par* genes required for anterior posterior polarity and cell fate including *par-1*, *par-3* and *par-6*, equalized ring closure kinetics between the P0 daughter cells.

The PAR proteins are required to generate the robust cortical flows needed to ensure that ingression occurs asymmetrically in the P0 cell to set up anterior-posterior polarity and produce the larger, anterior AB cell and the smaller, posterior P1 cell. PAR-3 and PAR-6 are part of a complex that localizes to the anterior cortex, while PAR-1 and PAR-2 form a complex that localizes to the posterior cortex. The activities associated with each complex mutually exclude the other proteins to create distinct cortical domains that align the mitotic spindle to ensure that the first division occurs asymmetrically. Actomyosin contractility is also enriched at the anterior cortex and reinforces polarity through positive feedback. Therefore, depletion of *par-3* or *par-6* should cause expansion of the posterior domain causing an overall decrease in cortical contractility, while depletion of *par-1* should cause expansion of the anterior domain and spread of cortical contractility into the posterior. Interestingly, embryos depleted of *par-1*, *par-3* or *par-6* all had similar ring closure kinetics with short assembly phases resembling AB cells (Figure 21B). While we expected ring assembly to be faster in *par-1*-depleted embryos vs. *par-3* or *par-6*, the equalization of P0 daughters may still cause higher levels of actomyosin to be inherited compared to P1 cells, supporting faster ring assembly. Myosin levels were measured in *par-1* RNAi embryos compared to control and peak myosin levels were higher than in control P1 cells but not as high as control AB cells (78%; data not shown). It seems as though the higher levels of myosin in AB cells compared to P1 cells is due to its unequal inheritance from the initial P0 division which could mean that cell fate is an important factor in affecting cytokinesis.

We found that ring closure kinetics is cell fate-dependent in the early embryo, which could be due to the inheritance of higher levels of actomyosin and/or regulators in AB vs. P1 cells. To test this hypothesis, we depleted several regulators of actomyosin contractility. We partially knocked down ECT-2, the GEF required to generate active RhoA, the upstream regulator of

actomyosin assembly and force generation. As shown in Figure 22, *ect-2* RNAi caused a delay in ring assembly in P0, AB and P1 cells, but the kinetics still varied depending on cell type and were not equalized. We also determined how depletion of Rho kinase (LET-502) affects ring closure kinetics in the three cell types. Rho kinase is required for myosin activation and was previously shown to regulate cytokinesis in the early embryo (Piekny and Mains, 2002). These studies also found that in *let-502*-depleted or in maternal *let-502* mutant embryos, AB cells often completed cytokinesis after P1 cells (Piekny and Mains, 2002). However, these phenotypes were not quantified for ring closure, and we found that *let-502* depletion caused an increase in ring assembly and delays in constriction in P0 and AB cells (Figure 22). Interestingly, in P1 cells, we saw a bimodal distribution where some cells had kinetics that resembled control AB cells, and others had an extremely extended ring assembly phase followed by rapid constriction (Figure 22). This data supports that there could still be additional regulation contributing to ring closure kinetics vs. just differences in actomyosin levels. Further, there could be sharper thresholds for ring assembly in P1 cells compared to the other cell types.

Next, we determined if the Ran pathway, which is a mechanism that regulates ring assembly in human cells, could regulate the differences in ring closure kinetics in AB vs. P1 cells. Prior studies in our lab discovered a role for Ran-GTP in coordinating the position of the contractile ring with segregating chromosomes (Beaudet et al., 2017). We found that the contractile ring component anillin (ANI-1) requires importin-binding for its recruitment to the equatorial cortex and function in cytokinesis (Beaudet et al., 2020). We propose that the requirement for the Ran pathway could vary with different parameters including fate, size and geometry. Interestingly, decreasing the levels of active Ran by *ran-3* RNAi (Ran-GEF; RCC1) equalized ring closure kinetics between P0, AB and P1 cells, which assembled rings more rapidly compared to control

cells (Figure 23). This data is consistent with our studies in cultured human cells, where decreasing active Ran could lead to a corresponding increase in importins free to bind to NLS-containing proteins (Beaudet et al., 2017; Ozugergin and Piekny, 2021). We also depleted embryos of importin-alpha, encoded by *ima-3* and found that P0, AB and P1 cells in these embryos had ring closure kinetics similar to *ran-3* depletion. While this may seem counterintuitive, our prior data found that importin-beta directly binds to human anillin to regulate its function (Beaudet et al., 2020). Since importin-alpha/-beta heterodimers can bind to NLS sites, one model is that the heterodimer could have different impacts on protein function vs. importin-beta. Although not shown here, we have further evidence supporting this model as co-depletion with importin-beta suppressed the faster ring closure kinetics caused by *ima-3* RNAi. Importantly, we found that the regulation of ring closure kinetics in AB and P1 cells caused by *ran-3* or *ima-3* RNAi was not due to perturbations in spindle assembly or changes in cell fate (Figure 24). Further, the increase in ring closure kinetics was due to enhanced actomyosin contractility because co-depletion of *ran-3* and *ect-2* suppressed the faster ring closure kinetics caused by *ran-3* (Figure 25).

Another potential target of the Ran pathway that could control ring closure kinetics is anillin (ANI-1). As mentioned above, anillin is regulated by importin-beta-binding in cultured human cells, and we determined if ANI-1 could similarly be a target in *C. elegans*. The NLS in anillin is conserved in ANI-1, and indeed we found that it can similarly bind to importin-beta (data not shown). Depletion of *ani-1* RNAi caused mild changes in ring closure kinetics in P0, AB and P1 cells (Figure 26). Co-depletion with *ani-1* suppressed the faster ring closure kinetics caused by *ran-3* in P0 and AB cells, but not P1 cells. These results suggest that ANI-1 could have different thresholds of regulation by the Ran pathway depending on the cell type. This exciting result

suggests that there are other Ran pathway targets in P1 cells, and the early *C. elegans* embryo could be ideal to identify these other targets.

Chapter 4: Overview and Conclusions

4.1. Chapter 2 Conclusions

In this study, we described the cellular events required for *C. elegans* anterior morphogenesis, which occurs during mid-to-late embryogenesis and has never been characterized before (Chisholm and Hardin, 2005). During this time, multiple tissues arise and develop simultaneously, including the epidermis, neuronal and pharyngeal tissue. As embryos undergo ventral enclosure, the pharyngeal primordium forms as a ball of cells that differentiate to form the mature pharynx and needs to connect the digestive tract to the buccal cavity or mouth comprised of arcade cells (Mango 2009; Portereiko and Mango, 2001; Portereiko et al., 2004). Polarization and cell movements aligns the pharyngeal cells with the arcade cells, which then form adherens junctions with neighbouring epidermal cells to form a contiguous lumen (Portereiko and Mango, 2001). Our findings revealed that there is coordination between pharyngeal cells (arcade cells), the neuroblasts and the epidermal cells to give rise to a properly positioned and formed buccal cavity. Very few studies have followed the morphogenesis of multiple tissue types simultaneously, and our findings should provide crucial, fundamental knowledge of how different tissues are coordinated for a specific developmental event.

Our studies revealed several important findings. We discovered that 6 arcade cells form a stable, multicellular rosette just anterior to the previously well-characterized, large pharyngeal cyst (Figure 14; Rasmussen et al., 2012). The alignment of these rosettes likely ensures that a uniform lumen forms in the pharynx. The cells form a bulb with projections that coalesce at the anterior, and are the first marker of the future lumen. The enrichment of proteins that are typically associated with polarity at the ends of these projections supports that arcade cell shape changes occur through apical constriction. We propose that since the projections (also referred to as BFP) are the first

marker of the future lumen, there could be important chemical and/or mechanical cues associated with these cells that helps to position other cell types nearby including the neuroblasts. In support of this, disruption of arcade cells via depletion of *pha-4* or *zen-4* caused disorganization of nearby cell positions and delays or defective anterior morphogenesis.

Subsets of neuroblasts also form projections marked by proteins required for polarity (Figure 15). We found that some of the projections emanate from glial cells, while others are neuronal from the SMDD/AIY and SIAD/SIBV lineages, and others remain to be determined. Importantly, the projections associated with these cells form distinct patterns including two pentagons on either side of the arcade cell projections, and a semi-circle on the more ventral side. Importantly, the leading edge of the migrating anterior ventral and dorsal epidermal cells also come into close proximity to these projections, and may form close contacts. We hypothesize that chemical or mechanical cues associated with these neuroblasts (glial or neurons) guide epidermal cell migration for anterior morphogenesis. In support of this, we found that depleting *ani-1*, which is required for neuroblast division causes defects in epidermal cell migration and anterior morphogenesis, specifically in their ability to form F-actin rich projections at the leading edge (Figure 17).

It is not clear how signaling from the neuroblasts controls epidermal cell migration. We found that the arcade cell and neuroblast cell projections also are enriched in adhesion proteins, including the DAC (DLG-1 and AJM-1 complex) and CCC (cadherin/HMR-1 and α -catenin/HMP-1 complex (Figure 16; Costa et al., 1998; McMahon et al., 2001; Chisholm and Hardin, 2005; McMahon et al., 2001). While their relative timing seems to vary, with the CCC being enriched first, this could indicate that there is adhesion between these projections and the epidermal cells. Whether this provides mechanical coupling between the cells, similar to what was observed for

the amphid dendritic projections and epidermal cells or helps coordinate the cells for chemical signaling is not known. Strikingly, the dorsal epidermal cells need to migrate a further distance compared to the ventral epidermal cells, as the lumen is more ventrally positioned. Yet, their migration is well-coordinated, so they reach this position at the same time. This suggests that the cues controlling their movements could be different on the dorsal vs. ventral side. Since the semi-circle of foci are positioned ventrally, these could actually help slow down ventral epidermal cell migration. In support of the important role of the epidermal cells in anterior morphogenesis, disrupting their fate via *elt-1* depletion caused a re-positioning or shift of the lumen to a more ventral position.

4.2. Chapter 2 Perspectives

Multiple factors could influence the position of the pharyngeal and neuroblast cell types and their polarity, which is required to form projections, as well as anterior epidermal cell migration. The ventral epidermal cells move toward, but do not cross the position of a subset of ventrally positioned neuroblasts (marked by foci), while the dorsal epidermal cells move in close concert with a subset of dorsally positioned neuroblasts. This could be controlled mechanically or chemically. All cell types could have associated cues, that could influence cell polarity, position and epidermal cell migration. Several studies have identified key signalling pathways that regulate neuroblast position and epidermal cell migration during ventral enclosure which could also be regulating anterior morphogenesis. Our lab has started to screen these components and found that the Slit/Robo pathway plays a role in regulating anterior morphogenesis (Victoria Richard, unpublished observations). Depletion of Robo (SAX-3) and the Slit ligand (SLT-1) caused the disorganization of cells contributing to the PAR-6 foci, and delays in anterior ventral epidermal

cell migration. Robo was previously shown to function redundantly with other signaling pathways in ventral enclosure, and the proportion of embryos with anterior morphogenesis was lower compared to *ani-1* RNAi, supporting redundancy in this process as well (Bernadskaya et al., 2012). Other pathways that also function during ventral enclosure include the netrin and ephrin pathways (Bernadskaya et al., 2012). In addition, ephrin and semaphorin pathways signal redundantly between specific subsets of neuroblasts and migrating pocket epidermal cells to mediate their migration for the final steps of ventral enclosure (Ghenea et al., 2005; Ikegami et al., 2012). Further, canonical Wnt signalling is responsible for a subset of neuroblast cell migrations along the anterior-posterior axis (Mentink et al., 2014). All of these pathways are candidates for regulating epidermal cell migration for lumen positioning. Identifying genes required for tissue-specific contributions to the regulation of anterior morphogenesis by tissue-specific RNAi or by using an auxin-inducible degradation system (AID), would provide us with immense insight as to which tissues send and/or receive cues to influence migration of the anterior epidermal cells.

4.3. Chapter 3 Conclusions

We found that cells with different fates have unique ring closure kinetics regulated by different mechanisms. Using *C. elegans* as a model system, our data showed that in P0 or P1 cells, the contractile ring takes longer to assemble compared to AB cells. We found that this is at least partly due to cell fate and partitioning of contractile ring components, but also is due to different threshold requirements for the Ran pathway components in AB vs. P1 cells. This work is the first to our knowledge to show that the Ran pathway can regulate cytokinesis in the *C. elegans* embryo. Further, we found that while anillin (ANI-1) is a target of this pathway in AB cells, it is not a target in P1 cells. This suggests that other cortical proteins could also be regulated by importin-binding.

Our lab found that the Ran pathway regulates cytokinesis in cultured human cells, by controlling the localization and function of anillin at the equatorial cortex (Beaudet et al., 2017; Beaudet et al., 2020). The NLS of anillin binds to importin-beta, and disruption of this binding causes delays in its cortical recruitment and causes cytokinesis failure (Beaudet et al., 2017; Beaudet et al., 2020). We proposed that since importins are free to bind to NLS-containing proteins in regions of the cell where Ran-GTP levels are low, this mechanism coordinates ring positioning with chromosome segregation. We also hypothesized that the Ran pathway is more strongly required in some cell types vs. others. The Ran pathway is likely redundant in symmetrically dividing cells with large spindles, but could be crucial in cells with different fates, where the spindle machinery is not symmetrically positioned and/or is less robust and requires more cortical regulation. We used *C. elegans* embryos as a model to test this hypothesis, to determine how the requirement for the Ran pathway varies with parameters such as cell fate. Specifically, we focused on AB and P1 cell division, since the cells have different fates, and had not been previously characterized for cytokinesis.

As outlined above, we found that P0, AB and P1 cells all have unique ring closure kinetics, but P0 and P1 were more alike in having a longer ring assembly phase compared to AB cells (Figure 20). This suggests that while each of these cells may require different mechanisms to control cytokinesis, similar mechanisms could control ring assembly in the P lineage. Indeed, this difference was at least partly fate-dependent, since depletion of polarity regulators (*par-1*, *par-3* and *par-6*) caused ring closure to be identical in the two daughter cells (Figure 2; Kemphues et al., 1988; Rose and Kemphues, 1998; Bowerman, 2000; Wu et al., 2018; Lim et al., 2021). We expected ring closure kinetics of the *par*-depleted P0 daughter cells to be a hybrid of those observed for control AB and P1 daughter cells, and perhaps even faster for multiple phases in *par*-

I depleted embryos, but surprisingly, they were all similar to each other, and to control AB cells (Guo and Kemphues, 1995; Rose and Kemphues, 1998). This supports the idea of different thresholds of myosin or its regulators contributing to different ring assembly kinetics, where P1 cells have the least myosin and take the longest, but as soon as you move above this threshold, varying levels all result in similar kinetics.

We further tested the idea of myosin thresholds contributing to differences in ring assembly by depleting regulators of contractility. As RhoA is a known regulator of cytokinesis and required for actomyosin contractility, we depleted embryos of *ect-2* (Rho-GEF) and *let-502* (Rho kinase) to determine if decreasing contractility further delays assembly in P1 cells, and/or causes AB cells to have kinetics more similar to P1 cells (Kosako et al. 2000; Piekny and Mains, 2002; Piekny et al., 2005; Green et al., 2012). While partial *ect-2* depletion caused delays in ring closure kinetics in both cell types, ring assembly was not distinctly altered in AB cells (Figure 22). Interestingly, depletion of *let-502* caused different phenotypes in AB vs. P1 cells. While all phases of ring closure were even more severely delayed in *let-502* RNAi AB cells, P1 cells displayed a bimodal distribution of ring closure phenotypes. While one set of cells had dramatic delays in ring assembly, supporting our threshold model, the other set of cells had ring closure kinetics similar to AB cells. This phenomenon was previously reported, where P1 cells completed division before AB cells in *let-502* mutant embryos, (Piekny and Mains, 2002). One possibility is that cell fate has been altered in a subset of cells, given the role of contractility in establishing anterior-posterior polarity. Despite this finding, the tendency to maintain distinct ring closure kinetics regardless of decreasing contractility in AB cells suggests that there are differences in the mechanisms that control these kinetics.

Our lab previously showed that the Ran pathway regulates cytokinesis in mammalian cells by sensing chromatin position (Beaudet et al., 2017; Beaudet et al., 2020) and we found that this pathway could regulate cytokinesis differently in AB vs. P1 cells. Since importin-binding was shown to facilitate anillin's cortical recruitment in cultured human cells, we expected that decreasing Ran-GTP levels could cause an increase in ring assembly in *C. elegans* cells. Indeed, depleting *ran-3*, which encodes RCC1 (Ran-GEF), caused ring closure kinetics to be the same in both AB and P1 cells, and to resemble a curve more similar to control AB cells with a rapid assembly phase (Figure 23). These kinetics were suppressed by co-depletion of *ect-2*, supporting that they occur due to changes in contractility (Figure 25). We also determined how depletion of *ima-3*, which encodes importin-alpha, affects ring closure kinetics. Since importins bind to the NLS of proteins, we expected to see the opposite effect and delays in ring assembly. Surprisingly, we observed the same phenotype as in *ran-3* RNAi embryos (Figure 24). Importins typically bind to the NLS sites of proteins as a heterodimer, with importin-alpha binding first and acting as an adaptor for importin-beta (Ozugergin and Piekny, 2021). However, our data from cultured human cells found that importin-beta could directly bind to the NLS of anillin (Beaudet et al., 2020). Other emerging studies suggest that the heterodimer could have different impacts on protein function vs. importin-alpha or -beta alone (Ozugergin and Piekny, 2021). This led us to propose that importin-beta could facilitate the function of cortical proteins, such as anillin, while the heterodimer could inhibit them. Therefore, reducing IMA-3 could free up additional IMB-1 to facilitate target protein function for ring assembly/cytokinesis. To test this model, we co-depleted *ima-3* and *imb-1*, and indeed found full suppression of rapid ring closure kinetics in AB cells, but intermediate suppression in P1 cells (data now shown) implying that the pathway could function differently and via different importins and target proteins in the two cell types. We also have further support for

this hypothesis, since *ani-1* depletion suppressed the rapid ring closure kinetics caused by *ran-3* depletion in AB cells, but not in P1 cells (Figure 26).

4.4. Chapter 3 Perspectives

The unique ring closure kinetics that we observed in AB vs. P1 cells lead us to the hypothesis that there are distinct mechanisms governing ring assembly and ingression in cells with different fates. Different ring assembly kinetics seem to be due, at least in part, to different levels of ring components or their regulators. This is supported by data showing that actin and myosin localization is more highly enriched in the furrow in AB vs. P1 cells (Ozugerin et al., *in revision*). Furthermore, as *ran-3* RNAi increased the rate of ring assembly and equalized ingression kinetics in AB vs. P1 cells, the Ran pathway could be responsible for and/or contribute to the mechanisms controlling ring assembly in cells with different fates. Additionally, the differential response to importin alpha/beta depletion in AB vs. P1 cells suggests that the Ran pathway functions differently in the two cell types. In support of this, we determined through our co-depletion experiments that the Ran pathway does not target anillin in P1 cells which demonstrates that there are other targets of this pathway in cells fated to become the germline. This data supports our model that the importin gradient controls multiple NLS-containing cortical proteins. Some well-characterized possible candidates include ECT-2, MKLP1, and CYK-4 (Mishima et al., 2002; Mishima et al., 2004; Bement et al., 2005; Yuce et al., 2005; Petronczki et al., 2007; Burkard et al., 2009; Wolfe et al., 2009). Moreover, unpublished data from our lab identified several proteins that interact with importin-beta during anaphase in human cells including moesin and septins.

References

- Achilleos, A., Wehman, A. M., & Nance, J. (2010). PAR-3 mediates the initial clustering and apical localization of junction and polarity proteins during *C. elegans* intestinal epithelial cell polarization. *Development*, *137*(11), 1833–1842. <https://doi.org/10.1242/dev.047647>
- Albertson, D. G., & Thomson, J. N. (1976). The Pharynx of *Caenorhabditis elegans*. *Philosophical Transactions of the Royal Society B: Biological Sciences*, *275*(938), 299–325. <https://doi.org/10.1098/rstb.1976.0085>
- Albertson, D. G. (1984). Formation of the first cleavage spindle in nematode embryos. *Developmental Biology*, *101*(1), 61–72. [https://doi.org/10.1016/0012-1606\(84\)90117-9](https://doi.org/10.1016/0012-1606(84)90117-9)
- Amann, K. J., & Pollard, T. D. (2000). Cellular regulation of actin network assembly. *Current Biology : CB*, *10*(20), R728-30. [https://doi.org/10.1016/s0960-9822\(00\)00751](https://doi.org/10.1016/s0960-9822(00)00751)
- Amini, R., Goupil, E., Labella, S., Zetka, M., Maddox, A. S., Labbé, J. C., & Chartier, N. T. (2014). *C. Elegans* Anillin proteins regulate intercellular bridge stability and germline syncytial organization. *Journal of Cell Biology*, *206*(1), 129–143. <https://doi.org/10.1083/jcb.201310117>
- Armenti, S. T., & Nance, J. (2012). Adherens junctions in *C. elegans* embryonic morphogenesis. *Sub-Cellular Biochemistry*, *60*, 279–299. https://doi.org/10.1007/978-94-007-4186-7_12
- Asan, A., Raiders, S. A., & Priess, J. R. (2016). Morphogenesis of the *C. elegans* Intestine Involves Axon Guidance Genes. *PLoS Genetics*, *12*(4). <https://doi.org/10.1371/journal.pgen.1005950>
- Barnes, K. M., Fan, L., Moyle, M. W., Brittin, C. A., Xu, Y., Colón-Ramos, D. A., ... Bao, Z. (2020). Cadherin preserves cohesion across involuting tissues during *C. Elegans* neurulation. *ELife*, *9*, 1–19. <https://doi.org/10.7554/eLife.58626>
- Basant, A., & Glotzer, M. (2018). Spatiotemporal Regulation of RhoA during Cytokinesis. *Current Biology. Curr Biol*. <https://doi.org/10.1016/j.cub.2018.03.045>
- Basant, A., Lekomtsev, S., Tse, Y. C., Zhang, D., Longhini, K. M., Petronczki, M., & Glotzer, M. (2015). Aurora B Kinase Promotes Cytokinesis by Inducing Centralspindlin Oligomers that Associate with the Plasma Membrane. *Developmental Cell*, *33*(2), 204–215. <https://doi.org/10.1016/j.devcel.2015.03.015>
- Bement, W. M., Benink, H. A., & Von Dassow, G. (2005). A microtubule-dependent zone of active RhoA during cleavage plane specification. *Journal of Cell Biology*, *170*(1), 91–101. <https://doi.org/10.1083/jcb.200501131>

- Bernadskaya, Y. Y., Wallace, A., Nguyen, J., Mohler, W. A., & Soto, M. C. (2012). UNC-40/DCC, SAX-3/Robo, and VAB-1/Eph Polarize F-Actin during Embryonic Morphogenesis by Regulating the WAVE/SCAR Actin Nucleation Complex. *PLoS Genetics*, 8(8), e1002863. <https://doi.org/10.1371/journal.pgen.1002863>
- Bertrand, V., Bisso, P., Poole, R. J., & Hobert, O. (2011). Notch-dependent induction of left/right asymmetry in *C. elegans* interneurons and motoneurons. *Current Biology*, 21(14), 1225–1231. <https://doi.org/10.1016/j.cub.2011.06.016>
- Blankenship, J. T., Backovic, S. T., Sanny, J. S. S. P., Weitz, O., & Zallen, J. A. (2006). Multicellular Rosette Formation Links Planar Cell Polarity to Tissue Morphogenesis. *Developmental Cell*, 11(4), 459–470. <https://doi.org/10.1016/j.devcel.2006.09.007>
- Bos, J. L., Rehmann, H., & Wittinghofer, A. (2007). GEFs and GAPs: Critical Elements in the Control of Small G Proteins. *Cell*. <https://doi.org/10.1016/j.cell.2007.05.018>
- Bossinger, O., Fukushige, T., Claeys, M., Borgonie, G., & McGhee, J. D. (2004). The apical disposition of the *Caenorhabditis elegans* intestinal terminal web is maintained by LET-413. *Developmental Biology*, 268(2), 448–456. <https://doi.org/10.1016/j.ydbio.2004.01.003>
- Bossinger, O., Wiesenfahrt, T., & Hoffmann, M. (2015). Establishment and maintenance of cell polarity in the *C. Elegans* Intestine. In *Cell Polarity 2: Role in Development and Disease* (pp. 33–65). Springer International Publishing. https://doi.org/10.1007/978-3-319-14466-5_2
- Bowerman, B. (2000). Embryonic polarity: Protein stability in asymmetric cell division. *Current Biology*. Current Biology Ltd. [https://doi.org/10.1016/S0960-9822\(00\)00660-6](https://doi.org/10.1016/S0960-9822(00)00660-6)
- Bowerman, B., & Shelton, C. A. (1999). Cell polarity in the early *Caenorhabditis elegans* embryo. *Current Opinion in Genetics and Development*, 9(4), 390–395. [https://doi.org/10.1016/S0959-437X\(99\)80059-8](https://doi.org/10.1016/S0959-437X(99)80059-8)
- Brenner, S. (1974). The genetics of *Caenorhabditis elegans*. *Genetics*, 77(1), 71–94.
- Bringmann, H., & Hyman, A. A. (2005). A cytokinesis furrow is positioned by two consecutive signals. *Nature*, 436(7051), 731–734. <https://doi.org/10.1038/nature03823>
- Burkard, M. E., Maciejowski, J., Rodriguez-Bravo, V., Repka, M., Lowery, D. M., Clauser, K. R., ... Jallepalli, P. V. (2009). Plk1 self-organization and priming phosphorylation of HsCYK-4 at the spindle midzone regulate the onset of division in human cells. *PLoS Biology*, 7(5). <https://doi.org/10.1371/journal.pbio.1000111>
- Cabernard, C., Prehoda, K. E., & Doe, C. Q. (2010). A spindle-independent cleavage furrow positioning pathway. *Nature*, 467(7311), 91–94. <https://doi.org/10.1038/nature09334>

- Campanale, J. P., Sun, T. Y., & Montell, D. J. (2017). Development and dynamics of cell polarity at a glance. *Journal of Cell Science*, *130*(7), 1201–1207. <https://doi.org/10.1242/jcs.188599>
- Chang, Y. C., Nalbant, P., Birkenfeld, J., Chang, Z. F., & Bokoch, G. M. (2008). 3GEF-H1 couples nocodazole-induced microtubule disassembly to cell contractility via RhoA. *Molecular Biology of the Cell*, *19*(5), 2147–2153. <https://doi.org/10.1091/mbc.E07-12-1269>
- Chapa-Y-Lazo, B., Hamanaka, M., Wray, A., Balasubramanian, M. K., & Mishima, M. (2020). Polar relaxation by dynein-mediated removal of cortical myosin II. *Journal of Cell Biology*, *219*(8). <https://doi.org/10.1083/jcb.201903080>
- Chin-Sang, I. D., George, S. E., Ding, M., Moseley, S. L., Lynch, A. S., & Chisholm, A. D. (1999). The ephrin VAB-2/EFN-1 functions in neuronal signaling to regulate epidermal morphogenesis in *C. elegans*. *Cell*, *99*(7), 781–790. [https://doi.org/10.1016/s0092-8674\(00\)81675-x](https://doi.org/10.1016/s0092-8674(00)81675-x)
- Chin-Sang, I. D., & Chisholm, A. D. (2000, December 1). Form of the worm: Genetics of epidermal morphogenesis in *C. elegans*. *Trends in Genetics*. Elsevier. [https://doi.org/10.1016/S0168-9525\(00\)02143-0](https://doi.org/10.1016/S0168-9525(00)02143-0)
- Chin-Sang, I. D., Moseley, S. L., Ding, M., Harrington, R. J., George, S. E., & Chisholm, A. D. (2002). The divergent *C. elegans* ephrin EFN-4 functions in embryonic morphogenesis in a pathway independent of the VAB-1 Eph receptor. *Development*, *129*(23), 5499–5510. <https://doi.org/10.1242/dev.00122>
- Chisholm, A. D., & Hardin, J. (2005). Epidermal morphogenesis. *WormBook : The Online Review of C. Elegans Biology*. <https://doi.org/10.1895/wormbook.1.35.1>
- Clarke, P. R., & Zhang, C. (2008). Spatial and temporal coordination of mitosis by Ran GTPase. *Nature Reviews Molecular Cell Biology*. *Nat Rev Mol Cell Biol*. <https://doi.org/10.1038/nrm2410>
- Colombo, K., Grill, S. W., Kimple, R. J., Willard, F. S., Siderovski, D. P., & Gönczy, P. (2003). Translation of polarity cues into asymmetric spindle positioning in *Caenorhabditis elegans* embryos. *Science*, *300*(5627), 1957–1961. <https://doi.org/10.1126/science.1084146>
- Cordova-Burgos, L., Patel, F. B., & Soto, M. C. (2021). E-cadherin/hmr-1 membrane enrichment is polarized by wave-dependent branched actin. *Journal of Developmental Biology*, *9*(2). <https://doi.org/10.3390/jdb9020019>
- Cortes, D. B., Dawes, A., Liu, J., Nickaeen, M., Strychalski, W., & Maddox, A. S. (2018). Unite to divide – How models and biological experimentation have come together to reveal mechanisms of cytokinesis. *Journal of Cell Science*. Company of Biologists Ltd. <https://doi.org/10.1242/jcs.203570>

- Costa, M., Raich, W., Agbunag, C., Leung, B., Hardin, J., & Priess, J. R. (1998). A putative catenin-cadherin system mediates morphogenesis of the *Caenorhabditis elegans* embryo. *Journal of Cell Biology*, *141*(1), 297–308. <https://doi.org/10.1083/jcb.141.1.297>
- Couwenbergs, C., Labbé, J. C., Goulding, M., Marty, T., Bowerman, B., & Gotta, M. (2007). Heterotrimeric G protein signaling functions with dynein to promote spindle positioning in *C. elegans*. *Journal of Cell Biology*, *179*(1), 15–22. <https://doi.org/10.1083/jcb.200707085>
- Cuenca, A. A., Schetter, A., Aceto, D., Kempfues, K., & Seydoux, G. (2003). Polarization of the *C. elegans* zygote proceeds via distinct establishment and maintenance phases. *Development*. *Development*. <https://doi.org/10.1242/dev.00284>
- Daniels, B. R., Dobrowsky, T. M., Perkins, E. M., Sun, S. X., & Wirtz, D. (2010). MEX-5 enrichment in the *C. elegans* early embryo mediated by differential diffusion. *Development*, *137*(15), 2579–2585. <https://doi.org/10.1242/dev.051326>
- Davies, T., Kim, H. X., Spica, N. R., Lesea-Pringle, B. J., Dumont, J., Shirasu-Hiza, M., & Canman, J. C. (2018). Cell-intrinsic and -extrinsic mechanisms promote cell-type-specific cytokinetic diversity. *ELife*, *7*. <https://doi.org/10.7554/eLife.36204>
- Davis, R. H. (2004). The age of model organisms. *Nature Reviews Genetics*. Nature Publishing Group. <https://doi.org/10.1038/nrg1250>
- Dechant, R., & Glotzer, M. (2003). Centrosome separation and central spindle assembly act in redundant pathways that regulate microtubule density and trigger cleavage furrow formation. *Developmental Cell*, *4*(3), 333–344. [https://doi.org/10.1016/S1534-5807\(03\)00057-1](https://doi.org/10.1016/S1534-5807(03)00057-1)
- Deng, M., Suraneni, P., Schultz, R. M., & Li, R. (2007). The Ran GTPase Mediates Chromatin Signaling to Control Cortical Polarity during Polar Body Extrusion in Mouse Oocytes. *Developmental Cell*, *12*(2), 301–308. <https://doi.org/10.1016/j.devcel.2006.11.008>
- Douglas, M. E., Davies, T., Joseph, N., & Mishima, M. (2010). Aurora B and 14-3-3 Coordinately Regulate Clustering of Centralspindlin during Cytokinesis. *Current Biology*, *20*(10), 927–933. <https://doi.org/10.1016/j.cub.2010.03.055>
- Draper, B. W., Mello, C. C., Bowerman, B., Hardin, J., & Priess, J. R. (1996). MEX-3 is a KH domain protein that regulates blastomere identity in early *C. elegans* embryos. *Cell*, *87*(2), 205–216. [https://doi.org/10.1016/S0092-8674\(00\)81339-2](https://doi.org/10.1016/S0092-8674(00)81339-2)
- Duncan, L. H., Moyle, M. W., Shao, L., Sengupta, T., Ikegami, R., Kumar, A., ... Colón-Ramos, D. A. (2019). Isotropic light-sheet microscopy and automated cell lineage analyses to catalogue *Caenorhabditis elegans* embryogenesis with subcellular resolution. *Journal of Visualized Experiments*, *2019*(148), e59533. <https://doi.org/10.3791/59533>

- Etemad-Moghadam, B., Guo, S., & Kemphues, K. J. (1995). Asymmetrically distributed PAR-3 protein contributes to cell polarity and spindle alignment in early *C. elegans* embryos. *Cell*, 83(5), 743–752. [https://doi.org/10.1016/0092-8674\(95\)90187-6](https://doi.org/10.1016/0092-8674(95)90187-6)
- Etienne-Manneville, S. (2004). Cdc42 - The centre of polarity. *Journal of Cell Science*. *J Cell Sci.* <https://doi.org/10.1242/jcs.01115>
- Eweis, D. S., & Plastino, J. (2020). Roles of actin in the morphogenesis of the early *Caenorhabditis elegans* embryo. *International Journal of Molecular Sciences*. *Int J Mol Sci.* <https://doi.org/10.3390/ijms21103652>
- Fan, L., Kovacevic, I., Heiman, M. G., & Bao, Z. (2019). A multicellular rosette-mediated collective dendrite extension. *ELife*, 8. <https://doi.org/10.7554/eLife.38065>
- Fay, D. S. (2005). The cell cycle and development: Lessons from *C. elegans*. *Seminars in Cell and Developmental Biology*. Elsevier Ltd. <https://doi.org/10.1016/j.semcdb.2005.02.002>
- Fotopoulos, N., Wernike, D., Chen, Y., Makil, N., Marte, A., & Piekny, A. (2013). *Caenorhabditis elegans* anillin (*ani-1*) regulates neuroblast cytokinesis and epidermal morphogenesis during embryonic development. *Developmental Biology*, 383(1), 61–74. <https://doi.org/10.1016/j.ydbio.2013.08.024>
- Francis, R., & Waterston, R. H. (1991). Muscle cell attachment in *Caenorhabditis elegans*. *Journal of Cell Biology*, 114(3), 465–479. <https://doi.org/10.1083/jcb.114.3.465>
- Fumoto, K., Kikuchi, K., Gon, H., & Kikuchi, A. (2012). Wnt5a signaling controls cytokinesis by correctly positioning ESCRT-III at the midbody. *Journal of Cell Science*, 125(20), 4822–4832. <https://doi.org/10.1242/jcs.108142>
- Gally, C., Wissler, F., Zahreddine, H., Quintin, S., Landmann, F., & Labouesse, M. (2009). Myosin II regulation during *C. elegans* embryonic elongation: LET-502/ROCK, MRCK-1 and PAK-1, three kinases with different roles. *Development (Cambridge, England)*, 136(18), 3109–3119. <https://doi.org/10.1242/dev.039412>
- Gan, W. J., & Motegi, F. (2021, January 18). Mechanochemical Control of Symmetry Breaking in the *Caenorhabditis elegans* Zygote. *Frontiers in Cell and Developmental Biology*. *Front Cell Dev Biol.* <https://doi.org/10.3389/fcell.2020.619869>
- Gaudet, J., & Mango, S. E. (2002). Regulation of organogenesis by the *Caenorhabditis elegans* FoxA protein PHA-4. *Science*, 295(5556), 821–825. <https://doi.org/10.1126/science.1065175>
- George, S. E., Simokat, K., Hardin, J., & Chisholm, A. D. (1998). The VAB-1 Eph receptor tyrosine kinase functions in neural and epithelial morphogenesis in *C. elegans*. *Cell*, 92(5), 633–643. [https://doi.org/10.1016/S0092-8674\(00\)81131-9](https://doi.org/10.1016/S0092-8674(00)81131-9)

- Gillard, G., Shafaq-Zadah, M., Nicolle, O., Damaj, R., Pećreáux, J., & Michaux, G. (2015). Control of E-cadherin apical localisation and morphogenesis by a SOAP-1/AP-1/clathrin pathway in *C. elegans* epidermal cells. *Development (Cambridge)*, *142*(9), 1684–1694. <https://doi.org/10.1242/dev.118216>
- Glotzer, M. (2001). Animal cell cytokinesis. In *Annual Review of Cell and Developmental Biology* (Vol. 17, pp. 351–386). Annu Rev Cell Dev Biol. <https://doi.org/10.1146/annurev.cellbio.17.1.351>
- Glotzer, M. (2009). Cytokinesis: GAP Gap. *Current Biology*. Curr Biol. <https://doi.org/10.1016/j.cub.2008.12.028>
- Glotzer, M. (2017). Cytokinesis in metazoa and fungi. *Cold Spring Harbor Perspectives in Biology*, *9*(10). <https://doi.org/10.1101/cshperspect.a022343>
- Glotzer, M. (2009). The 3Ms of central spindle assembly: Microtubules, motors and MAPs. *Nature Reviews Molecular Cell Biology*. NIH Public Access. <https://doi.org/10.1038/nrm2609>
- Goldstein, B., & Hird, S. N. (1996). Specification of the anteroposterior axis in *Caenorhabditis elegans*. *Development*, *122*(5), 1467–1474. <https://doi.org/10.1242/dev.122.5.1467>
- Goldstein, B., & Nance, J. (2020). *Caenorhabditis elegans* Gastrulation: A model for understanding how cells polarize, change shape, and journey toward the center of an embryo. *Genetics*, *214*(2), 265–277. <https://doi.org/10.1534/genetics.119.300240>
- Goley, E. D., & Welch, M. D. (2006). The ARP2/3 complex: An actin nucleator comes of age. *Nature Reviews Molecular Cell Biology*. Nat Rev Mol Cell Biol. <https://doi.org/10.1038/nrm2026>
- Gönczy, P., & Rose, L. S. (2005). Asymmetric cell division and axis formation in the embryo. *WormBook : The Online Review of C. Elegans Biology*. WormBook. <https://doi.org/10.1895/wormbook.1.30.1>
- Gotta, M., Abraham, M. C., & Ahringer, J. (2001). Cdc-42 controls early cell polarity and spindle orientation in *C. elegans*. *Current Biology*, *11*(7), 482–488. [https://doi.org/10.1016/S0960-9822\(01\)00142-7](https://doi.org/10.1016/S0960-9822(01)00142-7)
- Gotta, M., & Ahringer, J. (2001). Axis determination in *C. elegans*: Initiating and transducing polarity. *Current Opinion in Genetics and Development*. Curr Opin Genet Dev. [https://doi.org/10.1016/S0959-437X\(00\)00206-9](https://doi.org/10.1016/S0959-437X(00)00206-9)
- Green, R. A., Paluch, E., & Oegema, K. (2012). Cytokinesis in animal cells. *Annual Review of Cell and Developmental Biology*. Annu Rev Cell Dev Biol. <https://doi.org/10.1146/annurev-cellbio-101011-155718>

- Grill, S. W., Gönczy, P., Stelzer, E. H. K., & Hyman, A. A. (2001). Polarity controls forces governing asymmetric spindle positioning in the *Caenorhabditis elegans* embryo. *Nature*, *409*(6820), 630–633. <https://doi.org/10.1038/35054572>
- Guedes, S., & Priess, J. R. (1997). The *C. elegans* MEX-1 protein is present in germline blastomeres and is a P granule component. *Development*, *124*(3), 731–739. <https://doi.org/10.1242/dev.124.3.731>
- Guillot, C., & Lecuit, T. (2013). Adhesion Disengagement Uncouples Intrinsic and Extrinsic Forces to Drive Cytokinesis in Epithelial Tissues. *Developmental Cell*, *24*(3), 227–241. <https://doi.org/10.1016/j.devcel.2013.01.010>
- Guo, H., Xu, Y., Li, Q., Du, S., He, D., Wang, Q., & Huang, Y. (2019). Improved Machine Learning Approach for Wavefront Sensing. *Sensors (Basel, Switzerland)*, *19*(16). <https://doi.org/10.3390/s19163533>
- Guo, S., & Kemphues, K. J. (1995). *par-1*, a gene required for establishing polarity in *C. elegans* embryos, encodes a putative Ser/Thr kinase that is asymmetrically distributed. *Cell*, *81*(4), 611–620. [https://doi.org/10.1016/0092-8674\(95\)90082-9](https://doi.org/10.1016/0092-8674(95)90082-9)
- Guse, A., Mishima, M., & Glotzer, M. (2005). Phosphorylation of ZEN-4/MKLP1 by aurora B regulates completion of cytokinesis. *Current Biology*, *15*(8), 778–786. <https://doi.org/10.1016/j.cub.2005.03.041>
- Hardin, J., King, R., Thomas-Virnig, C., & Raich, W. B. (2008). Zygotic loss of ZEN-4/MKLP1 results in disruption of epidermal morphogenesis in the *C. elegans* embryo. *Developmental Dynamics*, *237*(3), 830–836. <https://doi.org/10.1002/DVDY.21455>
- Harding, M. J., McGraw, H. F., & Nechiporuk, A. (2014). The roles and regulation of multicellular rosette structures during morphogenesis. *Development (Cambridge, England)*, *141*(13), 2549–2558. <https://doi.org/10.1242/dev.101444>
- Harrell, J. R., & Goldstein, B. (2011). Internalization of multiple cells during *C. elegans* gastrulation depends on common cytoskeletal mechanisms but different cell polarity and cell fate regulators. *Developmental Biology*, *350*(1), 1–12. <https://doi.org/10.1016/j.ydbio.2010.09.012>
- Heisenberg, C. P., & Bellaïche, Y. (2013). XForces in tissue morphogenesis and patterning. *Cell*, *153*(5). <https://doi.org/10.1016/j.cell.2013.05.008>
- Hickson, G. R. X., & O'Farrell, P. H. (2008). Anillin: A pivotal organizer of the cytokinetic machinery. *Biochemical Society Transactions*. Biochem Soc Trans. <https://doi.org/10.1042/BST0360439>

- Hird, S. N., Paulsen, J. E., & Strome, S. (1996). Segregation of germ granules in living *Caenorhabditis elegans* embryos: Cell-type-specific mechanisms for cytoplasmic localisation. *Development*, *122*(4), 1303–1312. <https://doi.org/10.1242/dev.122.4.1303>
- Hobert, O. (2010). Neurogenesis in the nematode *Caenorhabditis elegans*. *WormBook : The Online Review of C. Elegans Biology*. <https://doi.org/10.1895/wormbook.1.12.2>
- Horner, M. A., Quintin, S., Domeier, M. E., Kimble, J., Labouesse, M., & Mango, S. E. (1998). *pha-4*, an HNF-3 homolog, specifies pharyngeal organ identity in *Caenorhabditis elegans*. *Genes and Development*, *12*(13), 1947–1952. <https://doi.org/10.1101/gad.12.13.1947>
- Hung, T. J., & Kemphues, K. J. (1999). PAR-6 is a conserved PDZ domain-containing protein that colocalizes with PAR-3 in *Caenorhabditis elegans* embryos. *Development (Cambridge, England)*, *126*(1), 127–135. Retrieved from <http://www.ncbi.nlm.nih.gov/pubmed/9834192>
- Ikegami, R., Simokat, K., Zheng, H., Brown, L., Garriga, G., Hardin, J., & Culotti, J. (2012). Semaphorin and Eph receptor signaling guide a series of cell movements for ventral enclosure in *C. elegans*. *Current Biology : CB*, *22*(1), 1–11. <https://doi.org/10.1016/j.cub.2011.12.009>
- Jacinto, A., Martinez-Arias, A., & Martin, P. (2001). Mechanisms of epithelial fusion and repair. *Nature Cell Biology*. <https://doi.org/10.1038/35074643>
- Jantsch-Plunger, V., Gönczy, P., Romano, A., Schnabel, H., Hamill, D., Schnabel, R., ... Glotzer, M. (2000). CYK-4: A Rho family GTPase activating protein (GAP) required for central spindle formation and cytokinesis. *Journal of Cell Biology*, *149*(7), 1391–1404. <https://doi.org/10.1083/jcb.149.7.1391>
- Jewett, C. E., & Prekeris, R. (2018). Insane in the apical membrane: Trafficking events mediating apicobasal epithelial polarity during tube morphogenesis. *Traffic*. Blackwell Munksgaard. <https://doi.org/10.1111/tra.12579>
- Jiang, T., David, D. J. V., & Harris, T. J. C. (2015). Epithelial apicobasal polarity in the drosophila embryo. In *Cell Polarity I: Biological Role and Basic Mechanisms* (pp. 167–187). Springer International Publishing. https://doi.org/10.1007/978-3-319-14463-4_7
- Jordan, S. N., Davies, T., Zhuravlev, Y., Dumont, J., Shirasu-Hiza, M., & Canman, J. C. (2016). Cortical PAR polarity proteins promote robust cytokinesis during asymmetric cell division. *Journal of Cell Biology*, *212*(1), 39–49. <https://doi.org/10.1083/jcb.201510063>
- Kalab, P., & Heald, R. (2008). The RanGTP gradient - A GPS for the mitotic spindle. *Journal of Cell Science*, *121*(10), 1577–1586. <https://doi.org/10.1242/jcs.005959>
- Kaláb, P., Pralle, A., Isacoff, E. Y., Heald, R., & Weis, K. (2006). Analysis of a RanGTP-regulated gradient in mitotic somatic cells. *Nature*, *440*(7084), 697–701. <https://doi.org/10.1038/nature04589>

- Kalb, J. M., Lau, K. K., Goszczynski, B., Fukushige, T., Moons, D., Okkema, P. G., & McGhee, J. D. (1998). pha-4 is Ce-fkh-1, a fork head/HNF-3alpha, beta, gamma homolog that functions in organogenesis of the *C. elegans* pharynx. *Development*, *125*(12).
- Kamath, R. S., Martinez-Campos, M., Zipperlen, P., Fraser, A. G., & Ahringer, J. (2001). Effectiveness of specific RNA-mediated interference through ingested double-stranded RNA in *Caenorhabditis elegans*. *Genome Biology*, *2*(1), research0002.1. <https://doi.org/10.1186/gb-2000-2-1-research0002>
- Kardon, J. R., & Vale, R. D. (2009). Regulators of the cytoplasmic dynein motor. *Nature Reviews Molecular Cell Biology*. *Nat Rev Mol Cell Biol*. <https://doi.org/10.1038/nrm2804>
- Kemphues, K. J., Priess, J. R., Morton, D. G., & Cheng, N. S. (1988). Identification of genes required for cytoplasmic localization in early *C. elegans* embryos. *Cell*, *52*(3), 311–320. [https://doi.org/10.1016/S0092-8674\(88\)80024-2](https://doi.org/10.1016/S0092-8674(88)80024-2)
- Kemphues, K. J., & Strome, S. (1997). Fertilization and Establishment of Polarity in the Embryo. In *C. elegans II* (pp. 335–359). Retrieved from <https://pubmed.ncbi.nlm.nih.gov/21413241/>
- Kimura, K., & Kimura, A. (2020). Cytoplasmic streaming drifts the polarity cue and enables posteriorization of the *Caenorhabditis elegans* zygote at the side opposite of sperm entry. *Molecular Biology of the Cell*, *31*(16), 1765–1773. <https://doi.org/10.1091/mbc.E20-01-0058>
- Kiyomitsu, T., & Cheeseman, I. M. (2013). XCortical dynein and asymmetric membrane elongation coordinately position the spindle in anaphase. *Cell*, *154*(2), 391. <https://doi.org/10.1016/j.cell.2013.06.010>
- Kosako, H., Yoshida, T., Matsumura, F., Ishizaki, T., Narumiya, S., & Inagaki, M. (2000). Rho-kinase/ROCK is involved in cytokinesis through the phosphorylation of myosin light chain and not ezrin/radixin/moesin proteins at the cleavage furrow. *Oncogene*, *19*(52), 6059–6064. <https://doi.org/10.1038/sj.onc.1203987>
- Kotak, S., & Gönczy, P. (2013). Mechanisms of spindle positioning: Cortical force generators in the limelight. *Current Opinion in Cell Biology*. *Curr Opin Cell Biol*. <https://doi.org/10.1016/j.ceb.2013.07.008>
- Kotýnková, K., Su, K. C., West, S. C., & Petronczki, M. (2016). Plasma Membrane Association but Not Midzone Recruitment of RhoGEF ECT2 Is Essential for Cytokinesis. *Cell Reports*, *17*(10), 2672–2686. <https://doi.org/10.1016/j.celrep.2016.11.029>
- Kozłowski, C., Srayko, M., & Nedelec, F. (2007). Cortical Microtubule Contacts Position the Spindle in *C. elegans* Embryos. *Cell*, *129*(3), 499–510. <https://doi.org/10.1016/j.cell.2007.03.027>

- Kumar, A., Wu, Y., Christensen, R., Chandris, P., Gandler, W., McCreedy, E., ... Shroff, H. (2014). Dual-view plane illumination microscopy for rapid and spatially isotropic imaging. *Nature Protocols*, 9(11), 2555–2573. <https://doi.org/10.1038/nprot.2014.172>
- Labbé, J.-C., McCarthy, E. K., & Goldstein, B. (2004). The forces that position a mitotic spindle asymmetrically are tethered until after the time of spindle assembly. *Journal of Cell Biology*, 167(2), 245–256. <https://doi.org/10.1083/JCB.200406008>
- Labouesse, M. (2006). Epithelial junctions and attachments. *WormBook: The Online Review of C. Elegans Biology*, 1–21. <https://doi.org/10.1895/wormbook.1.56.1>
- Landmann, F., Quintin, S., & Labouesse, M. (2004). Multiple regulatory elements with spatially and temporally distinct activities control the expression of the epithelial differentiation gene *lin-26* in *C. elegans*. *Developmental Biology*, 265(2), 478–490. <https://doi.org/10.1016/J.YDBIO.2003.09.009>
- Lardennois, A., Pásti, G., Ferraro, T., Llense, F., Mahou, P., Pontabry, J., ... Labouesse, M. (2019). An actin-based viscoplastic lock ensures progressive body-axis elongation. *Nature*, 573(7773), 266–270. <https://doi.org/10.1038/s41586-019-1509-4>
- Lecaudey, V., Cakan-Akdogan, G., Norton, W. H. J., & Gilmour, D. (2008). Dynamic Fgf signaling couples morphogenesis and migration in the zebrafish lateral line primordium. *Development*, 135(16), 2695–2705. <https://doi.org/10.1242/dev.025981>
- Lekomtsev, S., Su, K. C., Pye, V. E., Blight, K., Sundaramoorthy, S., Takaki, T., ... Petronczki, M. (2012). Centralspindlin links the mitotic spindle to the plasma membrane during cytokinesis. *Nature*, 492(7428), 276–279. <https://doi.org/10.1038/nature11773>
- Leonelli, S., & Ankeny, R. A. (2012). Re-thinking organisms: The impact of databases on model organism biology. *Studies in History and Philosophy of Science Part C: Studies in History and Philosophy of Biological and Biomedical Sciences*, 43(1), 29–36. <https://doi.org/10.1016/j.shpsc.2011.10.003>
- Leung, B., Hermann, G. J., & Priess, J. R. (1999). Organogenesis of the *Caenorhabditis elegans* Intestine. *Developmental Biology*, 216(1), 114–134. <https://doi.org/10.1006/dbio.1999.9471>
- Lewellyn, L., Dumont, J., Desai, A., & Oegema, K. (2010). Analyzing the effects of delaying aster separation on furrow formation during cytokinesis in the *Caenorhabditis elegans* embryo. *Molecular Biology of the Cell*, 21(1), 50–62. <https://doi.org/10.1091/mbc.E09-01-0089>
- Lim, Y. W., Wen, F. L., Shankar, P., Shibata, T., & Motegi, F. (2021). A balance between antagonizing PAR proteins specifies the pattern of asymmetric and symmetric divisions in *C. elegans* embryogenesis. *Cell Reports*, 36(1). <https://doi.org/10.1016/j.celrep.2021.109326>

- Maddox, A. S., Habermann, B., Desai, A., & Oegema, K. (2005). Distinct roles for two C. elegans anillins in the gonad and early embryo. *Development*, *132*(12), 2837–2848. <https://doi.org/10.1242/dev.01828>
- Maddox, A. S., Lewellyn, L., Desai, A., & Oegema, K. (2007). Anillin and the Septins Promote Asymmetric Ingression of the Cytokinetic Furrow. *Developmental Cell*, *12*(5), 827–835. <https://doi.org/10.1016/j.devcel.2007.02.018>
- Mangal, S., Sacher, J., Kim, T., Osório, D. S., Motegi, F., Carvalho, A. X., ... Zanin, E. (2018). TPXL-1 activates Aurora A to clear contractile ring components from the polar cortex during cytokinesis. *Journal of Cell Biology*, *217*(3), 837–848. <https://doi.org/10.1083/jcb.201706021>
- Mango, S. E. (2009). The molecular basis of organ formation: insights from the C. elegans foregut. *Annual Review of Cell and Developmental Biology*, *25*, 597–628. <https://doi.org/10.1146/annurev.cellbio.24.110707.175411>
- Mango, S. E. (2007). The C. elegans pharynx: a model for organogenesis. *WormBook: The Online Review of C. Elegans Biology*. WormBook. <https://doi.org/10.1895/wormbook.1.129.1>
- Mango, S. E., Lambie, E. J., & Kimble, J. (1994). The pha-4 gene is required to generate the pharyngeal primordium of Caenorhabditis elegans. *Development*, *120*(10), 3019–3031. <https://doi.org/10.1242/dev.120.10.3019>
- Manolaridis, I., Kulkarni, K., Dodd, R. B., Ogasawara, S., Zhang, Z., Bineva, G., ... Barford, D. (2013). Mechanism of farnesylated CAAX protein processing by the intramembrane protease Rce1. *Nature*, *504*(7479), 301–305. <https://doi.org/10.1038/nature12754>
- Martin, A. C., & Goldstein, B. (2014). Apical constriction: themes and variations on a cellular mechanism driving morphogenesis. *Development*, *141*(10), 1987–1998. <https://doi.org/10.1242/dev.102228>
- Matsumura, F. (2005). Regulation of myosin II during cytokinesis in higher eukaryotes. *Trends in Cell Biology*. Trends Cell Biol. <https://doi.org/10.1016/j.tcb.2005.05.004>
- Matsumura, F., & Hartshorne, D. J. (2008). Myosin phosphatase target subunit: Many roles in cell function. *Biochemical and Biophysical Research Communications*, *369*(1), 149–156. <https://doi.org/10.1016/j.bbrc.2007.12.090>
- McMahon, L., Legouis, R., Vonesch, J. L., & Labouesse, M. (2001). Assembly of C. elegans apical junctions involves positioning and compaction by LET-413 and protein aggregation by the MAGUK protein DLG-1. *Journal of Cell Science*, *114*(Pt 12), 2265–2277. Retrieved from <http://www.ncbi.nlm.nih.gov/pubmed/11493666>

- Mishima, M., Kaitna, S., & Glotzer, M. (2002). Central spindle assembly and cytokinesis require a kinesin-like protein/RhoGAP complex with microtubule bundling activity. *Developmental Cell*, 2(1), 41–54. [https://doi.org/10.1016/S1534-5807\(01\)00110-1](https://doi.org/10.1016/S1534-5807(01)00110-1)
- Mishima, M., Pavicic, V., Grüneberg, U., Nigg, E. A., & Glotzer, M. (2004). Cell cycle regulation of central spindle assembly. *Nature*, 430(7002), 908–913. <https://doi.org/10.1038/nature02767>
- Morton, D. G., Hoose, W. A., & Kempfues, K. J. (2012). A genome-wide RNAi screen for enhancers of par mutants reveals new contributors to early embryonic polarity in *Caenorhabditis elegans*. *Genetics*, 192(3), 929–942. <https://doi.org/10.1534/genetics.112.143727>
- Motegi, F., Plachta, N., & Viasnoff, V. (2020). Novel approaches to link apicobasal polarity to cell fate specification. *Current Opinion in Cell Biology*. Elsevier Ltd. <https://doi.org/10.1016/j.ceb.2019.09.003>
- Motegi, F., & Sugimoto, A. (2006). Sequential functioning of the ECT-2 RhoGEF, RHO-1 and CDC-42 establishes cell polarity in *Caenorhabditis elegans* embryos. *Nature Cell Biology*, 8(9), 978–985. <https://doi.org/10.1038/ncb1459>
- Müller, H. A. J., & Bossinger, O. (2003). Molecular networks controlling epithelial cell polarity in development. *Mechanisms of Development*. Elsevier Ireland Ltd. <https://doi.org/10.1016/j.mod.2003.06.001>
- Munro, E., Nance, J., & Priess, J. R. (2004). Cortical Flows Powered by Asymmetrical Contraction Transport PAR Proteins to Establish and Maintain Anterior-Posterior Polarity in the Early *C. elegans* Embryo the anterior cortex and are thus called the anterior PAR complex (Boyd et al The initial cue that determines polarity in the newly fertilized embryo is unknown, but meshwork away from the site of sperm entry, that the. *Developmental Cell*, 7, 413–424. Retrieved from <http://www.developmentalcell.com/cgi/content/>
- Nakao, F., Hudson, M. L., Suzuki, M., Peckler, Z., Kurokawa, R., Liu, Z., ... Takagi, S. (2007). The plexin PLX-2 and the ephrin EFN-4 have distinct roles in MAB-20/semaphorin 2A signaling in *Caenorhabditis elegans* morphogenesis. *Genetics*, 176(3), 1591–1607. <https://doi.org/10.1534/genetics.106.067116>
- Nance, J. (2005). PAR proteins and the establishment of cell polarity during *C. elegans* development. *BioEssays*. Bioessays. <https://doi.org/10.1002/bies.20175>
- Nance, J., Lee, J. Y., & Goldstein, B. (2005). Gastrulation in *C. elegans*. *WormBook : The Online Review of C. Elegans Biology*. WormBook. <https://doi.org/10.1895/wormbook.1.23.1>
- Nance, J., Munro, E. M., & Priess, J. R. (2003). *C. elegans* PAR-3 and PAR-6 are required for apicobasal asymmetries associated with cell adhesion and gastrulation. *Development*, 130(22), 5339–5350. <https://doi.org/10.1242/dev.00735>

- Nance, J., & Priess, J. R. (2002). Cell polarity and gastrulation in *C. elegans*. *Development*. <https://doi.org/10.1242/dev.129.2.387>
- Nechiporuk, A., & Raible, D. W. (2008). FGF-dependent mechanosensory organ patterning in zebrafish. *Science (New York, N.Y.)*, *320*(5884), 1774–1777. <https://doi.org/10.1126/science.1156547>
- Nguyen-Ngoc, T., Afshar, K., & Gönczy, P. (2007). Coupling of cortical dynein and Ga proteins mediates spindle positioning in *Caenorhabditis elegans*. *Nature Cell Biology*, *9*(11), 1294–1302. <https://doi.org/10.1038/ncb1649>
- Oegema, K., & Hyman, A. A. (2006). Cell division. <https://doi.org/10.1895/wormbook.1.72.1>
- Osorio, D., Chan, F., Saramago, J., Leite, J., Silva, A., Sobral, A., ... Carvalho, A. (2018). Flow-independent accumulation of motor-competent non-muscle myosin II in the contractile ring is essential for cytokinesis. *BioRxiv*, 333286. <https://doi.org/10.1101/333286>
- Ozugerin, I., & Piekny, A. (2021). Complementary functions for the Ran gradient during division. *Small GTPases*. <https://doi.org/10.1080/21541248.2020.1725371>
- Page, B. D., Zhang, W., Steward, K., Blumenthal, T., & Priess, J. R. (1997). *Elt-1*, a Gata-like transcription factor, is required for epidermal cell fates in *caenorhabditis elegans* embryos. *Genes and Development*, *11*(13), 1651–1661. <https://doi.org/10.1101/gad.11.13.1651>
- Pantaloni, D., & Carlier, M. F. (1993). How profilin promotes actin filament assembly in the presence of thymosin β 4. *Cell*, *75*(5), 1007–1014. [https://doi.org/10.1016/0092-8674\(93\)90544-Z](https://doi.org/10.1016/0092-8674(93)90544-Z)
- Pásti, G., & Labouesse, M. (2015). Epithelial junctions, cytoskeleton, and polarity *. <https://doi.org/10.1895/wormbook.1.56.2>
- Patel, F. B., Bernadskaya, Y. Y., Chen, E., Jobanputra, A., Pooladi, Z., Freeman, K. L., ... Soto, M. C. (2008). The WAVE/SCAR complex promotes polarized cell movements and actin enrichment in epithelia during *C. elegans* embryogenesis. *Developmental Biology*, *324*(2), 297–309. <https://doi.org/10.1016/j.ydbio.2008.09.023>
- Patel, F. B., & Soto, M. C. (2013). WAVE/SCAR promotes endocytosis and early endosome morphology in polarized *C. elegans* epithelia. *Developmental Biology*, *377*(2), 319–332. <https://doi.org/10.1016/j.ydbio.2013.03.012>
- Paul, A., & Pollard, T. (2008). The Role of the FH1 Domain and Profilin in Formin-Mediated Actin-Filament Elongation and Nucleation. *Current Biology*, *18*(1), 9–19. <https://doi.org/10.1016/j.cub.2007.11.062>
- Petronczki, M., Glotzer, M., Kraut, N., & Peters, J. M. (2007). Polo-like Kinase 1 Triggers the Initiation of Cytokinesis in Human Cells by Promoting Recruitment of the RhoGEF Ect2 to

- the Central Spindle. *Developmental Cell*, 12(5), 713–725.
<https://doi.org/10.1016/j.devcel.2007.03.013>
- Piekny, A. J., Wissmann, A., & Mains, P. E. (2000). Embryonic morphogenesis in *Caenorhabditis elegans* integrates the activity of LET-502 Rho-binding kinase, MEL-11 myosin phosphatase, DAF-2 insulin receptor and FEM-2 PP2c phosphatase. *Genetics*, 156(4), 1671–1689. <https://doi.org/10.1093/genetics/156.4.1671>
- Piekny, A. J., & Glotzer, M. (2008). Anillin Is a Scaffold Protein That Links RhoA, Actin, and Myosin during Cytokinesis. *Current Biology*, 18(1), 30–36.
<https://doi.org/10.1016/j.cub.2007.11.068>
- Piekny, A. J., Johnson, J. L. F., Cham, G. D., & Mainz, P. E. (2003). The *Caenorhabditis elegans* nonmuscle myosin genes *nmy-1* and *nmy-2* function as redundant components of the let-502/Rho-binding kinase and mel-11/myosin phosphatase pathway during embryonic morphogenesis. *Development*, 130(23), 5695–5704. <https://doi.org/10.1242/dev.00807>
- Piekny, A. J., & Maddox, A. S. (2010). The myriad roles of Anillin during cytokinesis. *Seminars in Cell and Developmental Biology*. Elsevier Ltd.
<https://doi.org/10.1016/j.semcd.2010.08.002>
- Piekny, A. J., & Mains, P. E. (2002). Rho-binding kinase (LET-502) and myosin phosphatase (MEL-11) regulate cytokinesis in the early *Caenorhabditis elegans* embryo. *Journal of Cell Science*, 115(11), 2271–2282. <https://doi.org/10.1242/jcs.115.11.2271>
- Piekny, A. J., & Mains, P. E. (2002). Rho-binding kinase (LET-502) and myosin phosphatase (MEL-11) regulate cytokinesis in the early *Caenorhabditis elegans* embryo. *Journal of Cell Science*, 115(11), 2271–2282. <https://doi.org/10.1242/JCS.115.11.2271>
- Piekny, A., Werner, M., & Glotzer, M. (2005, December). Cytokinesis: Welcome to the Rho zone. *Trends in Cell Biology*. Trends Cell Biol. <https://doi.org/10.1016/j.tcb.2005.10.006>
- Pintard, L., & Bowerman, B. (2019). Mitotic cell division in *Caenorhabditis elegans*. *Genetics*, 211(1), 35–73. <https://doi.org/10.1534/genetics.118.301367>
- Pollard, T. D., Blanchoin, L., & Mullins, R. D. (2000). Molecular mechanisms controlling actin filament dynamics in nonmuscle cells. *Annual Review of Biophysics and Biomolecular Structure*. Annu Rev Biophys Biomol Struct.
<https://doi.org/10.1146/annurev.biophys.29.1.545>
- Portereiko, M. F., Saam, J., & Mango, S. E. (2004). ZEN-4/MKLP1 Is Required to Polarize the Foregut Epithelium. *Current Biology*, 14(11), 932–941.
<https://doi.org/10.1016/j.cub.2004.05.052>
- Portereiko, M. F., & Mango, S. E. (2001). Early morphogenesis of the *Caenorhabditis elegans* pharynx. *Developmental Biology*, 233(2), 482–494. <https://doi.org/10.1006/dbio.2001.0235>

- Priess, J. R., & Hirsh, D. I. (1986). *Caenorhabditis elegans* morphogenesis: The role of the cytoskeleton in elongation of the embryo. *Developmental Biology*, *117*(1), 156–173. [https://doi.org/10.1016/0012-1606\(86\)90358-1](https://doi.org/10.1016/0012-1606(86)90358-1)
- Prokopenko, S. N., Brumby, A., O’Keefe, L., Prior, L., He, Y., Saint, R., & Bellen, H. J. (1999). A putative exchange factor for Rho1 GTPase is required for initiation of cytokinesis in *Drosophila*. *Genes and Development*, *13*(17), 2301–2314. <https://doi.org/10.1101/gad.13.17.2301>
- Rai, A. K., Rai, A., Ramaiya, A. J., Jha, R., & Mallik, R. (2013). Molecular adaptations allow dynein to generate large collective forces inside cells. *Cell*, *152*(1–2), 172–182. <https://doi.org/10.1016/j.cell.2012.11.044>
- Rappaport, R. (1971). Cytokinesis in Animal Cells. *International Review of Cytology*, *31*(C), 169–214. [https://doi.org/10.1016/S0074-7696\(08\)60059-5](https://doi.org/10.1016/S0074-7696(08)60059-5)
- Rapti, G., Li, C., Shan, A., Lu, Y., & Shaham, S. (2017). Glia initiate brain assembly through noncanonical Chimaerin–Furin axon guidance in *C. elegans*. *Nature Neuroscience* *20:10*, *20*(10), 1350–1360. <https://doi.org/10.1038/nn.4630>
- Rasmussen, J. P., Reddy, S. S., & Priess, J. R. (2012). Laminin is required to orient epithelial polarity in the *C. elegans* pharynx. *Development (Cambridge, England)*, *139*(11), 2050–2060. <https://doi.org/10.1242/dev.078360>
- Reyes, C. C., Jin, M., Breznau, E. B., Espino, R., Delgado-Gonzalo, R., Goryachev, A. B., & Miller, A. L. (2014). Anillin regulates cell-cell junction integrity by organizing junctional accumulation of Rho-GTP and actomyosin. *Current Biology*, *24*(11), 1263–1270. <https://doi.org/10.1016/j.cub.2014.04.021>
- Ridley, A. J. (2011). Life at the leading edge. *Cell*. <https://doi.org/10.1016/j.cell.2011.06.010>
- Roberts, P. J., Mitin, N., Keller, P. J., Chenette, E. J., Madigan, J. P., Currin, R. O., ... Der, C. J. (2008). Rho family GTPase modification and dependence on CAAX motif-signaled posttranslational modification. *Journal of Biological Chemistry*, *283*(37), 25150–25163. <https://doi.org/10.1074/jbc.M800882200>
- Rodrigues, N. T. L., Lekomtsev, S., Jananji, S., Kriston-Vizi, J., Hickson, G. R. X., & Baum, B. (2015). Kinetochore-localized PP1-Sds22 couples chromosome segregation to polar relaxation. *Nature*, *524*(7566), 489–492. <https://doi.org/10.1038/nature14496>
- Rojas, R., Ruiz, W. G., Leung, S. M., Jou, T. S., & Apodaca, G. (2001). Cdc42-dependent modulation of tight junctions and membrane protein traffic in polarized Madin-Darby canine kidney cells. *Molecular Biology of the Cell*, *12*(8), 2257–2274. <https://doi.org/10.1091/mbc.12.8.2257>

- Rose, L. S., & Kemphues, K. J. (1998). Early patterning of the *C. elegans* embryo. *Annual Review of Genetics*. *Annu Rev Genet*. <https://doi.org/10.1146/annurev.genet.32.1.521>
- Rose, L. S., Lamb, M. L., Hird, S. N., & Kemphues, K. J. (1995). Pseudocleavage Is Dispensable for Polarity and Development in *C. elegans* Embryos. *Developmental Biology*, *168*(2), 479–489. <https://doi.org/10.1006/dbio.1995.1096>
- Rose, L., & Gönczy, P. (2014). Polarity establishment, asymmetric division and segregation of fate determinants in early *C. elegans* embryos. *WormBook : The Online Review of C. Elegans Biology*. WormBook. <https://doi.org/10.1895/wormbook.1.30.2>
- Roubinet, C., Decelle, B., Chicanne, G., Dorn, J. F., Payrastra, B., Payre, F., & Carreno, S. (2011). Molecular networks linked by Moesin drive remodeling of the cell cortex during mitosis. *Journal of Cell Biology*, *195*(1), 99–112. <https://doi.org/10.1083/jcb.201106048>
- Roy, P. J., Zheng, H., Warren, C. E., & Culotti, J. G. (2000). *mab-20* encodes Semaphorin-2a and is required to prevent ectopic cell contacts during epidermal morphogenesis in *Caenorhabditis elegans*. *Development*, *127*(4).
- Sasidharan, S., Borinskaya, S., Patel, F., Bernadskaya, Y., Mandalapu, S., Agapito, M., & Soto, M. C. (2018). WAVE regulates Cadherin junction assembly and turnover during epithelial polarization. *Developmental Biology*, *434*(1), 133–148. <https://doi.org/10.1016/j.ydbio.2017.12.002>
- Sawa, M., Suetsugu, S., Sugimoto, A., Miki, H., Yamamoto, M., & Takenawa, T. (2003). Essential role of the *C. elegans* Arp2/3 complex in cell migration during ventral enclosure. *Journal of Cell Science*. The Company of Biologists Ltd. <https://doi.org/10.1242/jcs.00362>
- Sawyer, J. M., Harrell, J. R., Shemer, G., Sullivan-Brown, J., Roh-Johnson, M., & Goldstein, B. (2010). Apical constriction: A cell shape change that can drive morphogenesis. *Developmental Biology*, *341*(1), 5–19. <https://doi.org/10.1016/j.ydbio.2009.09.009>
- Schonegg, S., & Hyman, A. A. (2006). CDC-42 and RHO-1 coordinate actomyosin contractility and PAR protein localization during polarity establishment in *C. elegans* embryos. *Development*, *133*(18), 3507–3516. <https://doi.org/10.1242/dev.02527>
- Schroer, T. A. (2004). Dynactin. *Annual Review of Cell and Developmental Biology*. *Annu Rev Cell Dev Biol*. <https://doi.org/10.1146/annurev.cellbio.20.012103.094623>
- Sedzinski, J., Biro, M., Oswald, A., Tinevez, J. Y., Salbreux, G., & Paluch, E. (2011). Polar actomyosin contractility destabilizes the position of the cytokinetic furrow. *Nature*, *476*(7361), 462–468. <https://doi.org/10.1038/nature10286>
- Severson, A. F., & Bowerman, B. (2003). Myosin and the PAR proteins polarize microfilament-dependent forces that shape and position mitotic spindles in *Caenorhabditis elegans*. *The*

Journal of Cell Biology JCB The Journal of Cell Biology, 161(1), 21–26.
<https://doi.org/10.1083/jcb.200210171>

- Shafaq-Zadah, M., Brocard, L., Solari, F., & Michaux, G. (2012). AP-1 is required for the maintenance of apico-basal polarity in the *C. elegans* intestine. *Development*, 139(11), 2061–2070. <https://doi.org/10.1242/dev.076711>
- Shah, P. K., Tanner, M. R., Kovacevic, I., Rankin, A., Marshall, T. E., Noblett, N., ... Colavita, A. (2017). PCP and SAX-3/Robo Pathways Cooperate to Regulate Convergent Extension-Based Nerve Cord Assembly in *C. elegans*. *Developmental Cell*, 41(2), 195-203.e3. <https://doi.org/10.1016/j.devcel.2017.03.024>
- Shelton, C. A., Carter, J. C., Ellis, G. C., & Bowerman, B. (1999). The nonmuscle myosin regulatory light chain gene *mlc-4* is required for cytokinesis, anterior-posterior polarity, and body morphology during *Caenorhabditis elegans* embryogenesis. *Journal of Cell Biology*, 146(2), 439–451. <https://doi.org/10.1083/jcb.146.2.439>
- Singh, D., & Pohl, C. (2014). A function for the midbody remnant in embryonic patterning. *Communicative and Integrative Biology*, 7(4). <https://doi.org/10.4161/cib.28533>
- Soeda, S., Nakayama, Y., Honda, T., Aoki, A., Tamura, N., Abe, K., ... Yamaguchi, N. (2013). V-Src causes delocalization of Mklp1, Aurora B, and INCENP from the spindle midzone during cytokinesis failure. *Experimental Cell Research*, 319(10), 1382–1397. <https://doi.org/10.1016/j.yexcr.2013.02.023>
- Soto, M. C., Qadota, H., Kasuya, K., Inoue, M., Tsuboi, D., Mello, C. C., & Kaibuchi, K. (2002). The GEX-2 and GEX-3 proteins are required for tissue morphogenesis and cell migration in *C. elegans*. *Genes and Development*, 16(5), 620–632. <https://doi.org/10.1101/gad.955702>
- Straight, A. F., Field, C. M., & Mitchison, T. J. (2005). Anillin binds nonmuscle myosin II and regulates the contractile ring. *Molecular Biology of the Cell*, 16(1), 193–201. <https://doi.org/10.1091/mbc.E04-08-0758>
- Strome, S., & Wood, W. B. (1982). Immunofluorescence visualization of germ-line-specific cytoplasmic granules in embryos, larvae, and adults of *Caenorhabditis elegans*. *Proceedings of the National Academy of Sciences of the United States of America*, 79(5), 1558–1562. <https://doi.org/10.1073/pnas.79.5.1558>
- Sulston, J. E., Schierenberg, E., White, J. G., & Thomson, J. N. (1983). The embryonic cell lineage of the nematode *Caenorhabditis elegans*. *Developmental Biology*, 100(1), 64–119. [https://doi.org/10.1016/0012-1606\(83\)90201-4](https://doi.org/10.1016/0012-1606(83)90201-4)
- Sun, L., Guan, R., Lee, I. J., Liu, Y., Chen, M., Wang, J., ... Chen, Z. (2015). Mechanistic Insights into the Anchorage of the Contractile Ring by Anillin and Mid1. *Developmental Cell*, 33(4), 413–426. <https://doi.org/10.1016/j.devcel.2015.03.003>

- Suzuki, A., Ishiyama, C., Hashiba, K., Shimizu, M., Ebnet, K., & Ohno, S. (2002). aPKC kinase activity is required for the asymmetric differentiation of the premature junctional complex during epithelial cell polarization. *Journal of Cell Science*, *115*(18), 3565–3573. <https://doi.org/10.1242/jcs.00032>
- Tatsumoto, T., Xie, X., Blumenthal, R., Okamoto, I., & Miki, T. (1999). Human ECT2 is an exchange factor for Rho GTPases, phosphorylated in G2/M phases, and involved in cytokinesis. *Journal of Cell Biology*, *147*(5), 921–927. <https://doi.org/10.1083/jcb.147.5.921>
- Timmons, L., Court, D. L., & Fire, A. (2001). Ingestion of bacterially expressed dsRNAs can produce specific and potent genetic interference in *Caenorhabditis elegans*. *Gene*, *263*(1–2), 103–112. [https://doi.org/10.1016/S0378-1119\(00\)00579-5](https://doi.org/10.1016/S0378-1119(00)00579-5)
- Totong, R., Achilleos, A., & Nance, J. (2007). PAR-6 is required for junction formation but not apicobasal polarization in *C. elegans* embryonic epithelial cells. *Development*, *134*(7), 1259–1268. <https://doi.org/10.1242/dev.02833>
- Triplet, C. van O., Garcia, M. J., Bik, H. H., Beaudet, D., & Piekny, A. (2014). Anillin interacts with microtubules and is part of the astral pathway that defines cortical domains. *Journal of Cell Science*, *127*(17), 3699–3710. <https://doi.org/10.1242/jcs.147504>
- Tse, Y. C., Piekny, A., & Glotzer, M. (2011). Anillin promotes astral microtubule-directed cortical myosin polarization, 22. <https://doi.org/10.1091/mbc.E11-05-0399>
- Tse, Y. C., Werner, M., Longhini, K. M., Labbe, J. C., Goldstein, B., & Glotzer, M. (2012). RhoA activation during polarization and cytokinesis of the early *Caenorhabditis elegans* embryo is differentially dependent on NOP-1 and CYK-4. *Molecular Biology of the Cell*, *23*(20), 4020–4031. <https://doi.org/10.1091/mbc.E12-04-0268>
- Verbrugghe, K. J. C., & White, J. G. (2004). SPD-1 is required for the formation of the spindle midzone but is not essential for the completion of cytokinesis in *C. elegans* embryos. *Current Biology*, *14*(19), 1755–1760. <https://doi.org/10.1016/J.CUB.2004.09.055>
- Vicente-Manzanares, M., Ma, X., Adelstein, R. S., & Horwitz, A. R. (2009, November). Non-muscle myosin II takes centre stage in cell adhesion and migration. *Nature Reviews Molecular Cell Biology*. *Nat Rev Mol Cell Biol*. <https://doi.org/10.1038/nrm2786>
- Von Dassow, G., Verbrugghe, K. J. C., Miller, A. L., Sider, J. R., & Bement, W. M. (2009). Action at a distance during cytokinesis. *Journal of Cell Biology*, *187*(6), 831–845. <https://doi.org/10.1083/jcb.200907090>
- Von Stetina, S. E., & Mango, S. E. (2015). PAR-6, but not E-cadherin and β -integrin, is necessary for epithelial polarization in *C. elegans*. *Developmental Biology*, *403*(1), 5–14. <https://doi.org/10.1016/j.ydbio.2015.03.002>

- Vuong-Brender, T. T. K., Yang, X., & Labouesse, M. (2016). *C. elegans* Embryonic Morphogenesis. In *Current Topics in Developmental Biology* (Vol. 116, pp. 597–616). Curr Top Dev Biol. <https://doi.org/10.1016/bs.ctdb.2015.11.012>
- Walck-Shannon, E., Reiner, D., & Hardin, J. (2015). Polarized rac-dependent protrusions drive epithelial intercalation in the embryonic epidermis of *c. Elegans*. *Development (Cambridge)*, *142*(20), 3549–3560. <https://doi.org/10.1242/dev.127597>
- Wallace, A. G., Raduwan, H., Carlet, J., & Soto, M. C. (2018). The RhoGAP HUM-7/Myo9 integrates signals to modulate RHO-1/RhoA during embryonic morphogenesis in *Caenorhabditiselegans*. *Development (Cambridge, England)*, *145*(23). <https://doi.org/10.1242/dev.168724>
- Wang, S. C., Low, T. Y. F., Nishimura, Y., Gole, L., Yu, W., & Motegi, F. (2017). Cortical forces and CDC-42 control clustering of PAR proteins for *Caenorhabditis elegans* embryonic polarization. *Nature Cell Biology*, *19*(8), 988–995. <https://doi.org/10.1038/ncb3577>
- Wang, X., Roy, P. J., Holland, S. J., Zhang, L. W., Culotti, J. G., & Pawson, T. (1999). Multiple ephrins control cell organization in *C. elegans* using kinase-dependent and -independent functions of the VAB-1 Eph receptor. *Molecular Cell*, *4*(6), 903–913. [https://doi.org/10.1016/S1097-2765\(00\)80220-8](https://doi.org/10.1016/S1097-2765(00)80220-8)
- Watanabe, N., Madaule, P., Reid, T., Ishizaki, T., Watanabe, G., Kakizuka, A., ... Narumiya, S. (1997). p140mDia, a mammalian homolog of *Drosophila* diaphanous, is a target protein for Rho small GTPase and is a ligand for profilin. *EMBO Journal*, *16*(11), 3044–3056. <https://doi.org/10.1093/emboj/16.11.3044>
- Werner, M., Munro, E., & Glotzer, M. (2007). Astral Signals Spatially Bias Cortical Myosin Recruitment to Break Symmetry and Promote Cytokinesis. *Current Biology*, *17*(15), 1286–1297. <https://doi.org/10.1016/j.cub.2007.06.070>
- Wernike, D., Chen, Y., Mastronardi, K., Makil, N., & Piekny, A. (2016). Mechanical forces drive neuroblast morphogenesis and are required for epidermal closure. *Developmental Biology*, *412*(2), 261–277. <https://doi.org/10.1016/j.ydbio.2016.02.023>
- Williams-Masson, E. M., Malik, A. N., & Hardin, J. (1997). An actin-mediated two-step mechanism is required for ventral enclosure of the *C. elegans* hypodermis. *Development*, *124*(15).
- Williams, B. D., & Waterston, R. H. (1994). Genes critical for muscle development and function in *Caenorhabditis elegans* identified through lethal mutations. *Journal of Cell Biology*, *124*(4), 475–490. <https://doi.org/10.1083/jcb.124.4.475>
- Wissmann, A., Ingles, J., McGhee, J. D., & Mains, P. E. (1997). *Caenorhabditis elegans* LET-502 is related to Rho-binding kinases and human myotonic dystrophy kinase and interacts

- genetically with a homolog of the regulatory subunit of smooth muscle myosin phosphatase to affect cell shape. *Genes and Development*, 11(4), 409–422. <https://doi.org/10.1101/gad.11.4.409>
- Withee, J., Galligan, B., Hawkins, N., & Garriga, G. (2004). *Caenorhabditis elegans* WASP and Ena/VASP proteins play compensatory roles in morphogenesis and neuronal cell migration. *Genetics*, 167(3), 1165–1176. <https://doi.org/10.1534/genetics.103.025676>
- Wolfe, B. A., Takaki, T., Petronczki, M., & Glotzer, M. (2009). Polo-like kinase 1 directs assembly of the HsCyk-4 RhoGAP/Ect2 RhoGEF complex to initiate cleavage furrow formation. *PLoS Biology*, 7(5). <https://doi.org/10.1371/journal.pbio.1000110>
- Wu, Y., Han, B., Gauvin, T. J., Smith, J., Singh, A., & Griffin, E. E. (2019). Single-molecule dynamics of the P granule scaffold MEG-3 in the *Caenorhabditis elegans* zygote. *Molecular Biology of the Cell*, 30(3), 333–345. <https://doi.org/10.1091/mbc.E18-06-0402>
- Yüce, Ö., Piekny, A., & Glotzer, M. (2005). An ECT2-centralspindlin complex regulates the localization and function of RhoA. *Journal of Cell Biology*, 170(4), 571–582. <https://doi.org/10.1083/jcb.200501097>
- Zanin, E., Desai, A., Poser, I., Toyoda, Y., Andree, C., Moebius, C., ... Oegema, K. (2013). A conserved RhoGAP limits M phase contractility and coordinates with microtubule asters to confine RhoA during Cytokinesis. *Developmental Cell*, 26(5), 496–510. <https://doi.org/10.1016/j.devcel.2013.08.005>
- Zhang, H., Gally, C., & Labouesse, M. (2010). Tissue morphogenesis: How multiple cells cooperate to generate a tissue. *Current Opinion in Cell Biology*. *Curr Opin Cell Biol*. <https://doi.org/10.1016/j.ceb.2010.08.011>
- Zhang, H., & Labouesse, M. (2010, May). The making of hemidesmosome structures in vivo. *Developmental Dynamics*. *Dev Dyn*. <https://doi.org/10.1002/dvdy.22255>
- Zhang, H., Landmann, F., Zahreddine, H., Rodriguez, D., Koch, M., & Labouesse, M. (2011). A tension-induced mechanotransduction pathway promotes epithelial morphogenesis. *Nature*, 471(7336), 99–103. <https://doi.org/10.1038/nature09765>
- Zheng, G., Cochella, L., Liu, J., Hobert, O., & Li, W. (2011). Temporal and Spatial Regulation of MicroRNA Activity with Photoactivatable Cantimirs. *ACS Chemical Biology*, 6(12), 1332–1338. <https://doi.org/10.1021/CB200290E>
- Zilberman, Y., Abrams, J., Anderson, D. C., & Nance, J. (2017). Cdc42 regulates junctional actin but not cell polarization in the *Caenorhabditis elegans* epider. *Journal of Cell Biology*, 216(11), 3729–3744. <https://doi.org/10.1083/jcb.201611061>

Supplemental Figures

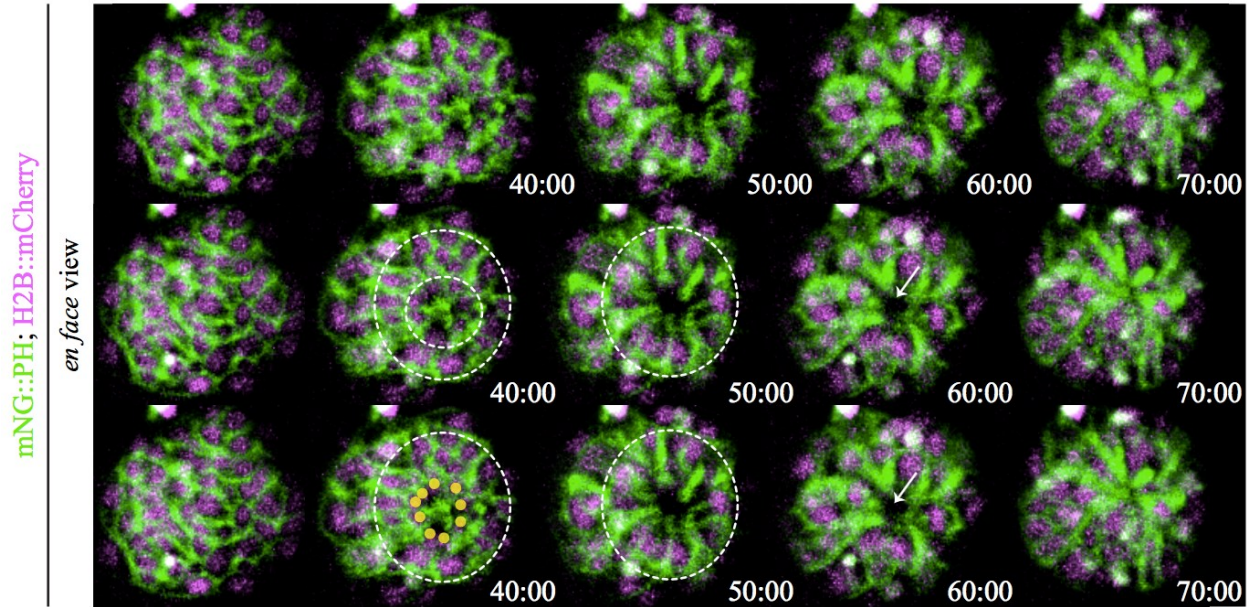


Figure S1. Cells ingress and form concentric rings during anterior morphogenesis. Time-lapse images obtained by sweptfield microscopy show *en face* views of an embryo co-expressing mNeonGreen::PH to visualize membranes (green) and H2B::mCherry to visualize nuclei (magenta) through anterior morphogenesis. A ‘ring in a ring’ of cells is highlighted (white dashed circles, inner yellow dots). The star-like pattern in the center marks the site of the future lumen, which forms after cells ingress into the embryo. Times are shown in minutes, and the scale bar is 10 μm .

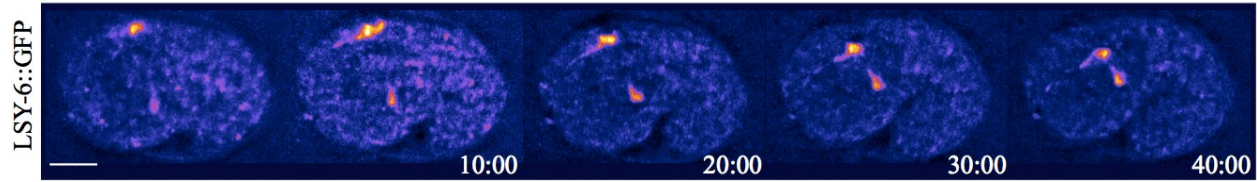


Figure S2. Distinct patterns of PAR-6 foci align with neuroblasts and epidermal cells during anterior morphogenesis. Time-lapse images show embryos expressing LSY-6::GFP, HLH-16::GFP, and MIR-228::GFP in Fire LUTs as indicated. For all embryos, times are shown in minutes, and the scale bar is 10 μ m.

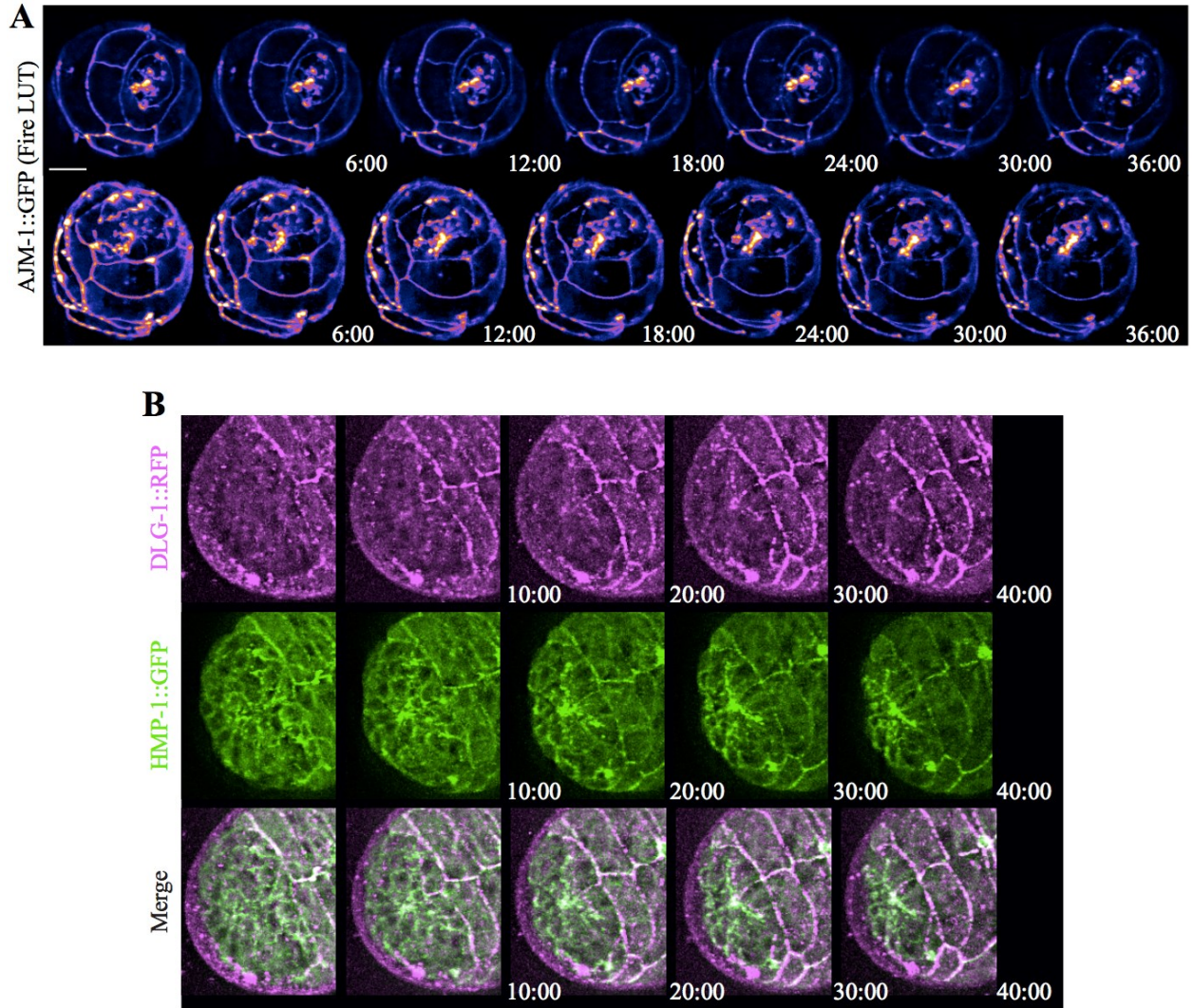


Figure S3. The epidermal cells form concentric rings around the lumen. A) Time-lapse images acquired using sweptfield microscopy show *en face* views of two different embryos expressing AJM-1::GFP (Fire LUTs) during anterior morphogenesis. B) Time-lapse images show ventral views (anterior to the left) of an embryo expressing HMP-1::GFP and DLG-1::RFP during anterior morphogenesis. Times are shown in minutes, and the scale bar is 10 μ m.

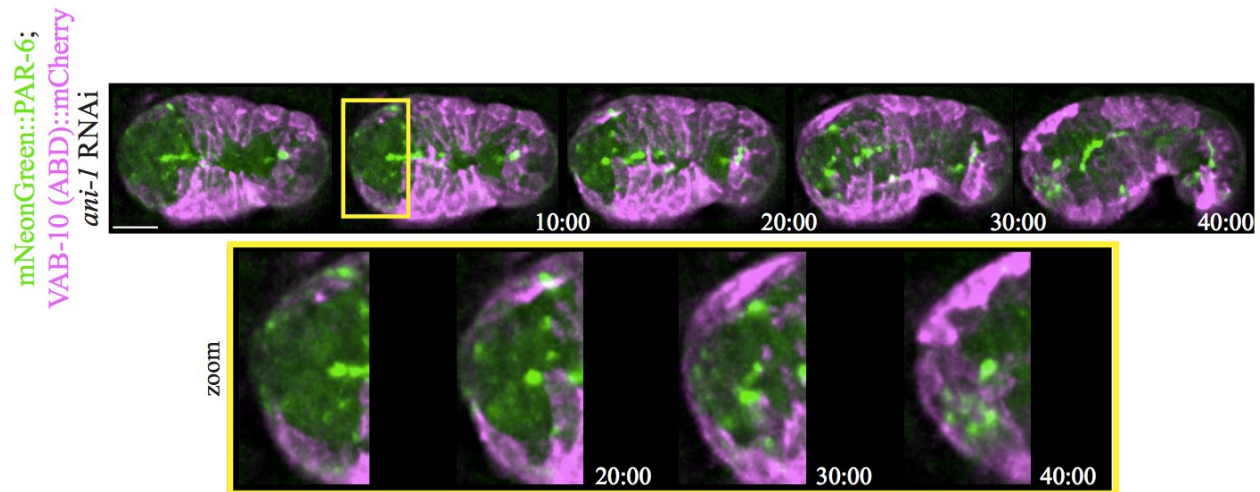


Figure S4. PAR-6 foci are disrupted after *ani-1* RNAi. Time-lapse images acquired using sweptfield microscopy show ventral views of an embryo co-expressing mNeonGreen::*PAR-6* (green) and *lin-26p*;VAB-10(ABD)::mCherry (magenta) after *ani-1* RNAi. The zoomed insets (yellow box) show the region where the foci would typically be found. While the BFP is still present, some of the foci associated with the pentagons and the semi-circle of foci are not visible. Times are shown in minutes, and the scale bar is 10 μ m.